Regulation of Microtubule Organization and Microtubule-dependent Transport by Septin 9

A Thesis

Submitted to the Faculty

of

Drexel University

by

Xiaobo Bai

in partial fulfillment of the

requirements for the degree

of

Doctor of Philosophy

Dec 2015

DEDICATION

This thesis is dedicated to my family, for all of their endless love and support, and also to those who helped me along the way. Life is short and make sure you have fun.

ACKNOWLEDGEMENT

I thank the United States of America for kindly giving me the chance to work on my PhD and have such a wonderful journey here. I thank my motherland, People's Republic of China, for raising me and providing me all those years of education and support, and for her recovery in the past years which give me so much pride and confidence.

Dr. Elias Spiliotis, my PhD thesis advisor and my mentor, deserves all of the gratitude a mentor can ever have. He has done every favor a mentor can do to his/her student. Without his full support, I could not have had any of my publications, nor to have attended so many conferences, or getting the career development opportunities that I had.

It was Dr. Donna Murasko, the Dean of College of Arts and Sciences, who introduced Drexel to me. She introduced me to the Drexel Biology Program and I am really grateful for her support. Upon arrival to Drexel, Alexis Finger, who is an Associate Teaching Professor in the Department of English & Philosophy, showed me her devotion and care, which I will never forget. Susan Cole, who was the graduate advisor, helped me with every step on my way and I really appreciate it.

My life as a Ph.D student could not have gone so well without those great scientists who served on my thesis committee: Drs. Aleister Saunders, Elias Spiliotis, Joseph Bentz, Daniel Marenda, Jennifer Stanford, and Kenneth Myers. Their suggestions and challenges drove my research and led me to all of my accomplishments. I thank Dr. Jennifer Stanford especially, who I also consider as a mentor. She gave me invaluable advice and guidance for my career development. I thank all of my collaborators, whose names are mentioned in the materials and methods sections for their reagents and help.

My colleagues gave me tremendous scientific and mental support, especially Jonathan Bowen, Lee Dolat, Dr. Jianli Hu, Eva Karasmanis, and Dimitrios Angelis, and it was their help

that made the tough times enjoyable. They are awesome people and it was an honor to work with them.

I thank my MS mentors in Nankai University, Drs. Wentao Qiao and Yunqi Geng. It was their care and training that launched my science career.

Last but certainly not least, I thank everyone in my family. My grandparents and parents raised me and suffered from all kinds of hardships along the way. My younger brother grow up with me, but I really should have done far more for him. My dear wife, Ying Yu, took care of my son Jason and all of the house work all by herself, and she gave me all support a wife can provide; I can't ask for a single bit more as a husband. She certainly deserves half of the credit I can get. My baby son, Jason gave me so much joy and pride. I could not have gotten to this point without them.

Table of Contents

LIST OF FIGURES

LIST OF ABBREVIATIONS

+TIPs	Microtubule plus end tracking proteins
AAA	ATPases Associated with diverse cellular Activities
AML	Acute myeloid leukemia
AMPA	α-amino-3-hydroxy-5-methyl-4-isoxazolepropionic acid
APC	Adenomatous polyposis coli
aPKC	Atypical protein kinase C
APP	Amyloid precursor protein
BBS-7	Bardet Biedl syndrome related proteins
CaMKII	Ca2+/calmodulin dependent protein kinase II
CAP-Gly	Cytoskeleton associated protein Gly-rich
CCP	Cytosolic carboxypeptidases
CENP-E	Centromere associated protein E
CH	Calponin homology
CLAMP	Chromatin linked adaptor for MSL proteins
CLASP	Cytoplasmic linker associated protein
CLIP 170	Cytoplasmic linker protein 170
CNS	Central nerve system
CRC	Colorectal cancer
CREB	Cyclic AMP responsive element-binding protein
DCLK1	Doublecortin like kinase 1
DCX	Doublecortin
EB	End-binding

EBH	End binding homology
ER	Endoplasmic reticulum
FEZ1	Fasciculation and elongation protein-ζ1
FRAP	Fluorescence recovery after photobleaching
GAPs	GTPase activating proteins
GEFs	Guanine nucleotide exchange factors
GluR2B	Glutamate receptor subunit 2B
GRIP1	Glutamate receptor interacting protein 1
GTP	Guanosine-5'-triphosphate
GTPase	Enzyme that can bind and hydrolyze GTP
HA	Haemagglutinin
HNA	Hereditary Neuralgic Amyotrophy
IFT	Intraflagellar transport
JNK	c-Jun N-terminal kinase
KAP	Kinesin associated protein
KHC	Kinesin heavy chain
KLC	Kinesin light chains
LIS1	Lissencephaly 1
MADD	MAPK activating death domain
MAP	Microtubule associated protein
MAPK	Mitogen activated protein kinase
MAP	MT associated protein
MBS	MAGUK binding stalk
MCAK	Mitotic centromere-associated kinesin

MDCK	Madin-Darby Canine Kidney
MLL	Lineage leukemia
mRNP	Messenger ribonucleoprotein
MT	Microtubule
MTOC	MT organizing center
NGF	Nerve growth factor
NMuMG	Mesenchymal normal murine mammary gland
NUDE	Nuclear distribution E
Op18	Oncoprotein 18
OSM3	Kinesin 2 family protein KIF17
PTMs	Post-translational modification
RanBP2	Ran-binding protein 2
RCC	Renal cell carcinoma
SBH	Subcortical band heterotopia
SEPT	Septins
STIM1	Stromal interaction molecule 1
STOPs	Stable tubulin only polypeptides
TGN	Trans-Golgi network
TOG	Tumor overexpressed gene
TTL	Tubulin Tyrosine ligase
TTLL	Tyrosine ligase-like
VAMP2	Vesicle-associated membrane protein 2
VSVG	Vesicular stomatitis virus G protein
XMAP215	Xenopus Microtubule Associated Protein 215

γTuRC	γ-tubulin ring complex

THESIS ABSTRACT

Regulation of Microtubule Organization and Microtubule-dependent Transport by Septin 9
Xiaobo Bai
Elias Spiliotis, Supervisor, Ph.D.

Microtubules (MTs) are a major component of the mammalian cytoskeleton. MTs are essential for cell morphogenesis and cellular functions including cell motility, cell division and intra-cellular transport. MT functions are tightly regulated by post-translational modifications (PTMs) and MT-associated proteins (MAPs). However, the underlying mechanisms are still elusive.

Septins are a family of GTP-binding proteins that can form hetero-oligomeric and polymeric structures, and function as scaffolds or diffusion barriers, controlling the localization of membrane and cytoplasmic proteins. Mammalian septins interact with MTs and actin filaments, Septins are also involved in Golgi-to-plasma membrane vesicle transport and chromosome alignment. Interestingly, septins have been shown to interact with the centromere-associated protein E (CENP-E), a mitotic kinesin-like motor that links kinetochores to the ends of spindle MTs. However, it is unknown whether septins interact directly with MTs and how they affect MT organization and intracellular transport.

In the first part of this thesis, I studied how MT organization is regulated by septins. I showed that the N-terminal domain of SEPT9 contains the novel repeat motifs K/R-x-x-E/D and R/K-R-x-E, which bind and bundle MTs by interacting with the acidic C-terminal tails of β-tubulin. Alanine scanning mutagenesis revealed that the K/R-R/x-x-E/D motifs pair electrostatically with one another and the C-terminal tails of β-tubulin, enabling septin-septin interactions that link MTs together. *SEPT9* is the only gene linked to hereditary neuralgic amyotrophy (HNA), a rare autosomal-dominant neuropathy. SEPT9 isoforms lacking repeat

motifs or containing the HNA-linked mutation R88W, which maps to the R/K-R-x-E motif, diminished intracellular MT bundling and impaired asymmetric neurite growth in PC-12 cells. These findings provide the first insight into the mechanism of septin interaction with MTs and the molecular and cellular basis of HNA.

In the second part of this thesis, I discovered a novel interaction between SEPT9 and KIF17, a kinesin 2 family motor that is important for learning and memory, mediating the transport of the NMDA glutamate receptor in hippocampal neurons. I found that SEPT9 associates directly with the cargo-binding C-terminal tail of KIF17 and competes with mLin-10/Mint1, a cargo adaptor/scaffold protein, which links KIF17 to the NMDA receptor subunit 2B (NR2B). Significantly, SEPT9 down-regulates NR2B transport into the dendrites of hippocampal neurons. Because SEPT9 does not affect the microtubule-dependent motility of KIF17, my results suggest that SEPT9 modulates the interaction of KIF17 with NR2B cargo. These results provide the first evidence of an interaction between septins and a non-mitotic kinesin, and suggest that SEPT9 modulates specifically the interactions of KIF17 with membrane cargo.

These findings advanced our knowledge of how septins associate with MTs and revealed the mechanism of MT binding and bundling by septins. My studies also provided the first clue about the etiology of HNA, which might be helpful in developing therapies for this disease in the future. In addition, the results of this work provided the first insight into how septins may regulate kinesin-dependent transport and the transport of a neurotransmitter to dendrite membrane. This knowledge could potentially be helpful in developing treatment for diseases associated with misregulation of MT organization and MT based transport.

CHAPTER I: Introduction

Microtubules (MTs)

MTs are a major component of cytoskeleton. MTs are essential in a variety of cellular structures and functions that include forming the mitotic spindle for faithful segregation of chromosomes, providing tracks for intra-cellular transport and constituting the axoneme of cilia and flagella for cell sensation and motility.

MTs are cylindrical structures. Each MT is usually 25 nm in external diameter, and is made of 13 linear protofilaments, which is formed by head to tail association of α- and β-tubulin heterodimers. MTs are intrinsically dynamic, the α-tubulin pointing end (minus end) is usually stabilized at the cell's MT organization center, while the β-tubulin pointing end (plus end) grows and shrinks. This dynamic behavior at the end of an individual microtubule is termed "dynamic instability" (Mitchison and Kirschner, 1984). MTs switch from growth to rapid shrinkage, which is called MT "catastrophe" (Atherton et al., 2013), and transition from shrinkage to growth, which is called MT "rescue". The terminal β-tubulin subunits of a growing plus end are bound to GTP (GTP cap), which stabilizes the microtubule structure (Conde and Caceres, 2009). When GTP is hydrolyzed to GDP, protofilaments splay apart and the microtubule rapidly depolymerizes (Conde and Caceres, 2009) (Figure 1.1 A).

Regulation of MT organization, dynamics and functions

MT organization and dynamics are tightly regulated in cells. Most MT nucleation occurs *in vivo* at the MT organizing center (MTOC). The initiation of MT growth is controlled spatially and temporally by the γ-tubulin ring complex (γTuRC) and related γ-tubulin complexes (Kollman

et al., 2011). γTuRC functions as a MT template, forcing the tubulin to form 13-protofilament MTs, whereas MT protofilaments spontaneously forms 14-protofilament MTs (Evans et al., 1985).

MT structures and dynamics, in addition to its functions are further regulated through the diversity of tubulin isotypes, post-translational modifications (PTMs) and MT-associated proteins (MAPs).

Tubulin isotypes

Tubulin isotypes have been identified in many species since their first discovery in 1981 (Krauhs et al., 1981; Ponstingl et al., 1981). The number of tubulin isotypes varies among different species, with two α- and one β-tubulin in budding yeast and up to seven α- and eight β-tubulin isotypes in humans (Sirajuddin et al., 2014). Tubulin molecules consist of a highly structured and thus evolutionarily conserved tubulin body and unstructured and less conserved C-terminal tails (Sullivan and Cleveland, 1986). To date, the function of different tubulin isotypes is still not well understood. Although it has been shown that some isotypes of tubulin can be interchangeable (Bond et al., 1986; Lewis et al., 1987), specificity of tubulin isotypes has also been shown. For example, β-tubulin isotype III is neuron specific and isotype I, II and IV also assemble into neuronal MTs (Joshi and Cleveland, 1989). It has also been shown that tubulin isotype composition affects MT kinetics and dynamics (Luduena, 1993; Panda et al., 1994) as well as MT motor activity (Sirajuddin et al., 2014). The importance of tubulin isotypes is further underscored by the discovery of tubulin isotype mutations that cause neuronal disorders (Jaglin et al., 2009; Tischfield et al., 2010). It should be noted that although some studies suggest that the C-terminal tails of α- and β-tubulins are redundant (Westermann and Weber, 2003), it has been shown that modifications of the tubulin C-terminal tails affect the polymerization property of αβ tubulin dimers (Mejillano and Himes, 1991), and a testis-specific β2-tubulin which lacks the C-

terminal domain fails to assemble into a functional axoneme in Drosophila (Fackenthal et al., 1993).

Post-translational modifications (PTMs)

Post-translational modifications of tubulin include phosphorylation, ubiquitylation, palmitoylation and sumoylation (Westermann and Weber, 2003; Wloga and Gaertig, 2010). Although these PTMs have been shown to occur frequently on other proteins and efficiently regulate their structure and functions, their function in MT structure and function regulation is much less understood. Most of our knowledge about tubulin post-translational modifications is about acetylation/deacetylation, polyglutamylation, polyglycylation, detyrosination/tyrosination and Δ2 tubulin (Figure 1.1 B).

I. Aceylation/deacetylation

Most post-translational modifications in tubulin occur at the C-terminal tail, except for acetylation/deacetylation, which was first discovered in flagella of *Chlamydomonas*. Acetylation takes place on the ε- amino group of a conserved lysine residue at amino acid position 40 in α-tubulin (Lhernault and Rosenbaum, 1985). Acetylation occurs after MT assembly and is mostly associated with stable MTs in structures like axonemes in cilia (Westermann and Weber, 2003). Several enzymes for tubulin acetylation have been identified, including ARD1-NAT1 (arrest-defective 1-amino-terminal, α-amino, acetyltransferase 1) (Ohkawa et al., 2008) and αTAT1 (α-tubulin *N*-acetyltransferase 1) (Shida et al., 2010). Several proteins have been shown to increase acetylation of lysine 40, including ELP complex (elongator protein complex), GCN5 (general control of amino acid synthesis 5) and MAP1B (MT associated protein 1B) (Conacci-Sorrell et al., 2010; Creppe et al., 2009; Takemura et al., 1992). Two deacetylation enzymes have been reported:

HDAC6 (histone deacetylase 6) and SIRT2 (NAD-dependent deacetylase sirtuin-2) (Hubbert et al., 2002; North et al., 2003). So far, the function of tubulin acetylation/deacetylation is still elusive. Interestingly, although acetylated tubulin is widely used as a marker for stable MT structures (Kull and Sloboda, 2014), it has been reported that acetylation of MTs actually increases their sensitivity to MT severing enzyme katanin (Sudo and Baas, 2010).

II. Polyglutamylation

Polyglutamylation is a modification of creating a chain formed by up to 20 glutamine residues from the γ-carboxylate group of a glutamic acid amino acid in the tubulin C-terminal tail. This modification occurs on both α- and β-tubulin (Mary et al., 1994; Redeker et al., 1998), and can be detected on multiple neighboring residues (Schneider et al., 1998). A decade after the discovery of tubulin polyglutamylation, TTLL1 (tyrosine ligase-like 1) was identified as the catalytic subunit for tubulin polyglutamylase in a multiprotein complex. Subsequently, TTLL4, 5, 6, 7, 11, 13 were identified as the mammalian polyglutamylases and TtTtll6Ap was identified as β-tubulin elongating polyglutamylase in *Tetrahymena thermophila* (van Dijk et al., 2007). Each enzyme showed specific preference for either α- or β-tubulin, and preference for generating short or long polyglutamate chains. Mammalian depolyglutamylating enzymes were identified in the CCP (cytosolic carboxypeptidases) family (Kimura et al., 2010; Rogowski et al., 2010). Similar to polyglutamylases, each depolyglutamylating enzyme has a preference for either removing the glutamyl side chain from a branch point or hydrolyzing a peptide bond between glutamyl residues in a side chain (Rogowski et al., 2010). Hydrolysis of glutamyl chain also results in hydrolysis of the last amino acid residue of detyrosinated tubulin and the formation of Δ2-tubulin (Rogowski et al., 2010).

Polyglutamylation is involved in many cellular activities. Studies showed that it regulates MT length, stability and timely severing of MTs during cytokinesis by katanin and spastin (Connell et al., 2009; Sharma et al., 2007); spastin-mediated MT severing seems to be more effective on MTs with long Glu chains than those with short Glu ones (Lacroix et al., 2010). Interestingly, some MAPs (microtubule associated proteins) like MAP1A bind to MTs with long Glu chains, suggesting an alternative mechanism for regulation of MT stability (Bonnet et al., 2001; Hu et al., 2008). The length of the side chain also determines interactions between MTs and other MAPs. For example, some kinesins and tau have the strongest affinity to MTs containing glutamate side chain with three residues (Audebert et al., 1994). Evidence also suggests polyglutamylation might regulate MT affinity and processivity of some kinesins (Janke et al., 2005). In neurons, for example, it has been shown that decreased polyglutamylation led to the mislocalization of Kinesin KIF1A, but does not affect KIF3A (Ikegami et al., 2007). Increase of polyglutamylation, on the other hand, was shown to inhibit the KIF5 based transport (Maas et al., 2009).

Polyglutamylation is increased at the onset of mitosis, suggesting its importance in cell division (Regnard et al., 1999). It is also enriched in centrioles, which are characterized by particularly long Glu side chains (Bobinnec et al., 1998). It has been proposed that polyglutamylation might help to recruit specific proteins to build the centriolar matrix and anchor MTs, generating and maintaining the MT organization center (Westermann and Weber, 2003). Polyglutamylation was also shown to be enriched in cilia and flagella, playing an important role in basal body maturation and cilia assembly, as well as cilia beating by affecting the interaction between ciliary dynein and MTs (Kubo et al., 2010; Suryavanshi et al., 2010).

Regulation of polyglutamylation level is important during development. Polyglutamylase activity peaks in the early stage of brain development, when MTs are highly dynamic. At later

stages, the overall activity of polyglutamylase is low, but MTs are stable and highly polyglutamylated. Furthermore, the timing of polyglutamylation for α- and β-tubulin is different during neuronal development. α-tubulin polyglutamylation is abundant in very young neurons, while β-tubulin polyglutamylation is low in young neurons and only start to accumulate during differentiation (Audebert et al., 1994). Interestingly, deglutamylase CCP1, which is highly expressed in brain (Rogowski et al., 2010), is absent in a mouse model for Purkinje cell degeneration (*pcd*) (Mullen et al., 1976). Hyperglutamylated MTs accumulate in the brain region that is prone to degeneration (Greer and Shepherd, 1982), raising the possibility that hyperglutamylation might promote neuron degeneration.

III. Polyglycylation

Polyglycylation of MTs takes place on glutamate residues of the C-terminal tail of α- or β-tubulin, forming side chains of various lengths (Westermann and Weber, 2003). The difference from polyglutamylation is that Glycine is added instead of Glutamate, and the length of Glycine chain can contain up to 34 residues (Plessmann and Weber, 1997). Similar to the polyglutamyl branching formed from the γ-carboxylate group of the glutamate, the first glycine of the nascent side chain is bound to a glutamate residue of the tubulin polypeptide chain through a Glu COOH-Gly αNH2 isopeptide bond (Glu-Gly), and the linkage between glycine residues is through Gly αCOOH-Gly αNH2 peptide bonds (Gly-Gly) (Westermann and Weber, 2003). Polyglycylation takes place mostly on polymerized tubulins after polymerization and therefore, even in cells with high tubulin polyglycylation level, the side chains of tubulin consist of only one to two glycine residues (Bre et al., 1998).

Glycylation enzymes belong to the same TTLL family as of polyglutamylases. Similar to polyglutamylases, each glycylase specifically modifies either α- or β-tubulin and generates either

short or long side chains. Little is known, however, about the residue specificity or the spatial and temporal control of each glycylase (Janke and Bulinski, 2011). Evidence suggests the existence of deglycylation enzymes (Bre et al., 1998), but none has been identified.

Glycylation was first detected in ciliary tubulin (Redeker et al., 1994), which is highly glycylated (mono- or poly-glycylated) in cilia and flagella. Glycylation is also the dominant modification of tubulin in mammalian sperm (Plessmann and Weber, 1997; Rudiger et al., 1995). In *Tetrahymena*, glycylation of β-tubulin seems to be more important than that of α-tubulin. While loss of α-tubulin glycylation has no observable effect, decrease of β-tubulin glycylation leads to slow growth and motility and defective cytokinesis. Lack of all β-tubulin glycylation is lethal (Xia et al., 2000). Glycylation is critical for axonemal stability and decrease of this modification results in the shortening of cilia in *T. thermophila* and defective cilia in zebra fish, which leads to phenotypes like randomized body asymmetry (Wloga et al., 2009). In D. melanogaster, depletion of tubulin glycylation in testis resulted into disassembly of sperm axonemes and sterility of male flies (Rogowski et al., 2009). Although glycylation is essential to cilia in many organisms, it does not exist in cilia of organisms such as *Trypanosoma spp.* and *Plasmodium spp.* (Schneider et al., 1997). Interestingly, evolutionary exchange of two amino acids within the human elongating glycylase TTLL10 resulted in the loss of its polyglycylation capability. The mechanism of its function compensation is still elusive (Rogowski et al., 2009).

IV. Detyrosination/tyrosination

Tubulin detyrosination is the process of removing the last tyrosine of α-tubulin, which is encoded in most α-tubulin genes, and this process is reversible by the process of tyrosination (Janke and Bulinski, 2011). Detyrosinated tubulin exposes a glutamic acid at its carboxy-terminal and therefore, it is referred to as Glu-tubulin. The enzyme that catalyses detyrosination has not

been identified. However, the enzyme that reverses this process, tubulin tyrosine ligase (TTL) was the first tubulin modification enzyme purified and cloned (Ersfeld et al., 1993; Schroder et al., 1985). Detyrosination of tubulin occurs on polymerized MTs (Kumar and Flavin, 1981), whereas tyrosination takes place exclusively on soluble α- and β-tubulin dimers (Raybin and Flavin, 1977). In fact, TTLs re-tyrosinate tubulins so efficiently and rapidly that almost none of the newly polymerized MT contains detyrosinated tubulin (Gundersen et al., 1987; Webster et al., 1987). Detyrosinated tubulin can be further modified to Δ2-tubulin by removing its C-terminal Glutamic acid (Paturle-Lafanechere et al., 1991), which is catalysed irreversibly by deglutamylase of the CCP family (Rogowski et al., 2010).

The function of detyrosination is not clear. TTL knockout mice are born without obvious abnormality, but die within the first day after birth, suggesting that detyrosination may play an important role in organ function (Westermann and Weber, 2003). Evidence also suggests that decreased TTL activity promotes tumorigenesis (Cai et al., 2009; Larcher et al., 1996). Detyrosination was suggested to coordinate different cytoskeletal elements, as vimentin intermediate filaments preferentially co-align with detyrosinated MTs (Reed et al., 2006). Detyrosination/tyrosination regulates MT stability. Studies suggest that MT depolymerizing kinesins such as KIF2C and KIF2A preferentially depolymerize tyrosinated MTs (Peris et al., 2009). In contrast, detyrosinated and Δ2-tubulin, which permanently locks MTs in detyrosinated states, cannot be depolymerized by these kinesins (Song and Brady, 2014). Detyrosinated tubulins have been shown to accumulate in neuronal axons (Konishi and Setou, 2009), increasing the affinity of KIF5 and dynein to MTs, and thereby, stimulating their activities in axonal transport (Dunn et al., 2008; Reed et al., 2006). It has also been shown that tubulin tyrosination is important for MT binding of plus tip proteins such as CLIP 170 (cytoplasmic linker protein 170) and $p150^{glued}$ (Peris et al., 2006; Weisbrich et al., 2007).

Studies indicate that a level of coordination may take place between the PTMs of tubulin. For example, although most brain tubulin is polyglutamylated, brain Δ2-tubulin seems to be polyglycylated specifically (Peris et al., 2009). In the axoneme of sea urchin sperm, tubulins in A-tubules are mostly unmodified while tubulins in B-tubules are detyrosinated and polyglycylated extensively (Paturle-Lafanechere et al., 1994). A gradient of polyglutamylation and polyglycylation along the flagellum of *S. similis* has been reported, decreasing from the proximal part to the distal part (Lechtreck and Geimer, 2000; Zilberman et al., 2009). Axonemal MTs are detyrosinated but not uniformly (Lechtreck and Geimer, 2000). The central pair of axonemal MTs are highly tyrosinated, whereas the outer MT doublet, the B-tubule is heavily detyrosinated and contains abundant Δ2-tubulin, compared with A-tubules (Johnson, 1998; Paturle-Lafanechere et al., 1994; Robson and Burgoyne, 1989). However, the function of this distribution of modified tubulin in axoneme is not known.

PTMs of tubulins might be inter-dependent. It is possible that manipulation of a specific PTM might affect others. For example, It was shown that loss of α-tubulin polyglutamylation in mice might also alter the tyrosination and polyglutamylation of β-tubulin (Ikegami et al., 2007). Therefore it is difficult to study the effect of a specific PTM as the phenotype can be misinterpreted.

Microtubule plus-end tracking proteins (MT +TIPs)

MT +TIPs are a diverse group of conserved proteins that accumulate at growing end of MT tips and regulate their dynamics, interaction with cellular structures and signaling factors (Akhmanova and Steinmetz, 2008). MT +TIPs vary in size and structure and can be multi-domain or multi-subunit. Despite this diversity, MT +TIPs contain conserved protein binding domains,

motifs or sequences. Therefore, they are usually categorized into different families based on their structural properties (Akhmanova and Steinmetz, 2008).

In the End-binding (EB) family, EB proteins have conserved N- and C-terminal domains (Lansbergen and Akhmanova, 2006). The N-terminal domain contains a globular calponin homology (CH) domain, which is shared by signaling proteins (Gimona et al., 2002) and some other MAPs such as CLAMP (Dougherty et al., 2005). The C-terminal of EB proteins contain an α-helical coiled-coil domain, which mediates the parallel dimerization of EB proteins (Honnappa et al., 2005). They also contain an end binding homology (EBH) domain, which contains around 50 amino acids, forming a deep hydrophobic cavity, which serves as an interaction site for binding partners (Slep et al., 2005). The last 20-30 amino acids of EB proteins are flexible and contain an EEY/F sequence motif, which is also found at the C- terminus of α-tubulin and in the cytoplasmic linker protein 170 (CLIP170), serving as binding partner of CAP-Gly domains (Weisbrich et al., 2007). The CAP-Gly (cytoskeleton-associated protein Gly-rich) family of proteins includes the Class II-associated invariant chain peptide proteins (CLIPs) and the dynactin complex subunit $p150^{glued}$ (Galjart, 2005; Schroer, 2004). The CAP-Gly domain is globular and contains a unique hydrophobic cavity, mediates interaction with MTs and EB proteins (Ligon et al., 2006). CLIPs and $p150^{glued}$ also contain coiled coil domains, mediating the formation of homodimers (Ligon et al., 2006).

Additional MT +TIPs include the adenomatous polyposis coli (APC), cytoplasmic linker associated protein (CLASP) and XMAP215 family MAPs that contain tumor overexpressed gene (TOG) like domains. APC is flexible and contains extensive basic and Ser residues, which mediate interaction with MTs and EB proteins (Nathke, 2004). Cytoplasmic linker associated protein (CLASP) family proteins contain basic and Ser-rich sequences.

MT plus ends are also bound by MT motors of either plus-end or minus-end direction (Wu et al., 2006). Motor proteins interact with MT plus ends via sequences outside of their motor domains and rely on their interaction with other +TIPs (Akhmanova and Steinmetz, 2008).

Most MT +TIPs track on the growing ends of MTs, but some (e.g., XMAP215) can also bind to the depolymerzing ends (Brouhard et al., 2008). The detailed mechanism of how +TIPs accumulate at the ends of MTs is not clear, but the presence of GTP caps and curvature of MT protofilaments might provide cues for their binding (Akhmanova and Steinmetz, 2008). Some +TIPs (e.g., CLIPs) can interact with tubulin dimers and oligomers *in vitro*, suggesting that +TIPs can co-polymerize with tubulin dimers during MT polymerization (Folker et al., 2005). MT affinity of most +TIPs is weak and +TIPs such as MCAK, XMAP215 and dynactin diffuse along MTs to reach the MT plus ends (Brouhard et al., 2008; Culver-Hanlon et al., 2006; Helenius et al., 2006). Other +TIPs (eg. CLIPs, Bik1 and APC) are transported to the growing end of MTs by kinesin motors such as the Kip2 and kinesin-2 (Carvalho et al., 2004; Jimbo et al., 2002). Plus-end directed kinesins are retained at MT ends by associating with MT ends or other +TIPs, and transport other proteins to MT ends through "hitchhiking" (Bieling et al., 2007; Carvalho et al., 2003). A few +TIPs such as $p150^{glued}$ can also "hitchhike" on other +TIPs, like EB proteins, for accumulation at the MT plus end (Honnappa et al., 2006). The mechanism of accumulation at MT plus ends can be species specific. In fission yeast, for example, the CLIP homologue Tip1 depend on the EB homologue Mal3 for plus tip accumulation, but this is not the case in budding yeast (Carvalho et al., 2004; Wolyniak et al., 2006).

+TIPs have diverse effect on MT dynamics. MT +TIPs with extensive basic and Ser-rich sequences (CLASPs, APC) stabilize MTs (Galjart, 2005; Lansbergen and Akhmanova, 2006) by preventing catastrophe and promoting rescue (Mimori-Kiyosue et al., 2005). By contrast, MT +TIPs such as XMAP215 promote MT growth by adding tubulin dimers to the plus end of MTs

(Brouhard et al., 2008). EB proteins increase the dynamics of MTs, but can also decrease catastrophe events (Lansbergen and Akhmanova, 2006). The detailed mechanism is still not clear, but the fission yeast EB1 homologue Mal3 can bind to the seam of MTs with 13 protofilaments, suggesting that EB proteins may stabilize MTs by "zipping" them up (Sandblad et al., 2006). This MT binding of EB1 may modulate the interaction of kinesins with MTs (Akhmanova and Steinmetz, 2008). Conversely, EB1 interacts with MT depolymerizing kinesins MCAK and KLP10A, and targets them to MT plus ends (Lee et al., 2008; Niethammer et al., 2007). EB1, however, may antagonize the destabilizing activities of these kinesins (Niethammer et al., 2007). Members of kinesin-13 family destabilize and promote MT depolymerization and catastrophe (Moores and Milligan, 2006). MCAK, a member of the kinesin 13 family is well studied and is thought to bend and peel off individual protofilaments from MTs to generate protofilament rings (Moores and Milligan, 2006). +TIPs in CLIP family, on the other hand, rescue MTs from shrinking to growing (Komarova et al., 2002).

Another important function of +TIPs includes capturing and stabilizing MT ends at the cell cortex (Gundersen et al., 2004; Huisman and Segal, 2005). APC and CLASPs can link MT ends directly to actin or cortical factors (Moseley et al., 2007; Tsvetkov et al., 2007). EB1 interacts with the stromal interaction molecule 1 (STIM1), which is a endoplasmic reticulum (ER)-resident transmembrane protein, and thereby mediates MT growth-dependent extension of ER tubules (Grigoriev et al., 2008). Finally, +TIPs regulate MT functions by pushing and pulling MT ends during membrane reorganization and mitosis (Pearson and Bloom, 2004). It has been shown that the interaction between dynein and CLIP170 is important for the positioning of the MT spindle during cell division (Huisman and Segal, 2005; Pearson and Bloom, 2004).

Structural MAPs

Vertebrate structural MAPs mainly consist of MAP2/Tau family, MAP1 and doublecortin. MAP2/Tau family proteins includes MAP2, MAP4 and tau, all of which have alternative splice isoforms. Each isoform has a flexible structure and consists of a C-terminal MT binding domain that contains multiple MT binding motifs, and a flexible N-terminus extends outward (Amos and Schlieper, 2005). MAP2 and tau are specific for neuron cells. MAP2 concentrates in dendrites and tau concentrates in axons. MAP4 is expressed in non-neuronal cell types. All of these MAPs stabilize MTs as well as increase MT rigidity and bundle MTs (Dehmelt and Halpain, 2005). The physiological importance of MAP2 and tau has been studied in MAP2 or tau knockout mice. In the MAP2 knockout mice, MT density and dendrite length are decreased (Harada et al., 2002). In the tau knockout mice, microtubule stability is decreased and microtubule organization is significantly changed in some small-caliber axons (Harada et al., 1994).

MAP2 and tau bind along MTs and stabilize them by reducing the frequency and duration of catastrophe (Gamblin et al., 1996). MAP2 has also been shown to form clusters along MTs and to stop MT catastrophe at these clusters (Ichihara et al., 2001). MAP2 and tau have been reported to create spaces within MT bundles for the movement of motors through their N-terminal projection domains, which extend from the MT surface and create distance between MTs (Amos and Schlieper, 2005; Chen et al., 1992). However, overexpression of MAP2/Tau interferes with movement of kinesin- and dynein-dependent transport along MTs by competing for MT attachment (Ackmann et al., 2000; Lopez and Sheetz, 1993; Mandelkow et al., 1999; Stamer et al., 2002).

MAP4 stabilizes MTs and is important in regulating mitotic MT dynamics during metaphase (Ookata et al., 1995). oMAP4, a MAP4 isoform, is required for paraxial microtubule organization in muscle cells and prevents dynein- and kinesin-driven microtubule-microtubule

sliding, which is essential for cell elongation and cell-cell fusion (Mogessie et al., 2015). In addition, MAP4 was shown to negatively regulate dynein-dependent movement and positively regulates kinesin-2 based movement (Bulinski et al., 1997; Semenova et al., 2014).

I. MAP1A/1B

Similar to MAP2 and Tau, MAP1A and MAP1B are unstructured and highly flexible. MAP1 interacts with MTs through repetitive short motifs in its N-terminal MT binding domain, but the sequence of these motifs have little similarity with the ones in MAP2/Tau (Amos and Schlieper, 2005). MAP1A can increase MT nucleation and stimulate MT elongation, but is much less efficient compared with MAP2 (Pedrotti and Islam, 1994). MAP1B is important for axonal development and acts cooperatively with tau in neuronal morphogenesis (Takei et al., 2000).

II. Doublecortin

Doublecortin (DCX) was named after the disease "double cortex syndrome", which is officially known as subcortical band heterotopia (SBH) (des Portes et al., 1998). To date, the DCX family comprises 11 paralogues in human (Reiner et al., 2006). DCX proteins mediate neuronal migration through promoting MT polymerization and stabilization (Taylor et al., 2000) (Gleeson et al., 1999). DCX does not affect the growth rate of MTs, but rather stabilizes MTs by linking adjacent protofilaments and counteracting outward bending of depolymerizing MTs, acting as an anti-catastrophe factor (Moores et al., 2006). DCX interacts with MTs through its conserved DCX domain and this interaction is regulated by phosphorylation/dephosphorylation of their SP-rich domain (Schaar et al., 2004).

Some other structural MAPs that are involved in MT stabilization include STOPs (stable tubulin only polypeptides), which enable MTs to be cold-resistant (Bosc et al., 1999) as well as

LIS1 (lissencephaly-related protein 1), which enhances MT polymerization and bundling (Tanaka et al., 2004).

III. MT depolymerizing and severing MAPs.

Stathmin, which is also named as Op18 (Oncoprotein 18), is a tubulin sequestering protein that induces MT catastrophe (Cassimeris, 2002). It has been suggested that each Op18 molecule binds to the side of one tubulin heterodimer and its N-terminal domain caps the α-tubulin subunit to prevent its polymerization (Amos and Schlieper, 2005). However, the detailed mechanism of how Op18 regulate MT organization is still not clear. Kinesin-8, which glides along MTs, can accumulates at the plus ends and promote MT disassembly (Mayr et al., 2007). Kinesin-8 preferentially disassemble longer MTs over shorter ones and is important in spindle length control during mitosis (Su et al., 2013). MT severing enzymes including katanin, spastin and fidgetin are all members of the AAA (ATPases Associated with diverse cellular Activities) family. These proteins form transient hexamer in presence of ATP and sever MTs by disrupting the interaction between αβ tubulin heterodimers (Roll-Mecak and McNally, 2010). MT severing by these proteins has been shown to be important in the regulation of spindle length during mitosis, disassembly of cilia and flagella, as well as neuron axon branching (Roll-Mecak and McNally, 2010).

Microtubule dependent transport

MT-dependent intracellular transport is essential for survival and function of mammalian cells. Retrograde transport (toward MT minus end, usually from periphery to center of the cell) is carried out by dynein. Cytoplasmic dynein consists of the dynein heavy chain, which is encoded by one gene in mice and human (Pfister et al., 2006), and a large complement of additional

subunits. Five classes of associated subunits are encoded in metazoan genomes, including the intermediate chain (IC), light-intermediate chain (LIC) and three types of light chain (LC), which include T-complex testis-specific protein (TCTEX), LC8 and Roadblock (Roberts et al., 2013). These subunits also subject to splicing and are encoded by two different genes each, and can be regulated by phosphorylation, which further increases the diversity. Some of these subunits have restricted expression patterns (Roberts et al., 2013). Homodimerization of the dynein heavy chain is mediated by the dynein tail domain, which also serves as a scaffold for other non-catalytic subunits. All of these subunits function as dimers to form the complement of the cytoplasmic dynein complex. The dynein IC and LIC bind directly to the dynein heavy chain, and the LC assembles on the intermediate chain. The LC can mediate the interaction with other adaptor proteins, such as the p150 subunit of dynactin (Roberts et al., 2013). Dynactin complex comprises 11 subunits, including p150, the largest subunit, and a filament of actin-related protein 1 (ARP1). Dynactin is essential for almost all functions of cytoplasmic dynein, such as targeting dynein to specific cellular locations and increase dynein processivity. Dynactin also mediates the interaction between dynein complex and its cargo through its ARP1 filament, P150 or p50 subunits (Kardon and Vale, 2009). The activities and functions of cytoplasmic dynein are regulated by various factors including the lissencephaly 1 (LIS1) and nuclear distribution E (NUDE) proteins (Roberts et al., 2013).

Kinesins, which mediate anterograde transport (toward microtubule plus end, usually from center to periphery of the cell), are encoded by 45 genes, and most of which have alternative splice isoforms. Kinesins are categorized into 15 families, which are termed kinesin 1 to kinesin 14B (Hirokawa et al., 2009). Among them, kinesins in families 1-12 have a N-terminal motor domain and are responsible for anterograde transport (Vale and Fletterick, 1997). Kinesin 13 molecules have the motor domain located in the center, and they depolymerize MTs (Wordeman,

2005). Members in kinesin 14A and 14B family have C-terminal motor domains and are retrograde transporters that mediate MT cross-linking and sliding during mitosis (Peterman and Scholey, 2009).

Kinesins contain coiled-coil domains that mediate their dimerization. The majority of kinesins form homodimers that walk on MTs with a hand-over-hand mechanism (Hirokawa et al., 2009). Kinesin-1 family members form hetero-tetramers with two kinesin heavy chains (KHC) and two kinesin light chains (KLC) (Figure 1.2 A). In kinesin-2 family, KIF17 can form homodimers (Figure 1.2 B), while KIF3A and KIF3B form heterotrimers with the kinesin associated protein (KAP) (Hirokawa et al., 2009; Scholey, 2013). Kinesin-3 family members can exist either as monomers or homodimers. Kinesin-5 motors form homotetramers with two motor domains on each end of the complex, and therefore can slide MTs of the mitotic spindle (Verhey and Hammond, 2009) .

ER-to-Golgi transport involves dynein (Hirokawa et al., 2009; Presley et al., 1997), while Golgi-to-ER transport involves KIF5 and KIF3 (Santama et al., 2004; Stauber et al., 2006), but their roles are still under debate (Hirokawa et al., 2009). The positioning of the Golgi apparatus has been suggested to be due to a "tug-of-war" between the anterograde motor KIF20A and the retrograde motors dynein and KIFC3 (Echard et al., 1998; Xu et al., 2002).

Several kinesins have been reported to transport various cargos from Golgi to the plasma membrane. For example, KIF5 was found to transport the vesicular stomatitis virus G protein (VSVG) and neurotrophin receptor p75 toward the plasma membrane (Hirokawa et al., 2009). In contrast, KIFC3 was found to transport TGN derived vesicles containing annexin XIIIb and influenza haemagglutinin (HA) toward the cell membrane (Hirokawa et al., 2009; Lin and Clarkson, 2015).

The transport of lysosomes in cells involves the kinesin 1 motor KIF5B (Nakata and Hirokawa, 1995) and kinesin 2 motors (Brown et al., 2005). The intracellular transport of melanosomes, which are lysosome-related organelles, is mediated by cytoplasmic dynein, kinesin 5B and KIF3 (Gross et al., 2002). Early endosomes containing RAB4 or RAB5 are transported by cytoplasmic dynein, KIF5, KIF3 and KIFC2 (Imamura et al., 2003). Early endosomes that contain PtdIns(3,4,5)P3 associate with KIF16B (Nakagawa et al., 1997), while late endosomes associate with cytoplasmic dynein, KIF3 and occasionally KIFC2 (Bananis et al., 2004).

Protein transport in cilia and flagella, also known as intraflagellar transport (IFT), is carried out by kinesin 2 family motors (Cole et al., 1998). In the sensory cilium of *Caenorhabditis elegans*, KIF3A/B (KRP85/95) and KIF17 (OSM3) are responsible for IFT and work partially redundantly (Ou et al., 2005). In the middle segment of cilia, the Bardet-Biedl syndrome-related proteins BBS-7 and BBS-8 link KIF3 and KIF17 so that they jointly serve as IFT motors (Jenkins et al., 2006). In the distal segment of cilia, however, only KIF17 was detected (Jenkins et al., 2006).

MT-dependent transport has been studied in neurons. In axons, proteins are transported in synaptic vesicle precursors. The kinesin 3 motors KIF1A and KIF1Bβ transport synaptic vesicle precursors containing synaptic vesicle proteins such as synaptophysin, synaptotagmin and small GTPase RAB3A (Okada et al., 1995; Zhao et al., 2001). Binding of RAB3 to KIF1A and KIF1Bβ is mediated by the adaptor protein mitogen-activated protein kinase (MAPK)-activating death domain (MADD) (Hirokawa et al., 2009). KIF5 transports synaptic vesicle precursors containing synaptic proteins such as synaptotagmin and synaptobrevin (Diefenbach et al., 2002). In addition, KIF5 can also transport vesicles containing presynaptic plasma membrane proteins such as syntaxin 1 and SNAP25, which interacts directly with KIF5 (Diefenbach et al., 2002).

Mitochondria are crucial for energy production and are distributed over the full length of axon due to active transport by KIF1Bα and KIF5B/C (Lin and Sheng, 2015). Interaction between KIF5 and mitochondria can be mediated by multiple adaptor proteins such as syntabulin, the Ran-binding protein 2 (RanBP2) and the Milton-Miro complex (Cai et al., 2005; Cho et al., 2007; Glater et al., 2006).

Kinesin-driven transport is essential for the elongation of neurites. The hetero-trimeric complex formed by the kinesin 2 family motors KIF3A, KIF3B and KAP3 (KIF-associated protein 3) transports fodrin-associated vesicles, which might provide plasma membrane components at the tips of neurites (Takeda et al., 2000).

Neurons are highly polarized with an axon, which contains MTs with plus-ends pointing toward the distal end, and multiple dendrites that contain MTs of mixed polarity (Baas et al., 1989). KIF3A was reported to transport APC, the cell polarity protein PAR3 and PAR6, and the atypical protein kinase C (aPKC) to the tip of nascent axons (Shi et al., 2004). KIF13B transports PIP3-containing vesicles toward the tip of axons through the interaction with an adaptor protein PIP3BP/centaurin-α (Horiguchi et al., 2006), which might have potential role in determination of neuronal polarity.

In dendrites, transport of neurotransmitter receptors such as NMDA (N-methyl-D-aspartate) and AMPA (α-amn0-3-hydroxy-5-methyl-4-isoxazole propionic acid) receptors (NMDARs/AMPARs) is essential for synaptic transmission and plasticity (Basu and Siegelbaum, 2015). KIF5A/B/C transports the AMPA receptor subunit GluR2 in dendrites and GluR2 binds KIF5 via the adaptor protein glutamate receptor-interacting protein 1(GRIP1) (Setou et al., 2002). In dendrites, the kinesin 2 family protein KIF17 (OSM3) transports the NMDA receptor subunit NR2B. Interaction between KIF17 and NR2B is mediated by the mLin complex, which contains the scaffolding proteins mLin2, mLin7 and mLin10 that binds directly to the C-terminal tail of

KIF17 (Setou et al., 2000). KIF17 is also thought to mediate the dendritic transport of the kainate glutamate receptor GluR5 and the voltage-gated potassium channel Kv4.2 (Chu et al., 2006; Kayadjanian et al., 2007).

Local protein synthesis in dendrites has been proposed to be important in synapse plasticity (Tom Dieck et al., 2014), and KIF5A/B/C transports messenger ribonucleoprotein (mRNP) complexes, which contain more than 40 proteins and mRNAs for proteins such as CaMKIIalpha and Arc (Kanai et al., 2004).

Regulation of kinesin-based transport

Kinesin-based transport can by regulated in a variety of ways. Some kinesins can transform into a folded, "autoinhibited" formation in the absence of cargo, which can be relieved upon cargo binding. Kinesin activities on MTs with different PTMs may vary and can also be regulated by MAPs.

In the absence of cargo, motor proteins in kinesins 1, 2 (KIF17/OSM-3), 3 (KIF1A, KIF13B) and 7 (CENP-E) families exist in a folded conformation, a state referred to as "autoinhibition". It is used to preserve energy consumption (Verhey and Hammond, 2009) (Figure 1.2 C). The autoinhibition of kinesin-1, KIF17 and CENP-E is achieved by direct interaction between the tail and motor domains (Espeut et al., 2008). In contrast, the autoinhibition of the kinesin 3 motors KIF1A and KIF13B involves domains in between their motor and tail. In the autoinhibited KIF1A, the FHA domain and the adjacent coiled-coil segment interact with the motor domain. In the autoinhibited KIF13B, the MAGUK binding stalk (MBS) domain interacts with the motor domain, preventing its binding to MTs (Hammond et al., 2009; Yamada et al., 2007). The autoinhibition of kinesin-1 can be further strengthened by a second mechanism (Yamada et al., 2007). Its KLC subunit keeps the two KHC motor domains apart,

preventing the processive motility (Cai et al., 2007). In kinesin-2, the CC2+CC3 region in the stalk domain promotes the autoinhibition (Hammond et al., 2010a) and in kinesin-3 motor KIF1A, the CC1 domain prevents its processive motility by promoting the monomeric state (Hammond et al., 2009).

Autoinhibition of kinesin-1, kinesin-2 and kinesin-3 family motors is released by cargo binding on their tail domains. For kinesin-1, the proteins FEZ1 (fasciculation and elongation protein-ζ1) and JNK (Jun N-terminal kinase) bind to the inhibitory regions of the KHC tail and KLC subunits, respectively (Blasius et al., 2007). Relieving the autoinhibition of kinesin-7 family motors, however, is induced by phosphorylation of the C-terminal tail by the monopolar spindle protein 1 and/or CDK1-cyclin B (Espeut et al., 2008).

I. Regulation by PTMs

Kinesin-based transport can also be regulated by post-translational modifications (PTMs), the related studies have been mostly focused on Kinesin-1 (KIF5). It has been reported that α-tubulin acetylation enhances MT binding and the motility of kinesin-1 (Reed et al., 2006). This is further supported by the finding that hyper-acetylation of MTs in neurons affects the distribution of kinesin-1(Geeraert et al., 2010). However, pharmacological perturbation of tubulin acetylation does not affect the distribution of kinesin-1 (Hammond et al., 2010b). Detyrosinated α-tubulin has also been suggested to be important in kinesin-1 dependent transport in neuronal axons (Konishi and Setou, 2009), and *in vitro* experiments indicated that kinesin-1 binds more tightly to detyrosinated MTs (Dunn et al., 2008). However, other findings show that kinesin-1 does not bind preferentially to detyrosinated MTs, suggesting that detryrosination is not alone a factor for kinesin 1 to discriminate MT tracks. Polyglutamylation, on the other hand, also seems to regulate kinesin-dependent transport, but the results are also inconclusive. For example, total loss of β-

tubulin polyglutamylation inhibits kinesin-1 MT binding, but similar inhibition was also shown when the Glu side chain contains more than three glutamate acids (Larcher et al., 1996). It is therefore possible that the length of Glu side chain is important for the MT affinity of Kinesin-1. Polyglutamylation might also be important in transport of kinesin-3 motors (Ikegami et al., 2007). A recent study by Sirajuddin and Vale showed that the processivity of kinesin-1 can be increased by polyglutamylation and decreased by detyrosination. Similar to kinsin-1, the motility and processivity of kinesin-2 can be increased by polyglutamylation, but interestingly, they are also increased by detyrosination, which is the opposite of kinesin-1 (Sirajuddin et al., 2014).

Other non-major tubulin PTMs, such as polyglycylation, phosphorylation, palmitoylation and ADP-ribosylation, and different tubulin isotypes, might also be involved in the regulation of kinesin motility, but are much less studied.

II. Regulation by MAPs

The regulation of kinesin-based transport by MAPs has also been studied over the years. The inhibitory role of tau overexpression on kinesin-1 motility and the subsequent alteration of its cargo distribution are well documented (Dubey et al., 2008; Stoothoff et al., 2009). Specifically, it has been shown that overexpression of tau leads to accumulation of kinesin-1 in soma and fail to enter neuronal processes (Seitz et al., 2002). MAP2 has also shown to have similar effects as tau, inhibiting the motility of kinesin-1 motor and decreasing its cargo transport (Seitz et al., 2002). It is generally agreed that kinesin-1 velocity is not affected by tau/MAP2, but whether motility inhibition is due to the decrease of motor run length or reduction of motor attachment on MTs is still under debate (Seitz et al., 2002; Trinczek et al., 1999). Overexpression of MAP4 was also found to reduce motility of vesicle transport (Bulinski et al., 1997). *In vitro* studies showed that MAP4 inhibits MT gliding on kinesin-1, increasing MT pausing and decreasing MT run length

(Atherton et al., 2013). However, the effect of MAP4 on kinesin motility at physiological *in vivo* concentrations is not clear (Atherton et al., 2013).

Doublecortin (DCX)/doublecortin-like kinase-1(DCLK1) has also been shown to affect intracellular transport. Loss of DCX and DCLK inhibits vesicle-associated membrane protein 2 (VAMP2) and synaptophysin to enter axons (Deuel et al., 2006). Similarly Ensconsin/MAP7 has been shown to promote MT binding of kinesin-1 and relieve its autoinhibition (Barlan et al., 2013).

Finally, some evidence suggests that tubulin GTPase cycle may affect the regulation of kinesin motility. For example, it has been shown that small islands of GTP-bound tubulin exists along cellular MTs (Kueh and Mitchison, 2009). In vitro MT gliding assays showed that kinesin-1 driven GMPCPP-stabilized MTs move ~ 34% faster than paclitaxel-stabilized MTs (Vale et al., 1994). In vitro single molecule motility assay showed that kinesin-1 has shorter run length on GMPCPP stabilized MTs than on paclitaxel stabilized MTs (McVicker et al., 2011).

III. Regulation of cargo-motor association

Motor-cargo binding and cargo unloading are also tightly regulated. The simplest model of cargo selection is through a direct interaction between the motor and cargo molecules or membrane vesicles. For example, kinesin-1 has been suggested to interact directly with amyloid precursor protein (APP) in axons (Kamal et al., 2000). The pleckstrin homology (PH) domains of kinesin-3 KIF1A/KIF1Bβ/Unc-104 can interact with phosphatidylinositol-4,5-bisphosphate (PIP2) on synaptic vesicles (Klopfenstein et al., 2002), and the PX domain of kinesin-3 family member KIF16B can bind to phopatidylinositol-3-phosphate (PI(3)P) on early endosomes (Hoepfner et al., 2005). However, in many cases, protein adaptors are necessary for recruiting of motors. For example, association between kinesin-1 and TrkB needs Rab27b, Slp1 and CRMP-2, which

function as adaptors (Arimura et al., 2009). The recruitment of dynein-dynactin to late endosomes depends on Rab7, RILP, ORP1L and βIII spectrin (Johansson et al., 2007). The regulatory role of adaptor proteins can be further demonstrated by the fact that one kinesin can be used to transport different cargos by changing the adaptors. A good example is kinesin-1, which interacts with mitochondria in the presence of the GTPase Miro and the Milton1/TRAK1 adaptor protein (Glater et al., 2006), but in the presence of Rab6, it associates with exocytotic vesicles (Grigoriev et al., 2007).

Kinesins can be regulated by phosphorylation. Two kinases have been shown to regulate the function of KIF5. Phosphorylation of KIF5 KLC (kinesin light chain) by protein kinase A has been shown to inhibit association of KIF5 with synaptic vesicles (Sato-Yoshitake et al., 1992). KLC phosphorylation by Glycogen synthase kinase 3 inhibits association of KIF5 with membrane organelles (Morfini et al., 2002). As another example, the Ca^{2+}/calmodulin-dependent protein kinase CaMKII phosphorylates Ser 1020 in the tail domain of KIF17, leading to the dissociation of KIF17 from its adaptor protein mLin-10, resulting in the unloading of its NR2B containing vesicle (Guillaud et al., 2008). Phosphorylation can also regulate the MT binding of kinesins. Evidence suggests that phosphorylation of KIF5 by c-Jun N-terminal kinase (JNK) weakens the MT binding of KIF5. In addition, phosphorylation of adaptor proteins can regulate kinesin-cargo interactions. Phosphorylation of the adaptor protein UNC76 is required for the transport of synaptotagmin-containing vesicles by KIF5 in axons. Unphosphorylated UNC76 can no longer associate with synaptotagmin 1 (Gindhart et al., 2003). Furthermore, CamKII mediated phosphorylation of poly (ADP-ribose) polymerase 1(PARP1) leads to its dissociation from KIF4 (Midorikawa et al., 2006).

Rab GTPases are regulators of motor proteins. GTP-bound Rab6 localizes in the Golgi apparatus but the GDP-bound form does not. KIF20A associates with GTP-bound Rab6 in Golgi,

and GTP hydrolysis of Rab6 leads to dissociation of KIF20A from Golgi (Echard et al., 1998). In addition, GTP-bound Rab5 has been shown to recruit KIF16B and cytoplasmic dynein to early endosomes (Nielsen et al., 1999).

Rab3 is a synaptic vesicle protein and is transported by KIF1A and KIF1Bβ. It has been shown that only the GTP-bound form of Rab3 can be transported to axons, not the GDP-bound form, and the transport of Rab3 into axons involves the binding of MAPK activating death domain (MADD) to both GTP-bound Rab3 and the stalk domain of KIF1A and KIF1Bβ (Niwa et al., 2008). Since MADD is thought to be a GEF (guanine exchange factor) of Rab3, it might help to maintain Rab3 in its GTP-bound form during its long-range transport in axons.

Cargo-motor association can also be regulated by Ca^{2+} signaling. Mitochondria concentrate at regions with high energy requirements, such as pre- and post-synaptic area, where high influx of Ca^{2+} occurs, and high Ca^{2+} concentrations arrest the motility of mitochondria (Chang et al., 2006). Neuronal mitochondria are transported by kinesin 1 (e.g., KIF5) and kinesin 3 (e.g., KIF1Bα) motors (Nangaku et al., 1994). The KIF5-mitochondria interaction is bridged by the adaptor proteins Milton and Miro (Guo et al., 2005; Stowers et al., 2002). Miro contains two EF hand motifs, which are modulated by Ca^{2+}, suggesting the possibility that transport of mitochondria by KIF5 can be regulated by Ca^{2+} signaling (Wang and Schwarz, 2009).

Physiological role of kinesin-based transport

Disruption of the normal function of kinesins could lead to diverse consequences. Knockout and conditional knockout of various kinesins in mice have shed light on the physiological roles of kinesins. The effects of kinesin disruption have been mostly concentrated on neuronal development. Knockout of either KIF1A or KIF1Bβ, which transport synaptic vesicle precursors, causes severe neuronal degeneration and synaptic dysfunction in perinatal

period, and ultimately results in death (Yonekawa et al., 1998; Zhao et al., 2001). A mutation in KIF5A leads to a neuropathy named hereditary spastic paraplegia (Reid et al., 2002). Missense mutation of KIF21A, which is enriched in both axons and dendrites, is related to a human disease CFEOM1 (congenital fibrosis of the extraocular muscle type 1) (Yamada et al., 2003).

KIF2A is a kinesin that directly regulates the morphology of neurons, and its knockout in mice leads to abnormal elongation and collateral branching of axons, as well as inhibition of neuronal migration (Homma et al., 2004). KIF4A associates with PARP1, inhibiting its activity and restricting it in the nucleus (Midorikawa et al., 2006). Activation of PARP1 by CamKII phosphorylation results in dissociation of PARP1 from KIF4A and prevents apoptosis (Midorikawa et al., 2006). KIF4A knockout neurons, therefore, exhibit high survival rate and resistance to apoptosis (Midorikawa et al., 2006).

KIF17 has been extensively studied and is shown to be important in learning and memory. Transgenic mice that overexpress KIF17 have a significant improvement of working and spatial memories (Wong et al., 2002), while KIF17 knockout mice have impaired memories (Yin et al., 2011). Overexpression of KIF17 leads to the upregulation of intrinsic *Nr2b*, which encodes NR2B, a subunit of the NMDA receptor (Wong et al., 2002). The increase of NR2B expression occurred in parallel to the enhanced phosphorylation of the cyclic AMP-responsive element-binding protein (CREB) (Wong et al., 2002), which has putative binding sites in the enhancer region of *Nr2b* and *Kif17*. CREB, therefore, may further enhance the expression level of both NR2B and KIF17. It is posited that KIF17 overexpression enhances the transport of NR2B to synapses, which induces a positive-feedback loop that further enhances the expression of KIF17 and NR2B upon increase of local Ca^{2+} signaling and CREB phosphorylation, leading to improved learning and memory.

KIF3A/B knockout mice die at the mid-gestation stage and show randomization of left-right body determination (Nonaka et al., 1999; Takeda et al., 1999). KIF3 also functions as a tumor suppressor, transporting vesicles containing N-cadherin and β-catenin towards the plasma membrane, and down-regulating Wnt signaling, which promotes cell proliferation. Conditional inactivation of the KAP3 subunit of the KIF3 complex in neural progenitor cells results in embryonic brain tumors (Teng, 2005).

Septins

Septins are a group of GTP binding proteins that oligomerize and polymerize into filamentous structures. Septins were first identified during a screen for mutations that alter the cell division cycle of *Saccharomyces cerevistae* (Hartwell, 1971). The name "septin" was chosen by the laboratory of John Pringle to reflect their role in separation of mother and budding daughter cells (Hall, 2005). Septins are evolutionarily conserved from yeast to animals, and they are found in almost all species except for plants and Dictyostelium (Longtine et al., 1996). The number of septin genes in different organisms are highly variable, with two in *Caenorhabditis elegans*, five in Drosophila, seven in yeast, and thirteen in human (Hall and Russell, 2004). The nomenclature of mammalian septins was not standardized until 2002. Since then, the human and mouse septin genes are named as *SEPT1-SEPT14* and *Sept1-Sept14*, respectively (Macara et al., 2002); *SEPT13* was found to be a pseudogene of *SEPT7* and is thus named as *SEPT7P2*.

Human septins are classified phylogenetically into four homology groups: SEPT2 (includes SEPT1, 2, 4 and 5), SEPT3 (includes SEPT3, 9, 12), SEPT6 (includes SEPT6, 8, 10, 14) and SEPT7 (Kinoshita, 2003; Weirich et al., 2008) (Figure 1.3 A). Septin genes undergo complex alternative splicing, which increases the number of isoforms expressed. In the most extreme case, septin 9 expressing gene can create six 5' splice variants and three 3' splice variants, resulting in

18 transcripts (McIlhatton et al., 2001), which encodes 15 different proteins; note that two different 5' transcripts encode the same polypeptide (Figure 1.4). All the longest isoforms of the thirteen septins expressed in humans have a GTP-binding domain, which is flanked by an N-terminal polybasic region and a C-terminal septin unique domain (Versele and Thorner, 2005). Septins vary mainly in the sequence and length of their N-terminal and C-terminal tails.

Septins belong to the TRAFAC class of GTPase superfamily of P-loop NTPases, which include small GTPases like Ras, and ATPases like myosin and kinesin (Leipe et al., 2002). Unlike the small GTPases of the Ras superfamily, septin GTP turnover is not regulated by GTPase activating proteins (GAPs) or guanine nucleotide-exchange factors (GEFs) (Gasper et al., 2009; Weirich et al., 2008). Septins belong to a group of G proteins activated by nucleotide-dependent dimerization (GADs) (Gasper et al., 2009), but how their GTPase activities are regulated is still to be determined. Septins have a α-β-α core structure and a conserved GTP-binding domain, which has a similar basic structure with other members in TRAFAC (translation factor) families, such as Ras. Despite the similarity to other members of TRAFAC family, septin structure has four unique elements, including two β-hairpin inserts in the GTP-binding domain and two α-helixes flanking the GTP-binding core. Three of these elements are involved in septin oligomerization. EM and crystallography analysis (Sirajuddin et al., 2007) of the protein complex formed by SEPT2 indicates that SEPT2 is able to form elongated filaments through two different binding interfaces, which involve interactions between the core GTP-binding domains and between the N- and C-terminal helices that flank the GTP-binding domain. The G-dimer requires one β-hairpin insert and the two flanking α-helixes are necessary for the dimerization of the NC interface (Sirajuddin et al., 2007). The function of the GTP-binding domain is still not clear, though some studies suggest that GTP binding and hydrolysis may induce conformational changes that promote septin oligomerization (Mendoza et al., 2002; Weems et al., 2014). GTP

has also been shown to affect septin binding to PtdIns(4,5)P_2 (Zhang et al., 1999), which is important for septins to binding cell membranes (Xie et al., 1999).

Septins form non-polar heteromeric complexes (Figure 1.3 B), which assemble into higher order structures including filaments, rings and cage-like structures. These structures function as diffusion barriers and scaffolds at various cellular locations. For example, septins serve as a diffusion barrier at the cleavage furrow during cell division, as well as at the annuli of spermatozoa and the base of cilia and neuronal spines (Chih et al., 2012; Hagiwara et al., 2011; Hu et al., 2010; Ihara et al., 2005; Joo et al., 2005; Kim et al., 2010; Kinoshita and Noda, 2001; Kissel et al., 2005; Mostowy et al., 2011; Sellin et al., 2011; Tada et al., 2007; Xie et al., 2007). Septins also perform unique functions such as surrounding invasive bacteria and inhibiting their growth (Mostowy et al., 2010; Mostowy et al., 2009). Higher order septin structures may also be important for cell signaling. For example, ARTS (SEPT4) was found to be essential for TGFβ-induced apoptosis (Larisch et al., 2000), and the SEPT6-SEPT7 dimer interacts directly with Borgs, which is a downstream effector of the Cdc42 GTPase (Sheffield et al., 2003). Recently, septins were found to promote stress fiber-mediated maturation of focal adhesions and renal epithelial motility (Dolat et al., 2014b).

Septin filaments are non-polarized, which is also conserved throughout species. *C. elegans* contains only two septins: UNC-59 and UNC-61, and EM studies demonstrated that the septin complex formed with the GTP-binding domain of these proteins was in the order of UNC-59-UNC61-UNC-61-UNC-59 (John et al., 2007). Similarly, EM revealed that the oligomers formed by the S. cerevisiae septins Cdc3, Cdc10, Cdc11 and Cdc12 are non-polar octamers that follow the order of Cdc11-Cdc12-Cdc3-Cdc10-Cdc10-Cdc3-Cdc12-Cdc11 (McMurray and Thorner, 2009). The core structure of human septin filaments is now accepted to be the non-polar octamer SEPT9-SEPT7-SEPT6-SEPT2-SEPT2-SEPT6-SEPT7-SEPT9 (Mostowy and Cossart,

2012). In this complex, septins alternate between G and NC interfaces. Although the G-interface dimerization is favored by SEPT2, the interface between the two SEPT2 subunits in the octamer is an NC-interface. In the complex, SEPT2 and SEPT7 bind to GDP, but SEPT6 binds to GTP, which is very likely due to the lack of Threonine 78 in the switch I region of the SEPT6 GTP-binding domain, which is responsible for GTP hydrolysis (Sirajuddin et al., 2009).

Septin filaments are much less dynamic than MTs (Hu et al., 2008). Septin oligomerization and filament formation are regulated at different levels. GTP binding and hydrolysis trigger conformation changes within the GTP-binding domain of septins, affecting the stability of oligomeric interfaces (Sirajuddin et al., 2009). In addition, the TRiC/CCT chaperone system is involved in the folding and possibly dimerization of septins (Dekker et al., 2008). Cdc42 suppresses oligomerization of septin through Borg3, which directly interacts with SEPT6-SEPT7 dimer (Joberty et al., 2001). The Drosophila Orc6 subunit of the origin recognition complex interacts with the coiled-coil domain of the Drosophila septin Pnut, increasing its GTPase activity and enhancing septin filament formation (Huijbregts et al., 2009). In addition, post-translational modification of septins, including phosphorylation, sumoylation, acetylation and ubiquitylation have been reported to affect the higher order structure of septins (Hernandez-Rodriguez and Momany, 2012). Membrane association of septins is also important in the regulation of septin structure (Beise and Trimble, 2011). Finally, septin structure is highly interdependent with actin filaments and microtubules (Nagata et al., 2003; Schmidt and Nichols, 2004).

Septins and diseases

The current knowledge about tissue expression and functions of mammalian septins is largely from DNA microarray analysis and septin knockout mice. DNA microarray assay with

normal, disease, and tumour tissues suggested that SEPT2, SEPT5, SEPT6, SEPT7, SEPT9, and SEPT11 are ubiquitously expressed in nearly all tissues (Hall et al., 2005; Mostowy and Cossart, 2012). SEPT4, SEPT8 and SEPT10 are widely expressed except for some tissues. In contrast, SEPT1, SEPT3, SEPT12, and SEPT14 showed tissue specific expression (Cao et al., 2007). SEPT1 and SEPT3 are specifically expressed in lymphoid and central nerve system (CNS), respectively (Dolat et al., 2014a), and SEPT12 is lymphocyte and testis specific (Cao et al., 2007; Mostowy and Cossart, 2012). Finally, the expression of SEPT14 was only detected in CNS and testis (Cao et al., 2007). It should be noted that the expression profile of different isoforms of the same septin protein may vary (Kartmann and Roth, 2001). In the brain, the expression levels of septins changes dramatically during development (Tsang et al., 2011), but the variation of septin expression in other tissues during development is not well known.

Knockout mice have been generated for seven septins. *Sept7, Sept9 and Sept11* knockout are embryonically lethal. *Sept3, Sept5* and *Sept6* knockout mice were physiologically and functionally normal (Ono et al., 2005; Tsang et al., 2008), but the social interaction, rewarded goal approach and anxiety-related behavior seem to be altered in the *Sept5* knockout mice (Harper et al., 2012; Suzuki et al., 2009). The *Sept4* knockout mouse is the most well studied. Male *Sept4*$^{-/-}$ mice are sterile due to the immobility of the sperm (Ihara et al., 2005; Kissel et al., 2005). Maldevelopment and hypo-dopaminergic phenotypes have also been reported for *Sept4*$^{-/-}$ mice (Kinoshita, 2008). These mice are also more susceptible to tumor growth and liver fibrosis, and contain high levels of hematopoietic and hair follicle stem cells (Fuchs et al., 2013; Garcia-Fernandez et al., 2010; Iwaisako et al., 2008).

The first evidence for the association between septins and human diseases came from the discovery that *SEPT5* was fused to the C-terminal of the mixed lineage leukemia (MLL) protein in an acute myeloid leukemia (AML) patient with a t(11;22)(q23;q11.2) translocation (Megonigal

et al., 1998). MLL encodes a large histone methyltransferase that directly binds DNA and positively regulates gene transcription (Muntean and Hess, 2012). Chromosomal rearrangement of MLL gene leads to hematopoietic malignancies, which are associated with both acute myeloid leukemia and acute lymphoid leukemia (Muntean and Hess, 2012). More than 50 MLL fusion partners have been identified (Burmeister et al., 2009). Up to now, five septins, SEPT2, SEPT5, SEPT6, SEPT9 and SEPT11, are identified as fusion partners of MLL in human leukemic cells (Borkhardt et al., 2001; Cerveira et al., 2006; Kojima et al., 2004; Osaka et al., 1999), accounting for the largest known protein family associated with MLL rearrangement (Cerveira et al., 2011). The function of these fusions are not well known, but it has been shown that the in frame fusion of MLL-SEPT6 upregulates the expression of Hox-7a and Hox-9a, immortalizing hematopoietic progenitor cells (Ono et al., 2005).

Septins are involved in neuron functions and neuronal development. The SEPT3/SEPT5/SEPT7 complex was identified in mammalian brain (Fujishima et al., 2007). SEPT3 was found to enrich in the presynaptic terminals of neurons (Xue et al., 2004). SEPT2 and SEPT8 are involved in the release of neurotransmitter (Ito et al., 2009; Kinoshita et al., 2004) and Sept6 is involved in myelin formation (Buser et al., 2009). In addition, SEPT6 and SEPT7 were found to localize at the base of axonal filopodia and axon branch points in sensory neurons (Hu et al., 2012). Sept4 and Sept14 were found to play essential roles in neuronal migration during mouse brain development (Shinoda et al., 2010).

It is unknown whether septins are directly involved in the development of neurological disorders. However, septins are linked to a variety of neurological disorders. For example, SEPT1, SEPT2 and SEPT4 were identified in neurofibrillary tangles of Alzheimer's patients (Kinoshita et al., 1998), and SEPT5 was found to interact with Parkin in Parkinson's disease (Choi et al., 2003). Sept4 has also been found in cytoplasmic inclusions in Parkinson's disease and other

synucleinopathies (Ihara et al., 2003). In fetuses with Down syndrome, the expression of Sept6 and Sept7 is dramatically reduced in the brain (Sitz et al., 2008). Expression of SEPT5, SEPT6 and SEPT11 was found to increase in schizophrenia and bipolar disorders (Pennington et al., 2008), and SEPT9 is abnormally overexpressed in a mouse model of demyelinating neuropathy (Patzig et al., 2011).

Septins are linked to male infertility. SEPT1, 4, 6, 7 and 12 localize at the annulus of the sperm, establishing a diffusion barrier, and are critical for the compartmentalization of sperm proteins (Kwitny et al., 2010; Toure et al., 2011). Male mice that lack the *Sept4* or *Sept12* genes do not possess a functional annulus, and they are immotile and have L- shaped tails (Kissel et al., 2005). Defective annulus is also common among patients with sperm malformation, and SEPT4 has been used as a diagnostic marker to screen for this disease (Sugino et al., 2008). Genetic analysis of infertile man identified two missense mutation of SEPT12, T89M and D197N, both mutations disrupt filament formation of SEPT12. In addition, the patient with the D197N mutation does not have SEPT12 in their sperm annulus (Kuo et al., 2012).

Septins are involved in the development of multiple cancers. Some testicular cancer patients lack the expression of SEPT14, suggesting that SEPT14 may function as a tumor suppressor (Peterson et al., 2007). In sporadic ovarian cancers, the chromosomal locus 17q25.3, which contains the *SEPT9* gene, is partially deleted (Russell et al., 2000). Analysis of benign, malignant and borderline ovarian carcinoma samples showed the *SEPT9_i1* and *SEPT9_i4** transcripts are overexpressed in serious and mucinous borderline tumors (Scott et al., 2006). Upregulation of SEPT9_i1 could slow down the degradation of c-Jun-N-terminal kinase (JNK) and the hypoxia inducible factor HIF1α, leading to the enhancement of tumor growth and angiogenesis (Amir et al., 2009; Gonzalez et al., 2009). Similarly, SEPT9_i4 overexpression

enhances cell motility and resistance to anticancer drugs (Chacko et al., 2012), and might promote the malignant and metastatic potential of ovarian carcinomas (McDade et al., 2007).

In renal cell carcinomas (RCC), which is an aggressive and highly metastatic cancer of the kidney, expression of SEPT2, the Bradeion isoform of SEPT4 and SEPT11 are increased in patients with defective von Hippel-Lindau (VHL) tumor suppressor (Bongiovanni et al., 2012; Craven et al., 2006). Because upregulation of the Bradeion isoform of SEPT4 can be detected in urine samples from RCC and translational bladder cancers, quantification of this SEPT4 isoform has been used to diagnose urological cancers in Europe and Japan (Bongiovanni et al., 2012; Tanaka et al., 2003). Upregulation of the Radeion α and β isoforms of SEPT4 was also identified in mucinous carcinoma and rectal malignant melanoma (Tanaka et al., 2001; Zieger et al., 2000).

Finally, in colorectal cancer (CRC), SEPT9 expression was found to decrease progressively during tumorigenesis (Toth et al., 2011). Hypermethylation of *SEPT9* promoter was found in most colorectal tumors and has been used commercially as a colorectal cancer screen marker in a non-invasive diagnostic test (Molnar et al., 2015).

Hereditary Neuralgic Amyotrophy (HNA)

The name of HNA literally means: "lack of muscle growth accompanied by nerve pain". HNA is also known as brachial plexus neuropathy or neuritis with brachial predilection. HNA is an autosomal dominant neuralgic disorder, which is characterized by nerve damage and atrophy of upper-limb muscle preceded by sudden and severe non-abating pain. This disease is similar to the Parsonage-Turner syndrome in prognosis, which is the non-hereditary form of neuralgic amyotrophy. The onset of HNA is typically in the second or third decade (median age 28 years). In some families, HNA is characterized by anatomical deficiencies or deformities such as distinct craniofacial features, bifid uvula or cleft palate, short stature and/or partial syndactyly of the

fingers or toes (van Alfen N, 2008). During the development of this disease, brachial plexus nerves are attacked by the immune system and degenerate (Pellegrino et al., 1996). In some cases, phrenic nerves or the recurrent laryngeal may be affected (Holtbernd et al., 2011). As the neurons lose function, the muscles associated with them start to atrophy. With the degeneration of the branchial plexus, the deltoid muscle will atrophy, leading to severe pain and atrophy in the muscles of the arms and shoulders. If the phrenic nerve gets degenerated, the diaphragm would be affected, which might lead to impaired breath due to lack of muscle control of the diaphragm. In the cases where the laryngeal nerve gets affected, atrophy of the pharynx will occur, resulting in loss of vocal function (Chance and Windebank, 1996; van Alfen, 2007; van Alfen et al., 1993). HNA occurs sporadically, and some patients experience recurrent episodes (Orstavik et al., 1997). No systematic clinical trial has been executed and there is still a lack of effective treatment (van Alfen et al., 2009). With years of pursue; *SEPT9* has been found to be the only gene associated with HNA (Kuhlenbaumer et al., 2005; Meulemann et al., 1999; Pellegrino et al., 1996; Stogbauer et al., 1997). Approximately 75% of the patients are genetically linked to aberrations in SEPT9 expression which include the missense mutations R88W and S93F in SEPT9_i3, duplications of aa 19-233 (Figure 1.5), as well as the *SEPT9_v3* 5'-UTR -131G > C mutation (Kuhlenbaumer et al., 2005; Kuhlenbaumer et al., 2001; Landsverk et al., 2009; van Alfen N, 2008). The molecular etiology of HNA is unknown, but it has been shown that unlike the wild type SEPT9, the SEPT9 R88W and S93F mutants form filaments with SEPT4 along the stress fibers of murine mammary gland (NMuMG) cells (Sudo et al., 2007). These mutants also colocalize with SEPT11 at the cell-cell junctions of epithelial cells (Sudo et al., 2007). In addition, septin filaments containing the SEPT9_i3 R88W and S93F mutants are no longer disrupted by Rho/Rhotekin signaling, which is the case for the wild type SEPT9_i3 (Sudo et al., 2007). Furthermore, the HNA associated 5' UTR mutation were found to dramatically enhance the

translational efficiency of the *SEPT9_v4*, leading to elevated expression of SEPT9_i4 under hypoxic conditions (McDade et al., 2007).

Septins and microtubules

The first observation of a septin-microtubule interaction was reported in *S. cerevisiae* by Pringle lab, by staining yeast septin, Cdc 11, with an affinity purified antibody (Ford and Pringle, 1991). However, it was regarded as an antibody cross reaction with other MAPs. It was not until a decade later when a potential association between septins and MTs was reported again. In 2002, the Barral lab showed that the yeast septin Cdc12 is required for shrinkage of mitotic MTs and their cortical capture (Kusch et al., 2002). Additional studies in sporulating yeast showed that Cdc10, Cdc11 and Spr28 colocalize with MTs during meiosis and before the formation of the prospore membrane (Pablo-Hernando et al., 2008).

Proteomic screens have shown that septins associate with MTs in insects and mammals. Six rat septins (SEPT2, SEPT3, SEPT6, SEPT7 and SEPT9) were found to associate with MTs (Sakamoto et al., 2008). *Drosophila* septin Peanut 2 and rat SEPT9_i3 cosedimented strongly with prepolymerized MTs in vitro (Sakamoto et al., 2008; Sisson et al., 2000). Colocalization of septins and MTs in mammalian cells by immunofluorescence has also been reported by different groups. For example, SEPT2 and SEPT6 colocalize with mitotic spindle MTs in MDCK and Hela cells, and SEPT9 also colocalizes with a subset of interphase and mitotic spindle MTs (Joberty et al., 2001; Martinez et al., 2006; Nagata et al., 2003; Spiliotis et al., 2008).

The mechanism of interaction between septins and MTs is unknown. The GTPase domain of SEPT9_i3 was reported to interact with MTs (Nagata et al., 2003). However, whether GTPase activity is involved in the interaction has never been studied. Some evidence including

the finding that SEPT2 colocalizes with polyglutamylated MTs suggests the involvement of the highly acidic tail of tubulins in the interaction with septins (Spiliotis et al., 2008).

Unlike other MAPs, septins associate with a subset of perinuclear MTs during interphase and part of the MT spindle during mitosis in epithelial cells (Bowen et al., 2011; Schmidt and Nichols, 2004; Spiliotis, 2010). The mechanism for MT selection is not clear, but some evidence suggests that tubulin PTMs might be involved as SEPT2 was shown to colocalize with polyglutamylated MTs in MDCKs (Spiliotis et al., 2008). Furthermore, MT association with septins is also dependent on septin isoforms. For example, SEPT9 isoforms have been shown to determine the MT dependent arrangement of septin complexes (Sellin et al., 2012). Association between septins and MTs is important for the filamentous structure of septins. Septin filaments that colocalize with MTs disassemble upon MT depolymerization with nocodazole (Martinez et al., 2006; Surka et al., 2002).

The regulatory effect of septins on MT structure and dynamics is still far from clear, but the importance of septins on MT PTMs, dynamics and organization has been shown by several studies. Knocking down of SEPT7 in Hela cells increases MT resistance to nocodazole-induced depolymerization and tubulin acetylation (Kremer et al., 2005). Conversely, depletion of SEPT9 decreases the polymerization of MTs without affecting tubulin expression (Nagata et al., 2003). In addition, SEPT2 RNAi has been shown to decrease the levels of MT polyglutamylation in MDCK cells (Spiliotis et al., 2008). Septins have been shown to suppress MT catastrophe and guide the directionality of MT plus end movement (Bowen et al., 2011). Depletion of SEPT2 disrupts the organization of peripheral MTs as well as the apicobasal positioning of MTs (Spiliotis et al., 2008). Finally, SEPT2/6/7 competes with MAP4 for MT binding and inhibits MAP4-induced MT bundling (Spiliotis et al., 2008). Knocking down of SEPT2, which down-regulates the expression levels of SEPT6 and SEPT7 (Silverman-Gavrila and Silverman-Gavrila,

2008) decreases MT bundles in MDCK cells (Bowen et al., 2011; Spiliotis, 2010). Despite this knowledge, further studies are needed to clarify the role of septins in MT organization and dynamics.

Septins are involved in the regulation of MT-dependent activities. In budding yeast, septin rings at the budding neck capture and stabilize astral MTs, which is essential to the positioning of mitotic spindles during cell division (Kusch et al., 2002). Mammalian SEPT1, SEPT2, SEPT6 and SEPT9 have been found on mitotic spindles and the midbody (Nagata et al., 2003; Qi et al., 2005; Spiliotis et al., 2005). Importantly, depletion of SEPT2, SEPT6 and SEPT7 increase the percentage of cells with abnormal nuclei, indicating their function in cell division (Kremer et al., 2005). In addition, SEPT2 was found to be juxtaposed to the kinetochores of metaphase chromosomes and is required for the proper alignment and segregation of chromosomes by regulating the localization of the centromere-associated protein E (CENP-E) (Spiliotis et al., 2005), which drives the movement of chromosomes toward the midplane of the cell (Cleveland et al., 2003). This effect is likely due to the direct interaction between the C-terminal domain of SEPT7 and C-terminal tail of CENP-E (Zhu et al., 2008). Because the C-terminal tail domain of CENP-E is involved in the autoinhibition of CENP-E, which can be relieved by phosphorylation, SEPT7 might promote the motility of CENP-E by acting as a scaffold for mitotic kinases such as Aurora kinase. Alternatively, SEPT7 may allosterically affect CENP-E association and MTs. In addition, overexpression of SEPT9_i1 in human mammary epithelial cells results in higher mitotic index and defects in cytokinesis (Gonzalez et al., 2007).

Finally, recent discoveries suggest that septins might also be involved in the regulation of MT-dependent vesicle transport. In neurons, SEPT3 concentrates in presynaptic terminals, colocalizing with synaptophysin. Moreover, SEPT3 is enriched in synaptosomes, which suggests that SEPT3 might be involved in synaptic vesicle recycling (Xue et al., 2004). SEPT2 knock

down and microinjection of SEPT2 antibody have been shown to impede the transport of Golgi-derived vesicles to the plasma membrane of polarizing epithelia cells (Spiliotis et al., 2008). In the sperm cells of Sept4 knockout mice, the localization of kinesins on flagellar axoneme is disrupted (Ihara et al., 2005). Furthermore, because septins interact with the Par1-related kinases (McMurray and Thorner, 2009), septins may regulate motor based transport through scaffolding the interaction of MAPs with MARK/Par1 kinase.

Figures:

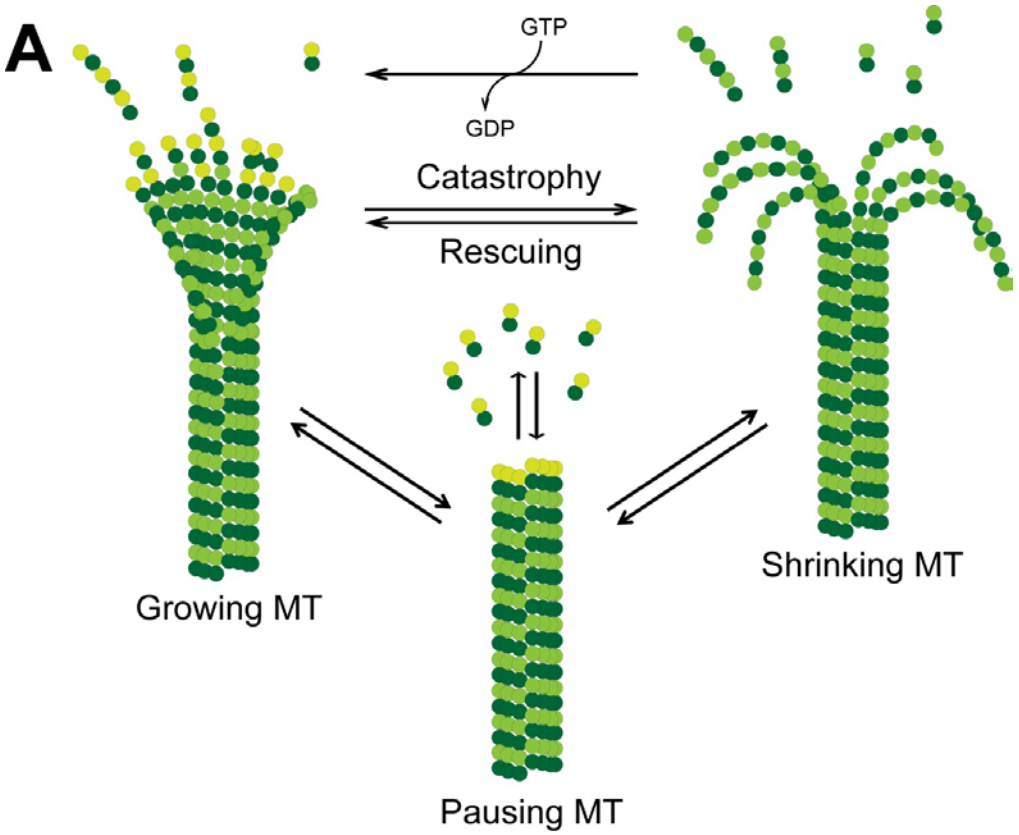
A
GTP
GDP
Catastrophy
Rescuing
Growing MT
Shrinking MT
Pausing MT

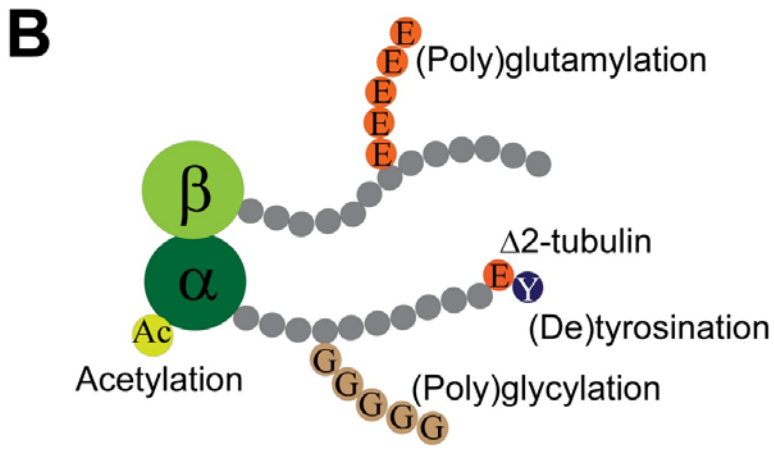
B
(Poly)glutamylation
β
α
Δ2-tubulin
(De)tyrosination
Ac
Acetylation
(Poly)glycylation

Figure 1.1. Dynamic instability of microtubules (MTs) and their post-translational modifications (PTMs)

(A) Dynamic instability of MTs.

(B) PTMs of MTs. Most of the modifications take place on the C-terminal tail of the tubulin monomers, except for acetylation that takes place on the N-terminal K40 amino acid of α-tubulin.

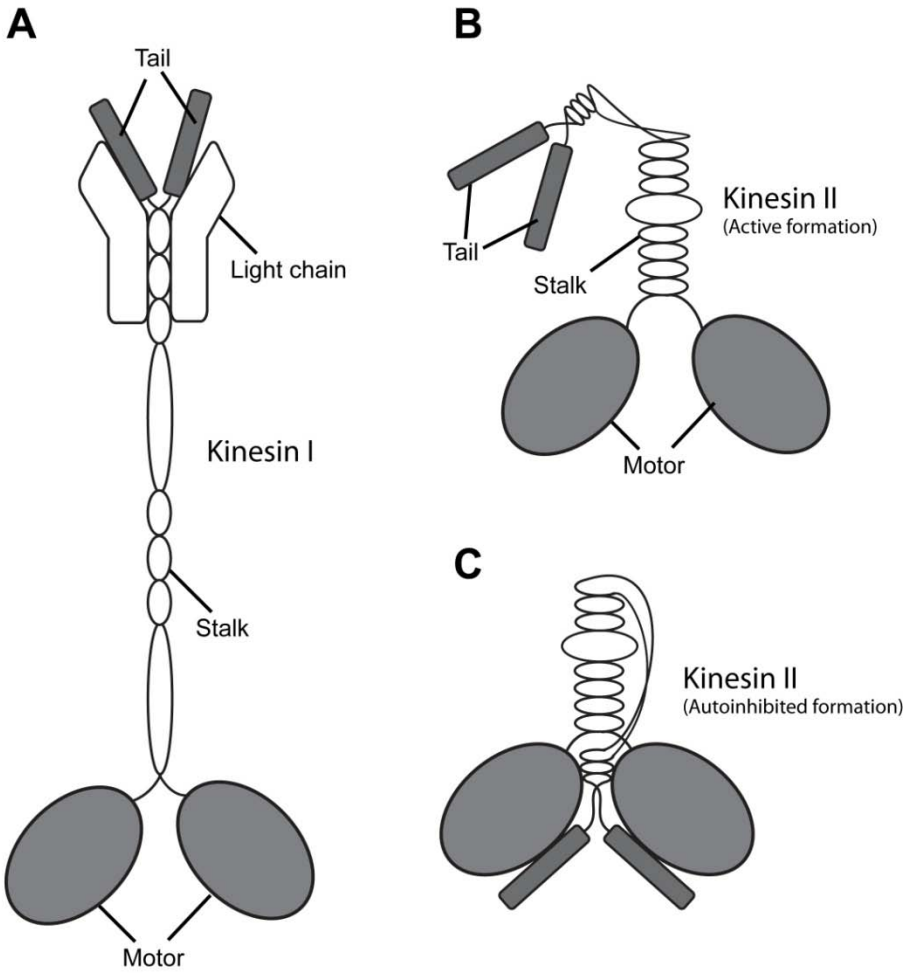

Figure 1.2. Structures of kinesin I and kinesin II motor proteins.

(A) Structure of Kinesin I.

(B) Structure of Kinesin II in its active formation.

(C) Structure of Kinesin II in its autoinhibited formation.

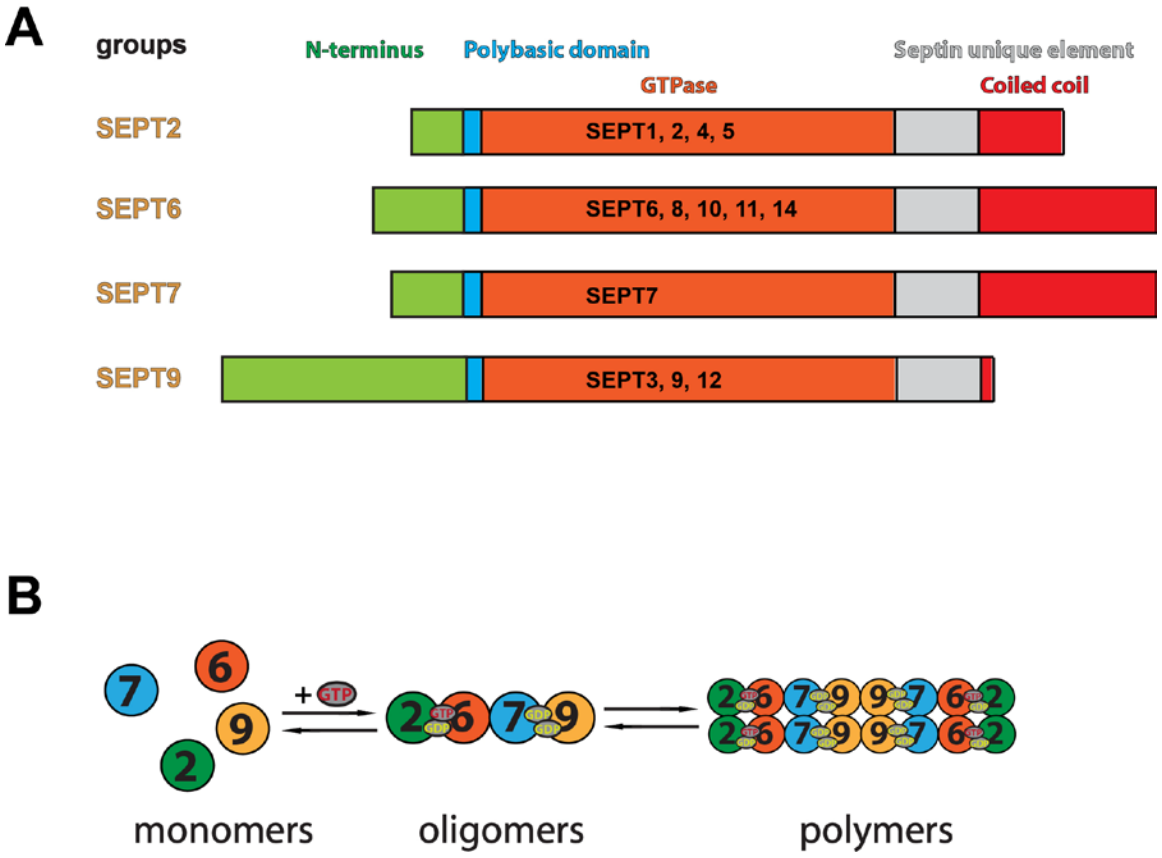

Figure 1.3. Human septin family.

(A) Human septins are categorized into four groups based on their sequence similarity.

(B) Septins can exist and transit among monomers, oligomers and polymers. The basic building block of septin filaments is a non-polarized octomer formed by SEPT2, SEPT6, SEPT7 and SEPT9.

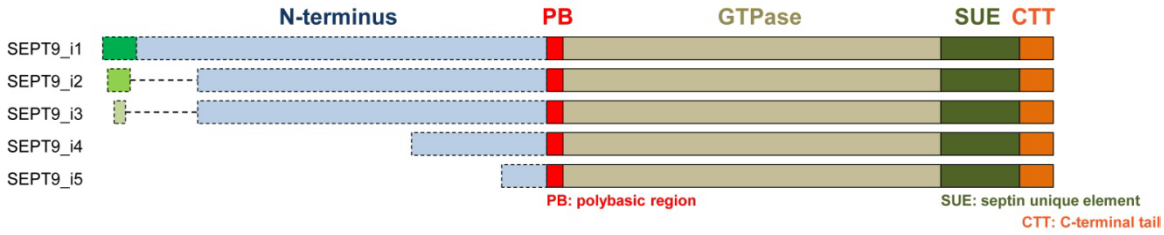

Figure 1.4. Isoforms of SEPT9.

Different domains of SEPT9 isoforms are labeled and marked in different colors. Regions at the N-terminals of SEPT9_i1, SEPT9_i2 and SEPT9_i3 N-terminus have different sequences. SEPT9_i4 and SEPT9_i5 differ from other isoforms only in the length of their N-terminus.

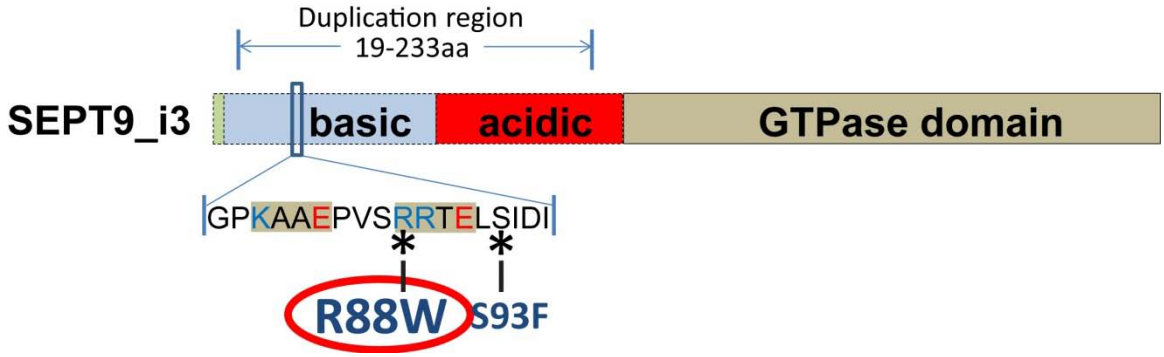

Figure 1.5. Genetic alternations of SEPT9 associated with HNA.

Alterations of SEPT9 sequence associated with HNA include duplications of amino acids 19-233, and the point mutations R88W and S93F of SEPT9_i3 N-terminus, with R88W to be the most frequently occurring mutation.

CHAPTER II: SEPT9 bundles MTs through novel repeat motifs mutated in HNA patients

Abstract

Septins are a family of GTP-binding proteins that form hetero-oligomeric complexes. These complexes can assemble into non-polar filamentous structures, and involve in multiple MT-dependent cellular processes such as mitosis and intracellular transport. In mammalian cells, septins are important in regulation of MT dynamics and post-translational modification. Septin depletion decreases MT bundling. However, the mechanism of septin-MT association and the regulatory role of septin in MT bundling is still elusive.

Here, I showed that SEPT9 binds and bundles MTs via a basic region in its N-terminal domain, which interacts with the acidic C-terminal tails of β-tubulin. Importantly, I showed that SEPT6/7/9 oligomers bundle MTs much more efficiently than SEPT2/6/7, indicating that SEPT9 is a key subunit for the bundling of MTs by septin complexes. Sequence analysis showed that the basic N-terminal domain of SEPT9 consists of the novel repeat motifs K/R-x-x-E/D and R/K-R-x-E. Alanine scanning mutagenesis reveals that the basic residues of these motifs interact with β-tubulin, while the acidic residues of K/R-x-x-E/D interact with the basic residues in R/K-R-x-E, enabling septin-septin interactions that join MTs together. I showed that lack of repeat motifs from truncated SEPT9 isoforms (e.g., SEPT9_i4) and the HNA-linked mutation R88W, which maps to the R/K-R-x-E motif, diminish intracellular MT bundling and impair asymmetric neurite outgrowth during nerve growth factor (NGF) - induced neuronal differentiation of PC12 cells. Thus, the SEPT9 repeat motifs bind and bundle MTs, and promote the development of neurite asymmetry during neuronal morphogenesis. My results provide the first insight into the mechanism of septin interaction with MTs and the molecular basis of HNA.

Introduction

The MT cytoskeleton is a highly dynamic structure and is important in cellular functions such as mitosis and polarization (Amos and Schlieper, 2005). The regulation of MT organization is mostly achieved through MT associated proteins (MAPs) (Dehmelt and Halpain, 2005). Post-translational modifications (PTMs) of tubulin are also involved in the regulation, which could further affect MT association of MAPs (Janke and Bulinski, 2011). Tau and MAP2 are two well-studied MAPs that induce MT bundling. Both of them have a C-terminal MT binding domain and a N-terminal domain that extend out from MTs, interacting with N-terminal domain of other MAPs, therefore mediate MT bundling (Dehmelt and Halpain, 2005).

Septins are a group of GTP-binding proteins that can oligomerize and polymerize into filamentous structures. It has been well accepted that SEPT2, SEPT6, SEPT7 and SEPT9 can oligomerize and form a non-polar octamer SEPT9-SEPT7-SEPT6-SEPT2-SEPT2-SEPT6-SEPT7-SEPT9, which can further oligomerize to form filaments (Beise and Trimble, 2011). Septins co-localize with a subset of peri-nuclear MT bundles and septin filaments dependent on MT cytoskeleton in some epithelial cells (Nagata et al., 2003). Septin knockdown decreases MT bundling in cells and disrupts septin organization (Spiliotis, 2010). However, how septins associate with MTs and how they mediate MT bundling are still elusive. Septin 9 (SEPT9) is a ubiquitously expressed septin subunit that caps the ends of septin heteromers (Fuchtbauer et al., 2011; Kim et al., 2011). Alternative splicing gives rise variable N and C termini, which differ in length and sequence, leading to the formation of 15 SEPT9 isoforms (Sellin et al., 2012), which may direct association of septin heteromers with MTs (Sellin et al., 2012). Missense mutations in the N-terminus of SEPT9 are genetically linked to hereditary neuralgic amyotrophy (HNA), an autosomal dominant peripheral neuropathy (Kuhlenbaumer et al., 2001). In HNA patients, a group of neurons named brachial plexus are affected and HNA patients suffer from severe pain

and atrophy of arm and shoulder muscle (Chance and Windebank, 1996). So far, only genetic alternation of *SEPT9* has been found to associate with this disease, but the mechanism of the disease development is still unclear.

Here I examined the interaction between septins and MTs and I found that SEPT9 is the strongest septin unit for MT binding. I identified some novel motifs in SEPT9 N-terminal domain that mediate MT binding and bundling. These motifs associate with asymmetric development of PC-12 neurites upon growth factor (NGF) treatment and may affect polarization of neurons. In addition, I found that the SEPT9_i3 R88W mutation, which is linked to HNA, decreases MT bundling both *in vitro* and *in vivo*. Finally, I showed that SEPT9_i3 R88W mutation affects the asymmetric neurite outgrowth of PC-12 cells, which provides the first clue about the possible cause of HNA.

Materials and methods

Cells, peptides, and plasmids

MDCK IIG cells were maintained in low glucose DME media (Sigma-Aldrich) supplemented with 10% FBS (Cell Generation) and 1 g/L NaHCO3. MDCK cells were transfected with the plasmids pEGFP-SEPT9_v1 and pEGFP-SEPT9_v4, which encode respectively for GFP-tagged SEPT9_i1 and SEPT9_i4, and were constructed by PCR amplification of SEPT9_v1 (AF189713) and SEPT9_v4 (AJ312322) from normal breast tissue cDNA and insertion into pEGFP-C2 (Connolly et al., 2011). PC-12 cells were maintained in high glucose DME supplemented with 6% donor-defined equine serum (Hyclone), 6% defined bovine calf serum (Hyclone), and 1 g/liter NaHCO3. PC-12 differentiation and neurite growth were induced after 24 h of transfection by incubation in low serum (1% horse serum, 1% bovine calf serum) DME containing 100 ng/ml 2.5S NGF (Harlan Biosciences). Embryonic fibroblasts derived from *Sept9*$^{cond/con}$ and *Sept9*$^{del/del}$ mice were provided by E. M. Füchtbauer (University of Aarhus, Aarhus, Denmark) and maintained in DME with 10% FBS as described previously (Fuchtbauer et al., 2011). Dermal cells were derived from skin biopsies taken from a healthy individual (control 1) and an HNA patient with the SEPT9_i3_R88W mutation (c.262C>T). Both subjects provided written informed consents and the biopsy protocol was approved by the University of Kiel ethics committee. Under local anesthesia, a standard skin-biopsy punch (diameter 3 mm; Kai Industries) was used to take a skin sample from the extensor surface of the upper arm. After removal of the subcutaneous fatty tissue, skin explants were cultured in high glucose DME media with 20% FBS for 5 - 7 d. Skin fibroblasts that grew out of the explants were isolated and passaged. Experiments with R88W and control 1 fibroblasts were performed at passages 7 - 11 and 9 - 13, respectively. The peptides NH2-CEVGVDSVEGEGEEEGEEY-COOH (α-tubulin CTT), NH2-CQETAEEYQDEEQGEADAEDFG-COOH (control, scrambled

βII-tubulin CTT), and NH2-CQYQDATAEEEEDFGEEAEEEA-COOH (βI tubulin CTT) were purchased at >95% purity from GenScript. The peptides NH2-CQYQDATADEQGEFEEEEGED EA-COOH (βII-tubulin CTT) and NH2-CQYQDATAEEEGEMYEDDEEESEAQGPK-COOH (βIII-tubulin CTT) were purchased at >95% purity from LifeTein, LLC.

His-SEPT9_i1-expressing plasmid was constructed by PCR amplifying human SEPT9_i1 (NP_001106963) using the primers 5 -CGTAAGCTTGCATGAAGAAGTCTTACTC-3′ and 5′-GTACTCGAGCTACATCTCTGGGGC-3′ and cloning the amplified fragment into the HindIII and XhoI sites of pET-28a(+). His-GFP-SEPT9_i1-expressing plasmid was constructed by PCR amplifying GFP-SEPT9_i1 from pEGFP-C2-SEPT9_v1 (see above) using the primers 5 -TCGAAGCTTCCATGGTGAGCAAGGGC-3′ and 5′-GTACTCGAGCTACATCTCTGGGGC-3′ and inserting the fragment into the HindIII and XhoI sites of pET-28a(+). His-SEPT9_i3-expressing plasmid was made by PCR amplifying human SEPT9_v3 (NP_006631) using the primers 5′-CATGCTAGCATGGAGAGGGACCGG-3′ and 5′-ACTAAGCTTTTACATCTCTGG GGC-3′ and cloning the amplified fragment into the NheI and HindIII sites of pET-28a(+). His-GFP-SEPT2-expressing plasmid was constructed by PCR amplifying human GFP-SEPT2 (NP_006146) from pEGFP-C1-SEPT2 using primers 5′-TCGGGATCCATGGTGAGCAAGGGC -3′ and 5′-TCGAAGCTTTCACACATGCTGCCCGAG-3′ and cloning the amplified fragment into the BamHI and HindIII sites of pET-28a(+). Plasmids expressing His-tagged SEPT9-N (aa 1-283 of SEPT9_i1), SEPT9-B (aa 1-142 of SEPT9_i1), SEPT9-A (aa 143-283 of SEPT9_i1), SEPT9-G (aa 284-586 of SEPT9_i1), SEPT9_i3 (R88W), SEPT9_i1(61-113), and its mutants were made with the QuikChange II Site-Directed Mutagenesis kit (Agilent Technologies) using the pET-SEPT9_v1 and pET-SEPT9_v3 plasmids. pGEX-SEPT9-N- and pGEX-SEPT9-G-expressing GST-tagged SEPT9-N and SEPT9-G were constructed by PCR amplifying SEPT9-N and SEPT9-G and inserting into HindIII and XhoI sites of pGEX-KT-ext.

For the bacterial expression of septin heterotrimers, the bicistronic plasmid SEPT6-H-SEPT7 was constructed for the simultaneous expression of non-tagged (NT) SEPT6 and His-tagged SEPT7. First, His-SEPT7 expressing plasmid was constructed by PCR amplifying the rat SEPT7 transcript variant 2 (NM 0011137.4) using the primer 5′-TCGGGATCCATGTCGGTCA GTGCG-3′ and 5′-GTAAAGCTTTTAAAAGATCTTGCC-3′ and cloning the amplified fragment into the BamHI and HindIII sites of pET-28a(+). Second, a His-tagged SEPT6 was constructed by PCR amplifying the human SEPT6_v3 (NP_665798) using the primer 5′-TCGGGATCCATG GCAGCGACCGATATAG-3′ and 5′-TCGAAGCTTTTAATTTTTCTTCTC-3′ and the amplified fragment was inserted into the BamHI and HindIII sites of pET-28a(+). Using the QuikChange II Site-Directed Mutagenesis kit, this plasmid was modified by removing the His tag in front of SEPT6 and inserting a SpeI site in front of the stop codon of SEPT6. Subsequently, the SEPT7 gene and the upstream ribosome-binding site were excised from pET-His-SEPT7 by digesting with XbaI and HindIII, and the fragment was subcloned into the SpeI and HindIII sites of the modified pET-SEPT6 to create a SEPT6-His-SEPT7-expressing plasmid. The plasmids encoding for NT-SEPT2 and NT-SEPT9_i1 were made from pET plasmids expressing His-SEPT9 (see above) and His-SEPT2, which was constructed by PCR amplifying mouse SEPT2 (NP_006146) using the primer 5′-TCGGGATCCATGTCTAAGCAACAACC-3′ and 5′-ATCCTCGAGTCACA CATGCTGCCCG-3′ and cloning into the BamHI and XhoI sites of pET-28a(+). The His-SEPT9 and His-SEPT2 sequences and their upstream ribosome binding sites were then excised using XbaI and XhoI, and subcloned into pET-15b, which contains an ampicillin resistance marker. His tag sequences were then truncated with the QuikChange II Site-Directed Mutagenesis kit to create NT-SEPT2-and NT-SEPT9_i1- expressing plasmids.

Expression and purification of recombinant proteins

Plasmids encoding for recombinant proteins were transformed into *Escherichia coli* BL21(DE3) (Invitrogen). After bacterial cultures reached an OD600 of 0.8, protein expression was induced with 0.5 mM IPTG for 16 h at 18°C. Bacteria were centrifuged at 5,000 rpm for 5 min at 4°C. Pellets were resuspended in buffer containing 1% Triton X-100, 50 mM Tris, pH 8.0, 150 mM NaCl, 10% glycerol, and 10 mM imidazole, and lysed using a French pressure cell (1,280 psi). Cell lysates were clarified by centrifuging at 14,000 *g* for 30 min at 4°C. Supernatants were loaded on columns containing 500 µl Ni-NTA beads (QIAGEN). Columns were washed with 10 ml washing buffer (50 mM Tris, pH 8, 300 mM NaCl, 10% glycerol, and 10 mM imidazole). Proteins were eluted with elution buffer (50 mM Tris, pH 8, 300 mM NaCl, 10% glycerol, and 250 mM imidazole) and dialyzed overnight in buffer containing 50 mM Tris, pH 8.0, 150 mM NaCl, and 10% glycerol. The heterotrimeric complexes SEPT2/6/7 and SEPT6/7/9_i1 were purified from *E. coli* BL21(DE3) by co-transforming the pET-28a(+) plasmid encoding for SEPT6-H-SEPT7 and the pET-15b plasmid encoding for NT-SEPT2 or NT-SEPT9_i1. The bacteria were selected on LB plates containing both kanamycin and ampicillin. The heterotrimeric complexes were purified using a Ni-NTA column. GST-tagged proteins were purified by lysing bacteria in GST binding buffer (25 mM Tris HCl, pH 7.5, 150 mM NaCl, 1 mM EDTA, and 0.5% Trition X-100) using a French press. Supernatants were clarified by centrifuging at 14,000 *g* for 30 min at 4°C and loaded on columns containing 500 µl Protino glutathione agarose 4B beads (Macherey Nagel). Columns were extensively washed with GST binding buffer and eluted with elution buffer (25 mM Tris HCl, pH 7.5, 150 mM NaCl, 5% glycerol, and 50 mM glutathione) and dialyzed overnight.

High and low speed MT cosedimentation and protein binding assays

Bovine brain tubulin (10 µM; >99% pure; Cytoskeleton, Inc.) was polymerized in G-PEM (80 mM Pipes, pH 6.9, 1 mM EGTA, 1 mM MgCl2, 1 mM GTP, and 10% glycerol) plus 80 µM paclitaxel for 30 min at 37°C. Subtilisin-cleaved MTs (S-MTs) were prepared by incubating pre-polymerized MTs with 30 µg/ml subtilisin (Sigma-Aldrich) at 37°C for 3 h. The reaction was terminated by addition of 2 mM PMSF. S-MTs were pelleted at 16,000*g* on a cushion buffer (80 mM K-Pipes, pH 6.9, 1 mM MgCl2, 1 mM EGTA, 60% glycerol, and 20 µM paclitaxel) for 10 min at room temperature and then resuspended in 20 µl G-PEM with 20 µM paclitaxel. S-MTs were obtained from the supernatant fraction after re-centrifugation on 40 µl of cushion buffer at 12,000 *g* for 5 min. In high speed sedimentation assays, untreated, mock-, or subtilisin-treated MTs were incubated with recombinant SEPT9 proteins (10 µM) or SEPT9(61 - 113) peptides (30 µM) for 20 min at room temperature. Each reaction was placed on cushion buffer and centrifuged at 39,000*g* (high speed) for 20 min at 25°C in an ultracentrifuge (Optima TL100; Beckman Coulter). In low speed sedimentation assays, MTs were incubated with recombinant SEPT9 proteins (2 µM), SEPT9(61 - 113) peptides (30 µM), or SEPT2/6/7, SEPT6/7/9_i1 complexes and SEPT9_i1 (0.2 µM; Figure 2.5 E and F) for 10 min at room temperature. Each reaction was placed on cushion buffer and centrifuged at 8,000 *g* for 5 min. Pellets were resuspended in PBS of the same volume with the supernatants. Equal volumes of pellet and supernatant were loaded onto 10% SDS-PAGE and gels were stained with Coomassie Brilliant Blue. Gels were scanned and protein band densities were quantified with the Odyssey infrared scanning system (LI-COR Biosciences).

Binding assays between GST- and His-tagged proteins were performed (Figure 2.10 F and G) by incubating 25 µg of purified GST-SEPT9-N or GST-SEPT9-G with 20 µl glutathione agarose 4B beads for 15 min. After washing three times with GST binding buffer, beads were

incubated with 20 µg His-SEPT2, His-SEPT9, His-SEPT9-N, or His-SEPT9-G for 1.5 h. Beads were washed with GST binding buffer five times before resuspended with loading buffer and boiled. Samples were loaded into 10% SDS-PAGE gels and stained with Coomassie Brilliant Blue.

Visualization of MT bundling by fluorescence and electron microscopy

X-rhodamine-labeled bovine brain tubulin (10 µM; Cytoskeleton, Inc.) was polymerized in G-PEM buffer containing 80 µM paclitaxel. MTs were incubated with recombinant proteins (20 nM) in G-PEM buffer containing 20 µM paclitaxel for 10 min at room temperature. An aliquot (5 µl) of each reaction mix was mounted on a slide and sealed with a glass coverslip and nail polish. Slides were imaged on a fluorescent microscope (Axio Observer; Carl Zeiss) equipped with a Plan-Apo 63×/1.40 NA objective, a deep-cooled CCD camera (ORCA-AG; Hamamatsu Photonics), and Slidebook 5.0 software (Intelligent Imaging Innovations). All images were taken in the TRITC channel at 50-ms exposures. MT lengths and intensities were quantified by masking individual MTs (>5 µm). MT length and average fluorescence intensity per pixel after background subtraction were measured using Slidebook 5.0 software.

For visualization of MT bundling by negative stain electron microscopy, pre-polymerized MTs (Cytoskeleton, Inc.) were mixed with recombinant SEPT9-FL and incubated with glow-discharged 300 mesh Holey carbon copper grids covered with a thin layer of carbon. Grids were washed with 2% uranyl formate and subsequently blotted and air dried. Images were collected with a transmission electron microscope (Tecnai T12; FEI) equipped with a CCD camera (UltraScan 4000; Gatan, Inc.) operating at accelerating voltage of 120 kV, defocus value of - 950 nm, and magnification of 52,000.

Western blots and overlay assays

Bovine brain tubulin (>99% pure; Cytoskeleton, Inc.) was separated by 7.5% SDS-PAGE and transferred to PROTRAN B85 nitrocellulose membranes (Whatman), which were stained with Ponceau S (Sigma-Aldrich) and scanned with a CanoScan LiDE 210 (Canon). After extensive wash with ddH2O, membranes were blotted with mouse antibody DM1A against α-tubulin (1:100,000; Sigma-Aldrich) or TUB2.1 antibody against β-tubulin (1:100,000; Sigma-Aldrich), and secondary Alexa Fluor 680 goat anti–mouse IgG (1:15,000; Invitrogen). For blot overlay assays, membranes were incubated for 1 h at 4°C in blocking buffer (10 mM Tris HCl, pH 6.8, 150 mM NaCl, 1 mM DTT, 0.1% Tween 20, 5% nonfat dry milk, and 0.5% BSA). Subsequently, membranes were overlayed with His-SEPT9_i1 (200 nM) in blocking buffer for 2 h. Membranes were washed with TBS containing 0.1% Tween 20 and incubated in the same buffer containing 2% BSA and mouse antibody against 6×His tag (1:5,000; R&D Systems) followed by secondary Alexa Fluor 680 goat anti–mouse IgG (1:15,000; Invitrogen). Blots were imaged with the Odyssey infrared imaging system (LI-COR Biosciences).

Immunofluorescence microscopy and image analysis

Cells (MDCK and skin fibroblasts) treated with paclitaxel (Sigma-Aldrich) or carrier (DMSO; Sigma-Aldrich) were fixed with PHEM buffer (60 mM Pipes-KOH, pH 6.9, 25 mM Hepes, 10 mM EGTA, and 2 mM MgCl2) containing 3% paraformaldehyde (Electron Microscopy Sciences), 0.05% glutaraldehyde (Electron Microscopy Sciences), and 0.5% Triton X-100. MTs were stained with mouse antibody DM1A against α-tubulin (Sigma-Aldrich) and donkey DyLight 594-conjugated F(ab') 2 to mouse IgG (Jackson ImmunoResearch Laboratories, Inc.). Samples were mounted with FluorSave (EMD Millipore) and imaged on a laser-scanning confocal microscope (FluoView 1000; Olympus) using a Plan Apochromat 60×/1.42 NA

objective. Serial optical sections were acquired from the bottom to the top of each cell at 0.2-µm steps. Each z-stack was imported into Slidebook 5.0 software for colocalization and MT fluorescence analyses. Background fluorescence was removed and fluorescence intensity segmentation was used to mask MTs and septin filaments, and colocalization values were automatically calculated using the Manders algorithm of the Slidebook 5.0 software. To determine the fraction of MT bundles relative to total MTs, we first measured the mean fluorescence intensity per pixel for the dimmest single MTs found in the periphery of each cell. Subsequently, MTs and MT regions with pixel values over 5 or 10 times the single MT pixel value were masked. The sum fluorescent intensity of these putative MT bundles was calculated as a fraction of the total MT fluorescence intensity in a 3D stack of images using Slidebook 5.0 software.

PC-12 cells were fixed with PHEM buffer (60 mM Pipes-KOH, pH 6.9, 25 mM Hepes, 10 mM EDTA, and 2 mM MgCl2) containing 3% paraformaldehyde (Electron Microscopy Sciences) and 5% sucrose. Cells were permeabilized with 0.5% Triton X-100 and stained for α-tubulin and imaged on a fluorescent microscope (Axio Observer; Carl Zeiss) equipped with a Plan-Apo 63×/1.40 NA objective, a deep-cooled CCD camera (ORCA-AG; Hamamatsu Photonics), and Slidebook 5.0 software. MT-positive protrusions with lengths longer than the diameter of the cell soma were scored as neurites.

Statistical analysis and prediction of intrinsic disorder

Datasets were plotted in box-and-whisker diagrams. The bold horizontal line marks the median value and the bottom and top of each box corresponds respectively to the 25th (Q1) and 75th (Q3) percentiles of the range of values shown. Whisker ends correspond to the minimum and maximum values of each dataset. Values 1.5 times more than the Q3 value or 1.5 times less than

the Q1 value were considered statistical outliers and were plotted outside the whisker portions of the diagram. Kolmogorov-Smirnov tests were performed to assess the normal distribution of each dataset and unpaired Student's *t* tests were used to derive P-values for normally distributed datasets with equal standard deviations (SDs). The Welch *t* test was used to compare datasets with unequal SDs and the Mann-Whitney test was used to compare datasets, which were not normally distributed.

The prediction of intrinsic disorder of SEPT9_i1 was performed by combining results from GlobProt (http://globplot.embl.de), DisEMBL (http://dis.embl.de), DISOPRED2 (http://bioinf.cs.ucl.ac.uk/psipred/?disopred=1), IUPred (http://iupred. enzim.hu), DISpro (http://www.ics.uci.edu/~baldig/dispro.html), OnD-CRF (http://babel. ucmp.umu.se/ond-crf/), and DRIP-PRD (http://www.sbc.su.se/~maccallr/disorder). The predicted intrinsic disorder of every amino acid was set to 1 or 0 for values that were above or below the intrinsic disorder cut-off points of each algorithm (Seeger et al., 2012).

Results

Basic region in SEPT9 N-terminus interacts with C-terminal tail of β-tubulin directly

The basic building block of septin filaments consists of SEPT2, SEPT6, SEPT7 and SEPT9, but it was debated regarding whether any of them interact with MTs directly. To test this, I expressed His-GFP-tagged SEPT2, SEPT6, SEPT7 and SEPT9_i1 in bacteria, purified them, and mixed each one of them with pre-polymerized Rhodamine-labeled MTs *in vitro*. SEPT2 did not show obvious MT binding, compared with SEPT6, which binds MTs weakly. In contrast, SEPT7 and SEPT9_i1 bound MTs strongly, with SEPT9_i1 being the strongest MT binding unit. It was also obvious that SEPT7 and SEPT9_i1 can induce the formation of long, thick and bright MT filaments (Figure 2.1), suggesting they can also bundle MTs. Because SEPT9 binds MTs best and it is also genetically associated with hereditary neurogical amyotrophy (HNA), an autosomal dominant neuropathy, I focused my study on SEPT9. From this point on, SEPT9_i1 will be referred to as SEPT9 unless otherwise specified.

To determine how SEPT9 interacts with MTs, I thought to identify the SEPT9 domains that are involved in SEPT9-MTs binding using *in vitro* assays. SEPT9 comprises a long N-terminus, which contains almost the same number of amino acids as the GTPase domain. The first half of SEPT9 N-terminus (aa 1-142) is very basic (pI=10.9) and therefore will be referred to as "basic region". On the other hand, the second half (aa 143-283) of SEPT9 N-terminus is very acid (pI=5.1), and therefore will be referred to as "acidic region" (Figure 2.3 A). I purified the full length, N-terminal domain, basic, acidic region of N-terminal domain and the GTPase domain, and performed high speed MT co-sedimentation assays. Full length SEPT9 co-sedimented with MTs and the Kd was found to be 3.2 μM (Figure 2.2 A). The N-terminus of SEPT9 bound MTs similarly to the full length SEPT9 (Figure 2.4 A, B and I). In contrast, the SEPT9 GTPase domain did not show obvious MT binding (Figure 2.4 C and I). In the N-terminal domain of SEPT9, the

basic region bound MTs and the acidic region did not (Figure 2.4 D, E and I). These results suggested that it is the basic region in SETP9 N-terminus that mediate MT binding of SEPT9.

To examine which SEPT9 fragment induces MT bundling, I used low speed MT co-sedimentation and visual assays to test MT bundling of each purified SEPT9 fragment. Full length SEPT9 (SEPT9-FL), the N-terminal domain (SEPT9-N) and basic region (SEPT9-G) increased MT sedimentation, while the GTPase domain (SEPT9-G) and acidic region (SEPT9-A) had no obvious effect (Figure 2.4 F- H and J), which was in agreement with the low speed co-sedimentation assay results. Mixing SEPT9 fragments with pre-polymerized Rhodamine-labeled MTs showed that SEPT9-FL, SEPT9-N and SEPT9-B can induce formation of long, thick and bright MT bundles, while SEPT9-G and SEPT9-A could not (Figure 2.5 A-C). Both of the tests therefore suggested that it is the basic region in N-terminus of SEPT9 that mediate MT bundling. MT bundling mediated by SEPT9 was also confirmed with negative stain electron microscopy, which showed that SEPT9 can mediate the formation of MT bundles, in which MTs are in close contact (Figure 2.5 D). Since all MTs used in the above assays were stabilized with paclitaxel (Taxol), which might have an effect on MT-SEPT9 interaction, I repeated the MT-binding assays with fluorescent MTs stabilized with nonhydrolyzable GTP analogue GMPCPP. These MTs were also decorated and bundled by His-GFP-tagged SEPT9 (Figure 2.2 B). All of these support my conclusion that basic region in SEPT9 N-terminus mediates SEPT9-MT binding and MT bundling.

SEPT9 forms hetero-oligomeric complexes with other septin subunits, therefore the ability of MT bundling induced by septin heteromer formed by SEPT6, SEPT7 and SEPT9 was tested using low speed MT co-sedimentation assay, which was compared with SEPT9 alone or septin heteromer formed by SEPT2, SEPT6 and SEPT7. The result showed that heteromers formed by SEPT6, SEPT7, SEPT9 was able to induce MT bundling at concentration of 0.2 μM,

at which neither SEPT9 alone nor septin heteromers formed by SEPT2, SEPT6 and SEPT7 were able to bundle MTs (Figure 2.5 E and F), suggesting SEPT9 is indeed a key subunit of septin complexes to induce MT bundling.

MTs comprise α- and β-tubulin. To determine whether SEPT9 binds α- or β-tubulin, I separated α- and β-tubulin into two distinct bands in a 7.5% SDS-PAGE mini-gel (Figure 2.7 A). Western blotting with antibody specifically recognizes α- and β-tubulin confirmed that the top band being α-tubulin and the bottom band being β-tubulin (Figure 2.7 A). I performed blot overlay assay with purified His-tagged SEPT9 and it was clear that SEPT9 preferentially interacted with β-tubulin. I used His-tagged SEPT2 as a control to perform the same assay, and SEPT2 did not show any observable binding to either band (Figure 2.7 A), as expected.

Electrostatic interactions between MTs and many MT associated proteins (MAPs) or kinesin motors involve the highly acidic C-terminal tail of tubulin and basic regions of MAPs or motors (Marx et al., 2006). Since the SEPT9 basic domain directly interacts with MTs, I hypothesized that the tubulin C-terminal tail may also mediate SEPT9-MT interaction. Consistent with this possibility, MT bundling by SEPT9 was attenuated by increasing ionic strength (Figure 2.2 C). I therefore tested this hypothesis by performing MT co-sedimentation assay and visual bundling assay with polymerized MTs treated with subtilisin, a serine protease originally obtained from *Bacillus subtillis* that can specifically cleave C-terminal tail of tubulins. Co-sedimentation assay showed that SEPT9 pelleted by subtilisin treated MTs was significantly less than mock treated MTs (Figure 2.6 A). In a bundling assay, both the length and intensity of MT bundles induced by SEPT9 were significantly less for the subtilisin treated MTs compared with the mock treated ones (Figure 2.6 B, C and D).

These results suggested that SEPT9 preferentially interacts with the C-terminal tail of β-tubulin. To further test this hypothesis, I performed SEPT9 blot overlay assay on tubulin of mock

or subtilisin treated MTs separated in 7.5% SDS-PAGE gel. Subtilisin treatment led to the decrease of SEPT9 overlay on β- tubulin band (Figure 2.6 E). Next, I performed SEPT9-MTs co-sedimentation assay in the presence of synthesized peptides, whose sequence correspond to C-terminal tail of α-tubulin, βII-tubulin and a scrambled sequence of βII-tubulin C-terminal tail. Peptide corresponding to the sequence of βII-tubulin C-terminal tail, but not the α-tubulin or scramble sequence, induced a decrease in SEPT9 sedimentation by MTs in a dose dependent manner (Figure 2.7 B and C), indicating that the C-terminal tail of β-tubulin is involved in MT binding and bundling by SEPT9. β-tubulin has multiple isoforms, which varies mostly in the C-terminal tail, therefore it is possible that different β-tubulin isoforms have different SEPT9 binding abilities. Thus I tested how synthetic peptides corresponding to C-terminal tail of βI- and βIII-tubulin MT-septin binding. βI-and βIII-tubulin did not affect MT co-sedimentation of SEPT9 (Figure 2.8 A and B). Based on these data, I concluded that interaction between basic region of SEPT9 N-terminus and βII- tubulin plays a fundamental role in SEPT9-MT binding and bundling.

Novel charged repeat motifs K/R-x-x-E/D and K/R-R-x-E in SEPT9 are involved in MT binding and bundling by SEPT9

To further determine the mechanism of SEPT9-MT interaction, I examined how SEPT9 contains MT binding motifs reported in MAPs, MT plus-end tracking proteins and kinesin motors in unstructured SEPT9 N-terminus (Figure 2.3 B). Though I was not able to identify any known MT binding motifs, I found eleven tetrapeptide motifs K/R-x-x-E/D and six K/R-R-x-E repeat motifs in the N-terminus of SEPT9_i1, which are often flanked by proline or serine residues (Figure 2.9 A). These repeats will be referred as monobasic repeats and dibasic repeats respectively. By truncating basic region in SEPT9 N-terminus, I found a minimum region that can

autonomously bind and bundle MTs, aa 61-113, which contains multiple tetrapeptide motifs (Figure 2.9 C-E).

I set out to determine the role of these repeat motifs in MT binding and bundling through MT co-sedimentation assays. This sequence contains two regions of repeat motifs. The first region, which will be referred to as "R1" thereafter, contains three monobasic repeat motifs. The second region, which will be referred to as "R2", contains one monobasic repeat motif flanked by two dibasic repeat motifs (Figure 2.9 B). Neither R1 nor R2 was able to bind or bundle MTs by themselves. Charged amino acids in this sequence were substituted with Alanines to elucidate their role in MT binding and bundling. Through high speed co-sedimentation assays, I showed that mutation of more than one basic residues in either R1 or R2 resulted in significant decreases in MT binding, suggesting all of the basic residues in these motifs are involved in MT binding (Figure 2.9 F, G and J). I then used low speed co-sedimentation assay to assess the effect of the same mutations in MT bundling. Strikingly, substitution of basic residues of the R-R-x-E motifs in R2 into alanines decreased MT bundling, but mutating basic residues in R1 did not decrease MT bundling by the peptide (Figure 2.9 H, I and K). These data suggested that although basic residues in all repeat motifs are involved in MT binding, only arginines of R-R-x-E in R2 are uniquely critical in MT bundling.

Next, I analyzed the role of acidic residues in these repeats. Mutation of more than one acidic residues in either R1 or R2 led to slight increase of MT binding by SEPT9 (Figure 2.10 A and C), which is likely due to the repulsive effect of these acidic residues to the highly acidic tubulin C-terminal tails. I then assessed the role of these residues in MT bundling. Surprisingly, mutating acidic residues in two of the K/R-x-x-E/D motifs in R1 decreased MT bundling, but alanine substitution of glutamates in the R-R-x-E motifs of the R2 only resulted in a marginal

decrease of MT bundling (Figure 2.10 B and D). These data suggested the acidic residues of the K/R-x-x-E/D motifs in R1 are uniquely critical for MT bundling.

Based on these data, I proposed that the acidic residues in K/R-x-x-E/D of R1 motifs interact with extra arginines in R-R-x-E of R2 repeat motifs, mediating homophilic trans-interaction between aa 61-113 of SEPT9. Additional interaction between C-terminal tail of βII-tubulin and basic residues of the repeat motifs therefore leads to cross linking and bundling of MTs (Figure 2.10 E). Consistent with this model, GST-tagged SEPT9 N-terminus was shown to directly interact with His-tagged SEPT9 N-terminus and full length SEPT9 (Figure 2.10 F and G), supporting the hypothesis that the N-terminus of SEPT9 mediates homophilic interaction between SEPT9 proteins.

SEPT9 repeat motifs are important in intracellular MT bundling and asymmetric neurite growth

My results show that repeat motifs identified in the SEPT9 N-terminus are involved in SEPT9-MT binding and SEPT9 mediated MT bundling *in vitro*, but their role in intracellular MT bundling is unknown. As stated in the introduction section, SEPT9 has multiple isoforms. Among which, SEPT9_i4 lacks aa 1-164 of SEPT9_i1, which includes the entire basic region of SEPT9 N-terminus, and most of the repeat motifs. Therefore I hypothesized that SEPT9_i4 overexpression would affect intracellular MT bundling and the physiological function of SEPT9_i1. To test this hypothesis, I overexpressed GFP-tagged SEPT9_i1 and SEPT9_i4 in MDCK cells, in which septins were previously shown to colocalize with a subset of MTs. GFP-tagged SEPT9_i1 colocalized strongly with peri-nuclear MTs, whereas SEPT9_i4 distributed as short fibers at the cell periphery and failed to colocalize with MTs (Figure 2.11 A). To assess the effect of SEPT9_i1 and SEPT9_i4 on inducing MT bundles, I defined MT bundles as MTs with

intensity of more than five times the average intensity of single MTs at the cell periphery. Using a segmentation analysis on 3D confocal image stacks as published previously (Bowen et al., 2011), the percentages of MT bundles over total MT intensity were shown to be significantly higher in SEPT9_i1 overexpressed cells compared with those that have SEPT9_i4 overexpression (Figure 2.11 A, C and D). Treating cells with paclitaxel, a MT stabilizing drug, resulted in the formation of thick MT bundles and stronger MT colocalization of SEPT9_i1, but SEPT9_i4 still showed very little colocalization with MTs (Figure 2.11 B and C). MT bundles of five or ten times intensity of the average single MTs was also much higher in SEPT9_i1 overexpressed cells than those with SEPT9_i4 overexpression (Figure 2.11 E). These data suggested that the SEPT9 repeat motifs are indeed important in intracellular MT bundling. In fibroblasts isolated from *Sept9* knockout mice, the percentage of MT bundles was also lower compared with those isolated from healthy control mice at steady state or upon treatment with paclitaxel (Figure 2.12). These results further stressed the critical role of SEPT9 in intracellular MT organization.

MT bundling mediated by MAPs like tau and MPA1B is required for neuronal development and morphogenesis (Sapir et al., 2012; Teng et al., 2001), in particular, MAPs promote the asymmetric growth of a neuron processes termed neurites; one neurite grows faster and longer and becomes the axon. To determine if SEPT9 and its repeat motifs mediated MT bundling are involved in this process, I assayed for nerve growth factor (NGF)-induced neurite formation in PC-12 cells. Upon NGF treatment for two and three days, the percentage of PC-12 cells with a single neurite in SEPT9_i1 overexpressing cells were significantly higher than cells that overexpress GFP (Figure 2.13). In contrast, SEPT9_i4 overexpression induced the opposite effect (Figure 2.13), increasing the percentage of cells having more than three neurites upon two and three days of NGF treatment. The percentage of cells contain a single neurite upon three days of NGF treatment was also significantly less in SEPT9_i4 overexpressed cells than the control

(Figure 2.13). In addition, the average length of neurites in SEPT9_i1 overexpressed cells was less than the average length of single neurites (2.3 vs. 3.3 times of the cell width). These results support the hypothesis that MT bundling mediated by K/R-R/x-x-E/D repeat motifs within SEPT9 N-terminus promote asymmetric neurite growth.

SEPT9 mutations associated with HNA impairs MT bundling and neurite asymmetric growth

SEPT9 is so far the only gene identified to associate with the development of hereditary neurological amyotrophy (HNA), but its molecular etiology is still unknown. Among the genetic alternations that lead to HNA, R88W and S93F mutations of SEPT9_i3 are two that alter the SEPT9 sequence. R88W is the most dominant form of mutation in HNA patient and maps to the first arginine of the K/R-R-x-E motif. To determine if this mutation affects MT binding or bundling properties of SEPT9_i3, MT co-sedimentation assays were performed. While this mutation did not affect MT binding by SEPT9_i3 (Figure 2.14 A and C), as shown by high speed co-sedimentation assay, it significantly decreased MT bundling by SEPT9_i3, as shown by the result of low-speed MT co-sedimentation assay (Figure 2.14 B and D). In fluorescent MT-bundling assays, R88W also decreased intensity and length of MT bundles induced by SEPT9_i3 (Figure 2.14 E-G). To determine whether this mutation affect MT bundling in cells, I obtained dermal fibroblasts from healthy control individual and a HNA patient with R88W genotype. The intensity of MT bundles with more than five times the intensity of a single MT was significantly lower than that from healthy control (Figure 2.14 H).

Given the role of SEPT9 N-terminal repeat motifs in neurite asymmetric growth. The effect of R88W mutation in neurite outgrowth of PC-12 cells was examined. It was clear that overexpression of GFP-tagged SEPT9_i3 increased the percentage of cells containing a single

neurite, compared with the control set with GFP overexpression. In contrast, R88W mutation led to significant decrease of cells with a single neurite and increase of cells with more than three neurites (Figure 2.14 I). Taken together, these data suggested that HNA associated mutation R88W in SEPT9_i3 adversely affect MT bundling and asymmetric development of neurites.

Discussion

Septin colocalization with MTs has been reported in many cases, but whether septins directly interact with MTs was controversial. Here, for the first time, I provide evidence for direct interaction between SEPT9 and MTs, and shed light on the mechanism of their interaction. There are 13 members in human septin family, my study showed that besides SEPT9, SEPT7 can also directly bind and bundle MTs, and SEPT6 can weakly interact with MTs. It is therefore likely that other septins may also bind and bundle MTs. Septins form heteromers that perform various functions in oligomerized form. Therefore, MT bundling is likely mediated by septin complexes, which might be more efficient than monomers. Indeed, as the result of my low speed MT co-sedimentation assay suggested, SEPT9 in complex with SEPT6 and SEPT7 bundles MTs are much more efficient than SEPT9 alone. It is apparent that SEPT6 and SEPT7 may contribute to the bundling effect, but the MT bundling ability of the complex seems to be better than the cumulative effect of each septin monomer. The model that I propose here suggests how SEPT9 alone mediates MT cross linking through interaction between charged SEPT9 repeat motifs. In septin heteromers, however, the C-terminal coiled-coil tail of SEPT6 and SEPT7 may interact with each other to mediate parallel or anti-parallel formation of septin complexes, while flexible SEPT9 N- terminus extend out of main structure and interact with MTs, leading to the cross-linking of MTs.

SEPT9 specifically interacts with the β-tubulin C-terminal tail, which is also bound by many kinesin motors during intracellular transport. Therefore, it is very likely that SEPT9 may regulate kinesin-based transport by competing with kinesin motors for MT binding, decreasing their speed or run length. Our findings suggest that tubulin isotypes are associated with SEPT9 mediated MT bundling, and SEPT9 mediated MT binding through SEPT9-βII tubulin interaction is involved in asymmetric neurite growth. This conclusion is supported by previous studies,

which indicate that the βII tubulin isotype occurs mostly in neurites after differentiation and is crucial for neurite outgrowth (Guo et al., 2010). The β tubulin isotype and its PTMs may explain why septins colocalize with subsets of MTs in most cells. In addition, it is possible that MTs with different PTMs may have different properties in attracting or repelling binding of SEPT9 and other septins, performing different functions spatially or temporally.

Novel repeat motifs in the N-terminus of SEPT9 that mediate SEPT9-MT have been discovered in this study. Similar repeats may exist in other septins. These repeats could contribute to the MT binding by SEPT6 and SEPT7, but this needs to be tested in future studies. Although these repeats are charged and form electrostatic interaction with MTs, which is similar to the MT binding motifs in other MAPs such as tau or MAP1, the sequence of these repeats does not appear to be present in known MAPs with the possible exception of titin. The uniqueness of these repeat motifs suggest the possibility that the SEPT9 N-terminus may be evolutionally adopted from other proteins.

As mentioned previously, SEPT9 has the biggest number of isoforms in septin family. The diversity of isoforms might be used to precisely regulate SEPT9 functions spatially and temporally. The expression profile of each isoforms and their specific function in cells or organs but are still far from clear. For example, it has been reported that the expression level of SEPT9_i1 and SEPT9_i4, and the methylation status of their gene promoters are dramatically changed during cancer development, which has been used clinically as a biomarker for cancer screening (Yu et al., 2015). Regarding their interaction with MTs, it is still to be defined how each isoform regulate MT structure and functions. Colocalization between septins and MTs varies dramatically in different cell types, and whether and how different septins, septin isoforms, or other MAPs are involved still needs to be studied.

My data suggest that the HNA associated mutation, R88W in SEPT9_i3, decreases MT bundling by SEPT9, and affects asymmetric development of neurites. It is thus possible that during the development of HNA, SEPT9 mutations decrease MT bundling, affecting the formation of neuromuscular junctions and leading to the development HNA. This hypothesis raises more questions than it can answer. For example, it cannot explain why HNA develops during the middle age of the patient and how some specific neurons are only affected. A great amount of work is therefore needed to understand the development mechanism of HNA and whether SEPT9 mediate MT bundling or asymmetric neurite development is involved in this process.

Finally, there is a large number of MAPs in cells and the number is still growing, but how septins play with other MAPs is not clear. There is no doubt that the interaction between septins and MTs is tightly regulated by different proteins. Therefore, further studies will be necessary to understand the interplay between septins, MAPs and MTs.

Figures:

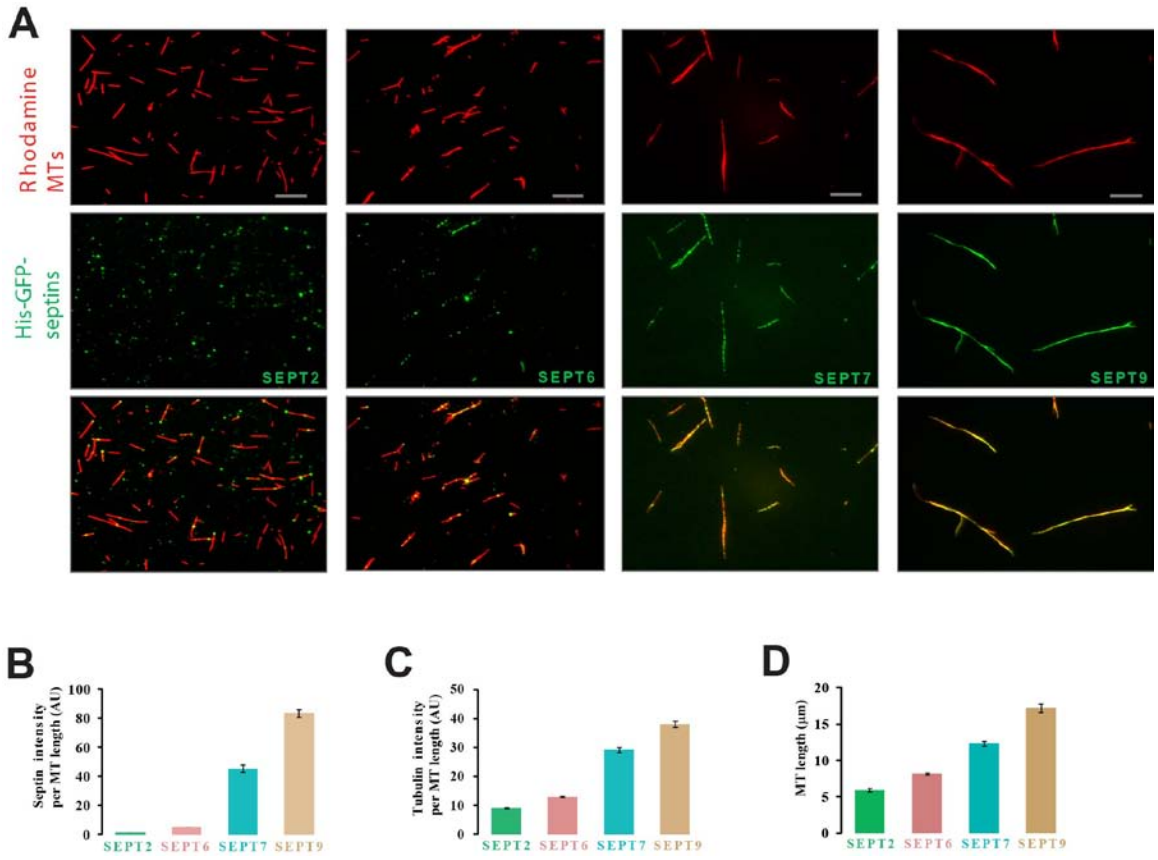

Figure 2.1. *In vitro* reconstitution of septin-MTs interaction.

(A) His-GFP-tagged septins (SEPT2, SEPT6, SEPT7 and SEPT9_i1) were expressed in bacteria, purified and mixed with prepolymerized MTs made with TRITC rhodamine-labeled tubulin (Cytoskeleton Inc). MT-septin complexes were mounted on a slide and imaged with fluorescence microscopy.

(B-D) Graphs show quantifications of GFP-septin intensity (B), MT intensity (C) and MT length (D) upon incubation with GFP-tagged septins. Note that both SEPT7 and SEPT9_i1 bind MTs strongly and appear to increase the intensity (bundling) and length of MTs.

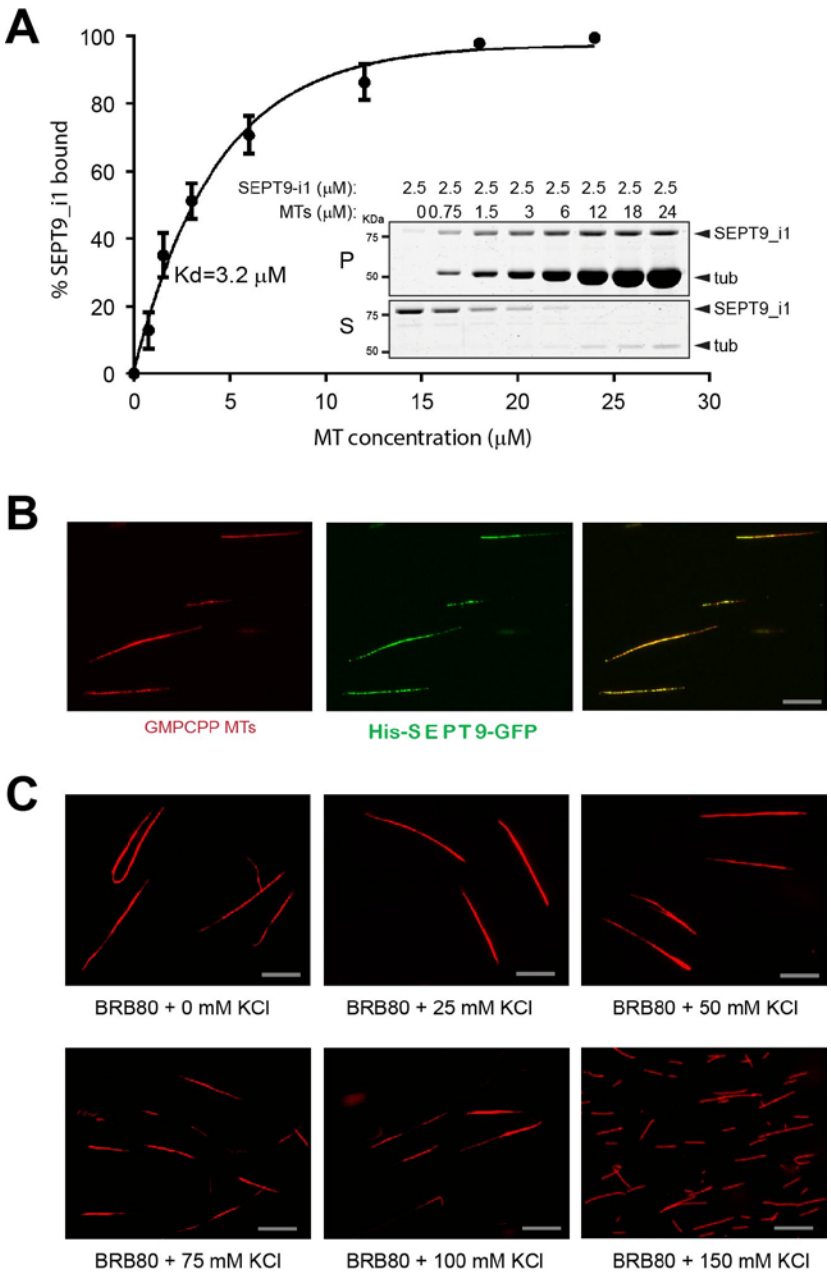
A
100
80
60
40
20
0
% SEPT9_i1 bound
Kd=3.2 μM
SEPT9-i1 (μM): 2.5 2.5 2.5 2.5 2.5 2.5 2.5 2.5
MTs (μM): 0 0.75 1.5 3 6 12 18 24
KDa
75
50
P
S
SEPT9_i1
tub
0 5 10 15 20 25 30
MT concentration (μM)
B
GMPCPP MTs
His-SEPT9-GFP
C
BRB80 + 0 mM KCl
BRB80 + 25 mM KCl
BRB80 + 50 mM KCl
BRB80 + 75 mM KCl
BRB80 + 100 mM KCl
BRB80 + 150 mM KCl

Figure 2.2. SEPT9_i1 interacts with MTs electrostatically.

(A) Pellet (P) and supernatant (S) fractions from a high speed MT-pelleting experiment. The percentage of total SEPT9_i1 pelleted with MTs was plotted against the concentration of tubulin and the dissociation constant (Kd) was calculated after applying a curve of best fit to the data.

(B) Images show X-rhodamine - labeled GMPCPP-stabilized MTs after mixing with His-GFP tagged SEPT9_i1. Scale bars, 10 μm.

(C) Fluorescence microscopy images show paclitaxel-stabilized X-rhodamine - labeled MTs after mixing with SEPT9-FL in BRB80 buffer (80 mM Pipes, 1 mM EGTA, and 1 mM MgCl2, pH 6.9) with increasing KCl concentrations. Scale bars, 10 μm.

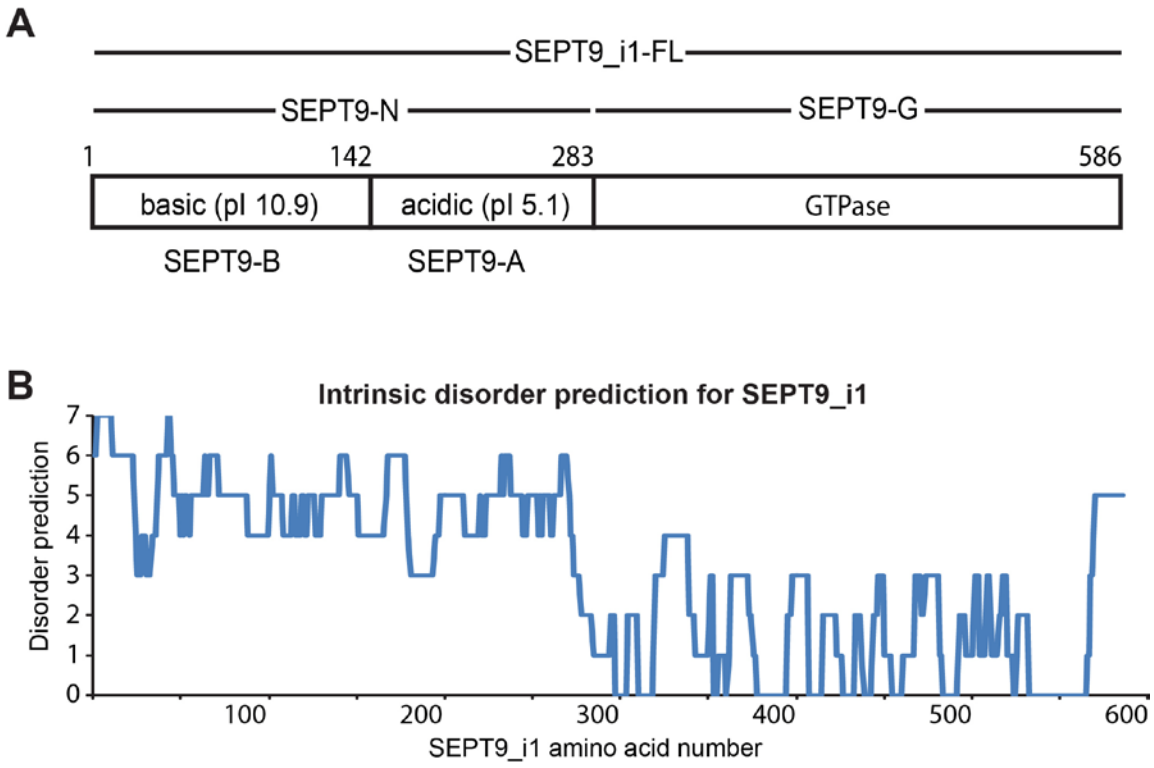

Figure 2.3. SEPT9 N-terminus is unstructured.

(A) Sequence and domains of SEPT9_i1.

(B) Graph shows the predicted intrinsic disorder for the protein sequence of SEPT9_i1. Predicted disorder is plotted as the cumulative result of seven different bioinformatic methods (GlobProt, DisEMBL, DISOPRED2, IUPred, DISpro, OnD-CRF, and DRIP-PRD). The predicted intrinsic disorder of every amino acid was set to 1 or 0 for values that were above or below the intrinsic disorder cut-off points of each algorithm. A maximum value of 7 indicates a prediction of structural disorder by all seven algorithms, and a minimum value of 0 indicates a high degree of structural order by all seven bioinformatic engines.

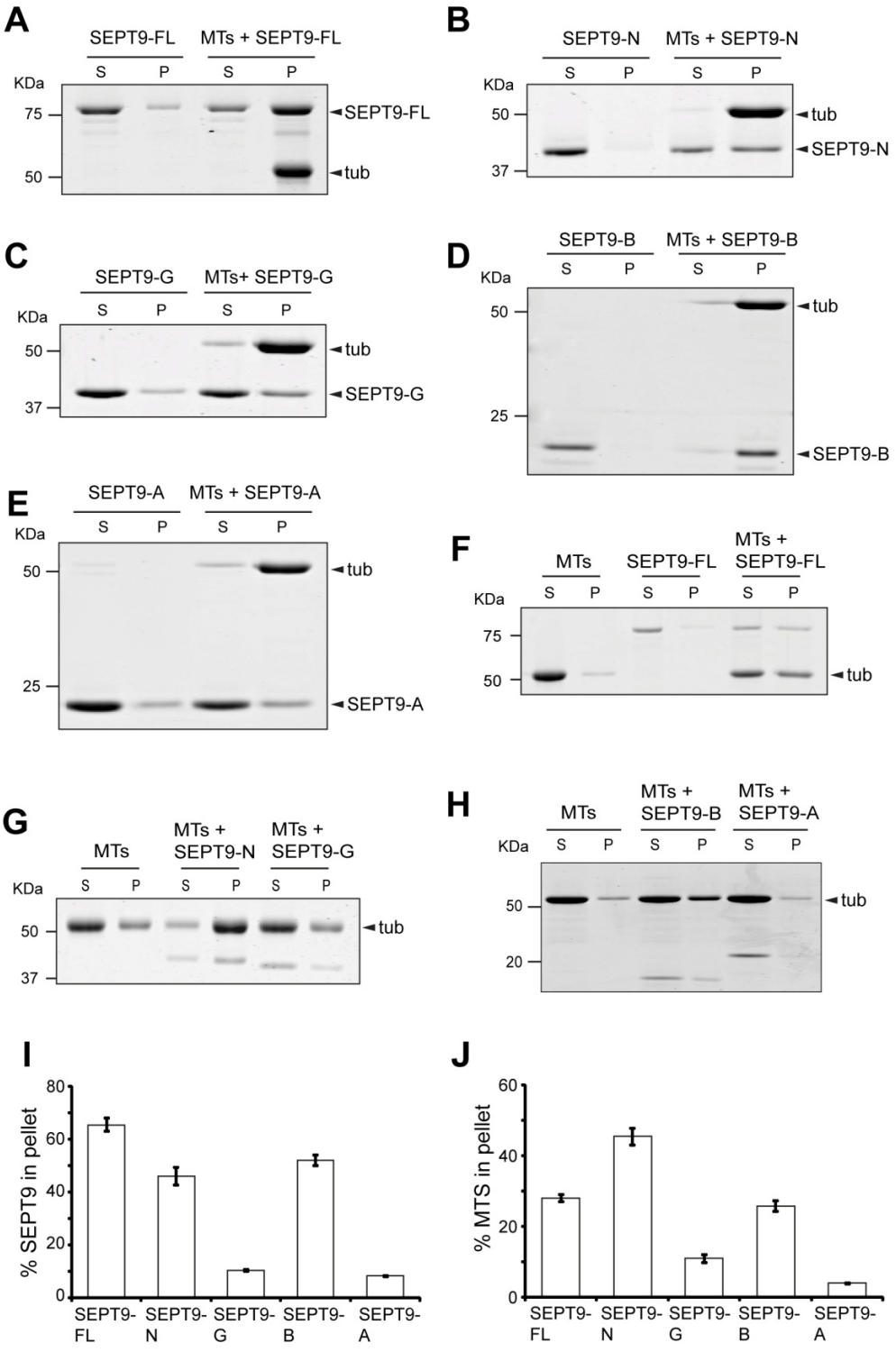
A
SEPT9-FL
MTs + SEPT9-FL
S P S P
KDa
75
50
SEPT9-FL
tub
B
SEPT9-N
MTs + SEPT9-N
S P S P
KDa
50
37
tub
SEPT9-N
C
SEPT9-G
MTs+ SEPT9-G
S P S P
KDa
50
37
tub
SEPT9-G
D
SEPT9-B
MTs + SEPT9-B
S P S P
KDa
50
25
tub
SEPT9-B
E
SEPT9-A
MTs + SEPT9-A
S P S P
KDa
50
25
tub
SEPT9-A
F
MTs
SEPT9-FL
MTs + SEPT9-FL
S P S P S P
KDa
75
50
tub
G
MTs
MTs + SEPT9-N
MTs + SEPT9-G
S P S P S P
KDa
50
37
tub
H
MTs
MTs + SEPT9-B
MTs + SEPT9-A
S P S P S P
KDa
50
20
tub
I
% SEPT9 in pellet
0
20
40
60
80
SEPT9-FL
SEPT9-N
SEPT9-G
SEPT9-B
SEPT9-A
J
% MTS in pellet
0
20
40
60
SEPT9-FL
SEPT9-N
SEPT9-G
SEPT9-B
SEPT9-A

Figure 2.4. MT co-sedimentation assays show the basic region of SEPT9_i1 N-terminal domain directly binds and bundles MTs.

(A - E) Coomassie-stained SDS-PAGE gels of the supernatant (S) and pellet (P) fractions after high speed (39,000 g) sedimentation of pre-polymerized paclitaxel-stabilized MTs with domains of SEPT9_i1.

(F - H) Low speed (8,000 g) sedimentation of MTs in the presence of SEPT9_i1 domains.

(I and J) Graphs show percentages of total protein pelleted with MTs at 39,000 g (I) and percentage of total MTs pelleted at 8,000 g (J) in three independent experiments.

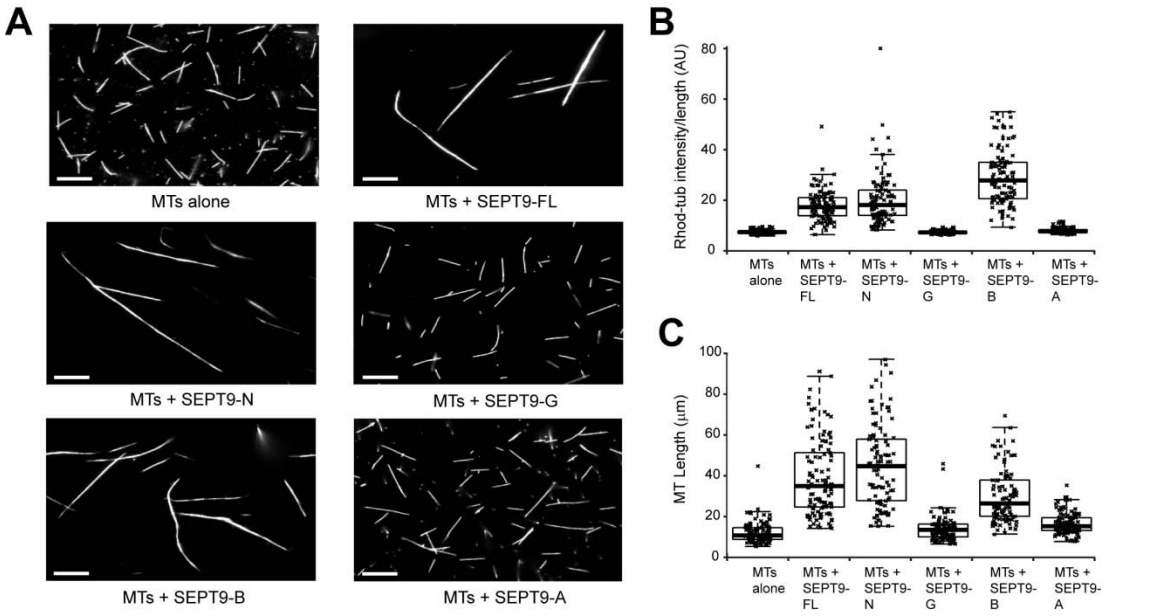
A
MTs alone
MTs + SEPT9-FL
MTs + SEPT9-N
MTs + SEPT9-G
MTs + SEPT9-B
MTs + SEPT9-A
B
Rhod-tub intensity/length (AU)
0
20
40
60
80
MTs alone
MTs + SEPT9-FL
MTs + SEPT9-N
MTs + SEPT9-G
MTs + SEPT9-B
MTs + SEPT9-A
C
MT Length (μm)
0
20
40
60
80
100
MTs alone
MTs + SEPT9-FL
MTs + SEPT9-N
MTs + SEPT9-G
MTs + SEPT9-B
MTs + SEPT9-A

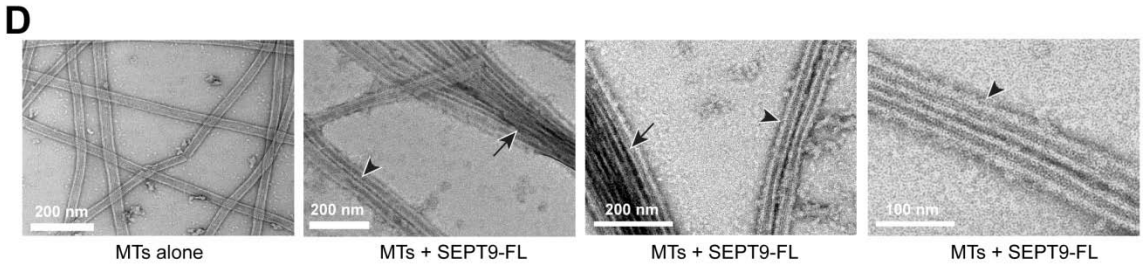
D
200 nm
MTs alone
200 nm
MTs + SEPT9-FL
200 nm
MTs + SEPT9-FL
100 nm
MTs + SEPT9-FL

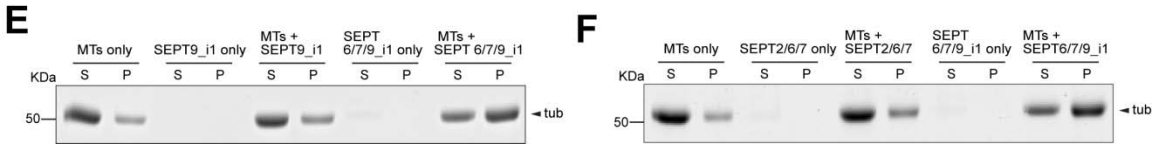
E
MTs only
SEPT9_i1 only
MTs + SEPT9_i1
SEPT 6/7/9_i1 only
MTs + SEPT 6/7/9_i1
KDa
S P S P S P S P S P
50
tub
F
MTs only
SEPT2/6/7 only
MTs + SEPT2/6/7
SEPT 6/7/9_i1 only
MTs + SEPT6/7/9_i1
KDa
S P S P S P S P S P
50
tub

Figure 2.5. The basic region of SEPT9_i1 N-terminus directly bundles MTs.

(A) Images show X-rhodamine-labeled MTs after mixing with recombinant SEPT9 fragments. Scale bars, 10 μm.

(B and C) Plots show the intensity of X-rhodamine fluorescence per micron of MT (B; n = 100) and the length of MTs (C; n = 100) per condition.

(D) Negative stain EM images of MTs before and after mixing with SEPT9_i1. Arrows and arrowheads point to MT bundles and doublets, respectively.

(E and F) Coomassie-stained gels show equal volumes of supernatant and pellet fractions from paclitaxel-stabilized MTs sedimented at 8,000 g alone or in the presence of 0.2 μM SEPT9_i1 and SEPT6/7 in complex with SEPT9_i1 (SEPT6/7/9_i1) or SEPT2 (SEPT2/6/7). Note that the in-gel amount of recombinant septins is below the detection limit of the Coomassie stain.

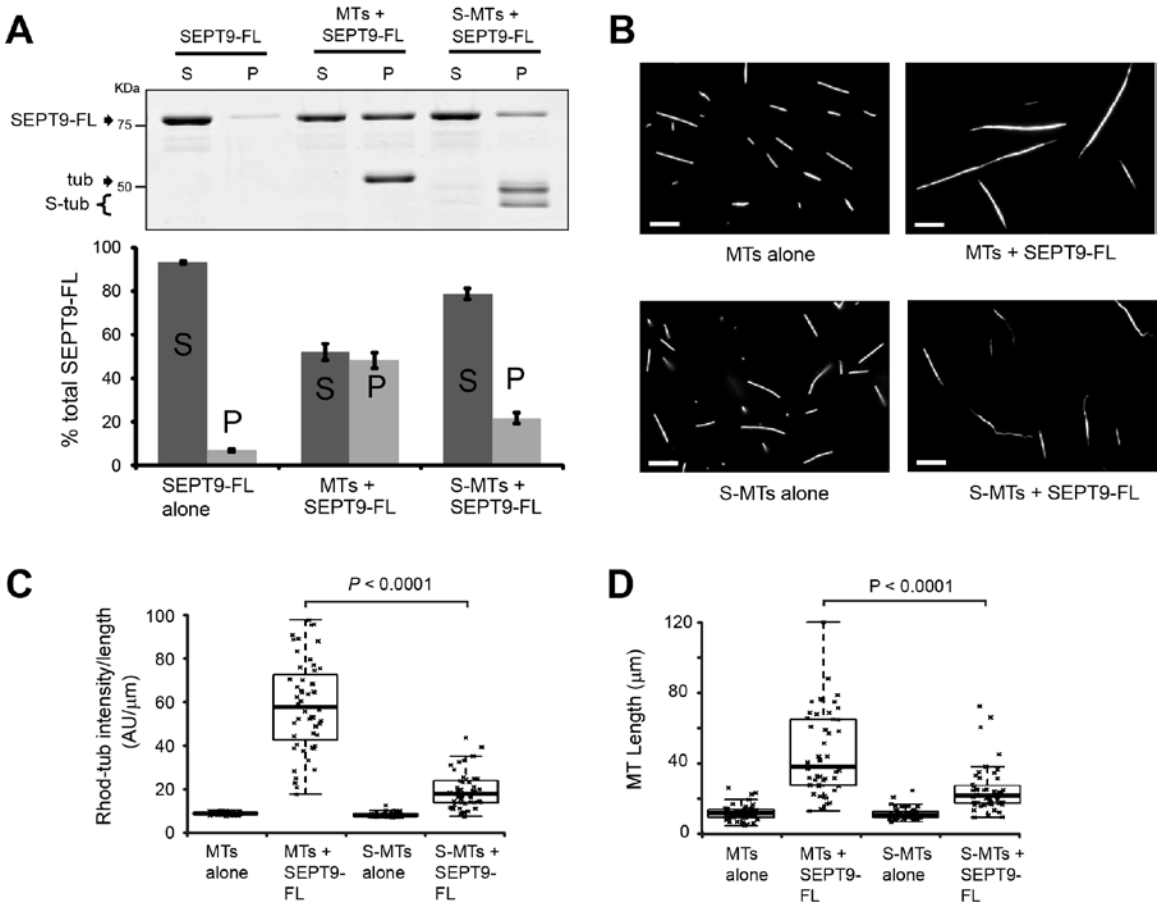
A
SEPT9-FL
MTs + SEPT9-FL
S-MTs + SEPT9-FL
S P S P S P
KDa
SEPT9-FL
75
tub
50
S-tub
% total SEPT9-FL
100
80
60
40
20
0
S
P
SEPT9-FL alone
MTs + SEPT9-FL
S-MTs + SEPT9-FL
B
MTs alone
MTs + SEPT9-FL
S-MTs alone
S-MTs + SEPT9-FL
C
P < 0.0001
Rhod-tub intensity/length (AU/µm)
MTs alone
MTs + SEPT9-FL
S-MTs alone
S-MTs + SEPT9-FL
D
P < 0.0001
MT Length (µm)
120
80
40
0
MTs alone
MTs + SEPT9-FL
S-MTs alone
S-MTs + SEPT9-FL

Figure 2.6. Tubulin C-terminal tail (CTT) mediates MTs-SEPT9_i1 binding.

(A) Gel shows supernatant (S) and pellet (P) fractions after sedimentation (39,000 g) of SEPT9-FL with untreated and subtilisin-treated MTs (S-MTs). Graph shows percentage of total SEPT9-FL in the S and P fractions.

(B) Images show untreated and subtilisin-treated X-rhodamine–labeled MTs after mixing with SEPT9-FL. Scale bars, 10 μm.

(C and D) Plots show the fluorescence intensity per micron of MT (C; n = 50) and the length of MTs (D; n = 50).

(E) Increasing amounts of bovine brain tubulin untreated (- sub) and subtilisin-treated (+ sub) MTs was separated by 7.5% SDS-PAGE and transferred to nitrocellulose membranes, which were overlaid with His-tagged SEPT9-FL, and blotted with anti-His antibodies.

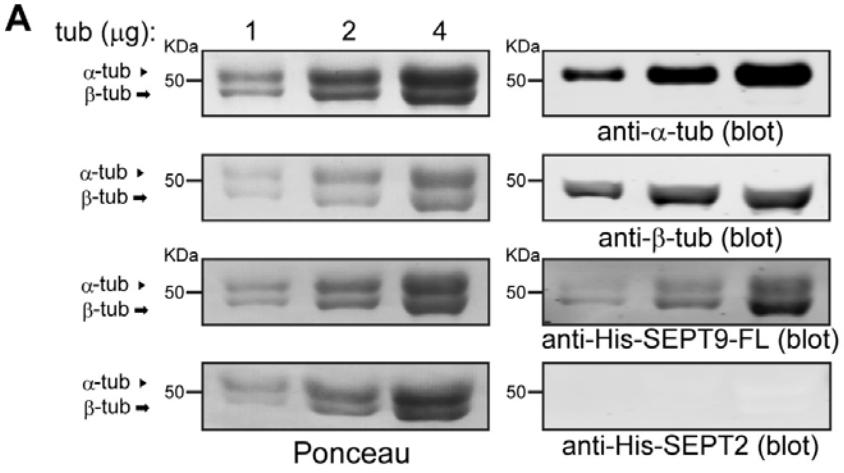
A
tub (μg):
1
2
4
KDa
α-tub
β-tub
50
anti-α-tub (blot)
anti-β-tub (blot)
anti-His-SEPT9-FL (blot)
Ponceau
anti-His-SEPT2 (blot)

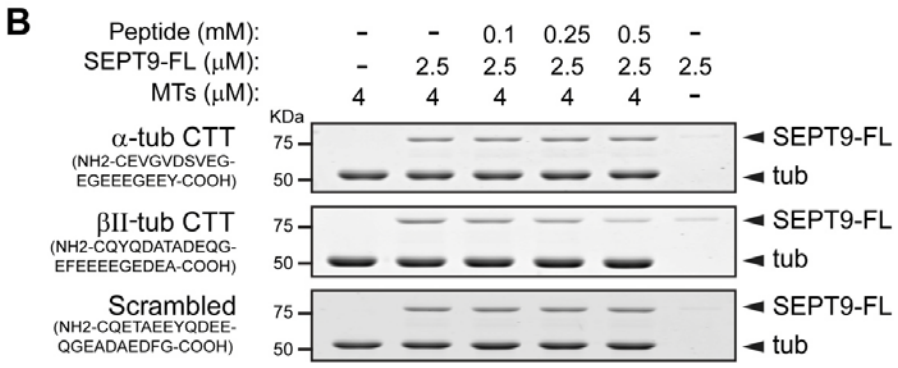
B
Peptide (mM):
SEPT9-FL (μM):
MTs (μM):
KDa
α-tub CTT
(NH2-CEVGVDSVEG-EGEEEGEEY-COOH)
βII-tub CTT
(NH2-CQYQDATADEQG-EFEEEEGEDEA-COOH)
Scrambled
(NH2-CQETAEEYQDEE-QGEADAEDFG-COOH)
75
50
SEPT9-FL
tub

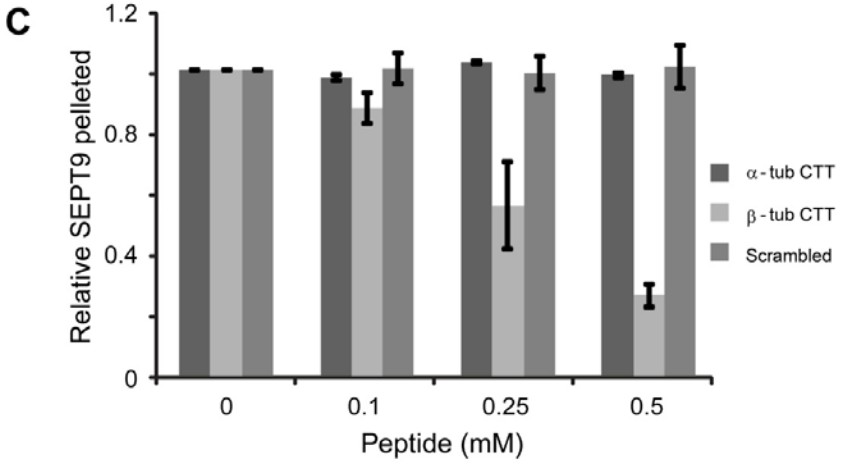
C
Relative SEPT9 pelleted
1.2
0.8
0.4
0
α-tub CTT
β-tub CTT
Scrambled
0
0.1
0.25
0.5
Peptide (mM)

Figure 2.7. SEPT9 preferentially interacts with β-tubulin.

(A) Increasing amounts of bovine brain tubulin was separated by 7.5% SDS-PAGE and transferred to nitrocellulose membranes, which were stained with Ponceau S red. Membranes were blotted with DM1A or TUB2.1 antibodies against α- and β-tubulin, respectively, and overlaid with His-tagged SEPT9-FL or SEPT2, which were detected with anti-His antibodies.

(B and C) Gels and graph shows fraction of SEPT9-FL pelleted with MTs in the presence of increasing concentrations of α-tubulin, βII-tubulin, and scrambled CTT peptide relative to no peptide in three independent experiments.

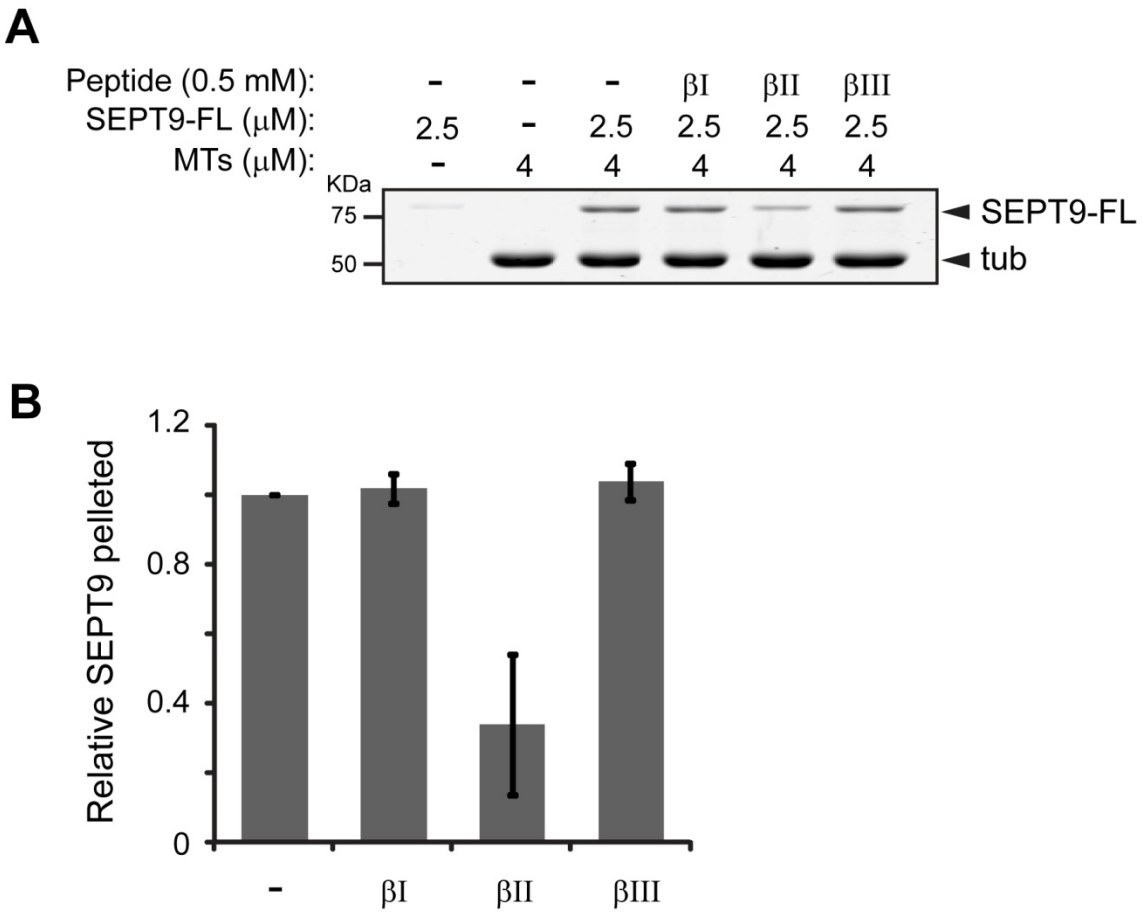

Figure 2.8. SEPT9 preferentially interacts with βII-tubulin tail.

(A) Gels show the pellet fractions after sedimentation of MTs with SEPT9-FL in the presence of βI-, βII-, and βIII-tubulin CTT peptides.

(B) Graph shows the fraction of SEPT9-FL pelleted in the presence of peptides relative to no peptide in three independent experiments.

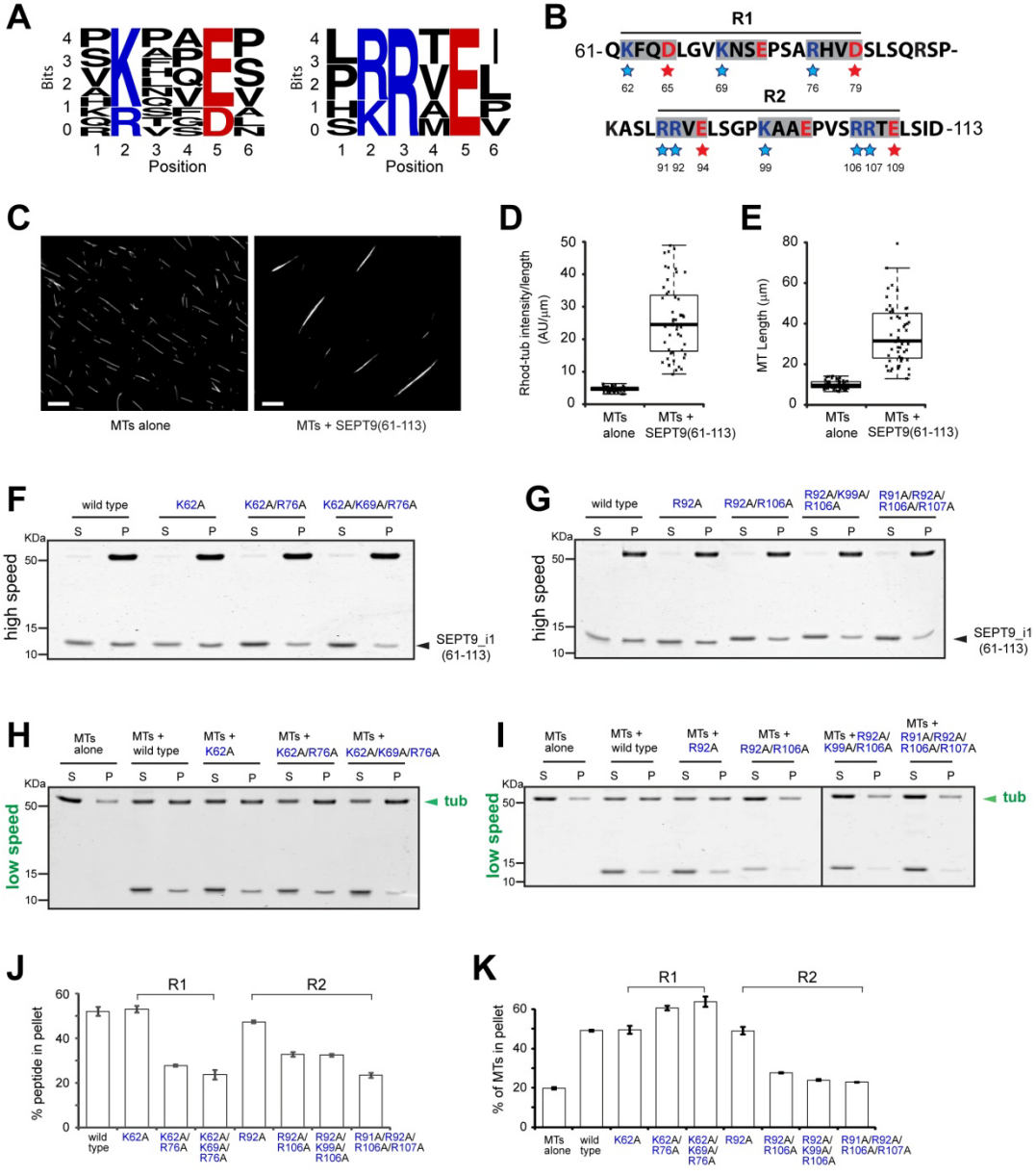
A
Bits
Position
B
R1
61-QKFQDLGVKNSEPSARHVDSLSQRSP-
62 65 69 76 79
R2
KASLRRVELSGPKAAEPVSRRTELSID-113
91 92 94 99 106 107 109
C
MTs alone
MTs + SEPT9(61-113)
D
Rhod-tub intensity/length (AU/μm)
MTs alone
MTs + SEPT9(61-113)
E
MT Length (μm)
MTs alone
MTs + SEPT9(61-113)
F
wild type
K62A
K62A/R76A
K62A/K69A/R76A
KDa
high speed
SEPT9_i1 (61-113)
G
wild type
R92A
R92A/R106A
R92A/K99A/ R106A
R91A/R92A/ R106A/R107A
high speed
SEPT9_i1 (61-113)
H
MTs alone
MTs + wild type
MTs + K62A
MTs + K62A/R76A
MTs + K62A/K69A/R76A
low speed
tub
I
MTs alone
MTs + wild type
MTs + R92A
MTs + R92A/R106A
MTs + R92A/ K99A/R106A
MTs + R91A/R92A/ R106A/R107A
low speed
tub
J
% peptide in pellet
R1
R2
wild type
K62A
K62A/ R76A
K62A/ K69A/ R76A
R92A
R92A/ R106A
R92A/ K99A/ R106A
R91A/R92A/ R106A/R107A
K
% of MTs in pellet
R1
R2
MTs alone
wild type
K62A
K62A/ R76A
K62A/ K69A/ R76A
R92A
R92A/ R106A
R92A/ K99A/ R106A
R91A/R92A/ R106A/R107A

Figure 2.9. Specific positively charged amino acids in charged repeats are involved in MT binding and bundling.

(A) WebLogo alignments of eleven hexapeptide sequences containing the K/R-x-x-E/D motif and six sequences containing the R/K-R-x-E motif within the N terminus (aa 1–286) of SEPT9_i1. The height of each residue indicates the frequency of its presence at the indicated positions.

(B) Sequence of aa 61 - 113 of SEPT9_i1. The blue and red stars highlight the basic and acidic residues mutated to alanine.

(C) Fluorescence microscopy images show paclitaxel-stabilized X-rhodamine-labeled MTs alone and after mixing with the SEPT9_i1(61 - 113) peptide. Scale bars, 10 μm.

(D and E) Plots show the intensity of X-rhodamine fluorescence per MT micron (D; n = 50) and MT length (E; n = 50) in the absence or presence of SEPT9_i1(61 - 113).

(F and G) Coomassie-stained SDS-PAGE gels show the supernatant (S) and pellet (P) fractions after sedimentation of the 61 - 113 peptide and the indicated mutants with pre-polymerized MTs at 39,000 g (high speed).

(H and I) Gels show the supernatant and pellet fractions after sedimentation of MTs with the 61 - 113 peptide and the indicated mutants at 8,000 g (low speed).

(G and K) Graphs show percentage of total SEPT9_i1(61 - 113) (wild-type and basic residue mutants) pelleted with MTs at 39,000 g (G), and percentage of total tubulin pelleted at 8,000 g (K) in three independent experiments.

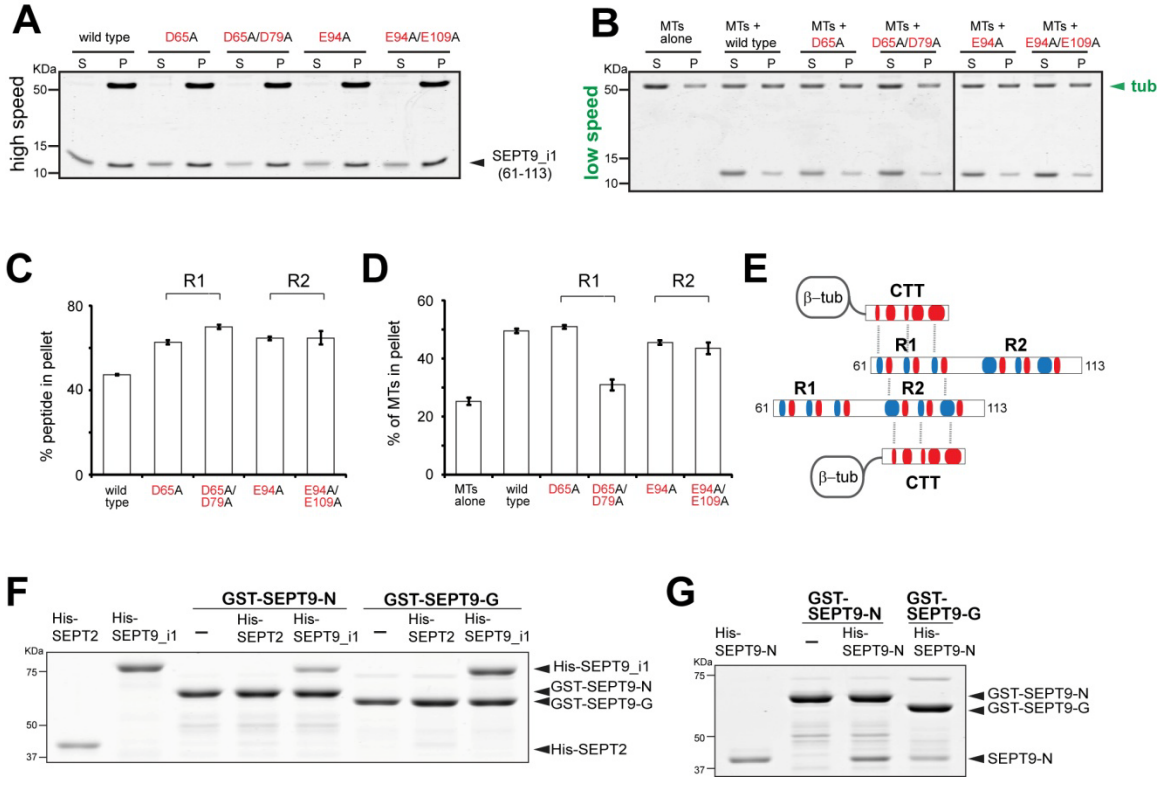
A
wild type
D65A
D65A/D79A
E94A
E94A/E109A
S P S P S P S P S P
KDa
high speed
50
15
10
SEPT9_i1
(61-113)
B
MTs alone
MTs + wild type
MTs + D65A
MTs + D65A/D79A
MTs + E94A
MTs + E94A/E109A
S P S P S P S P S P S P
KDa
low speed
50
15
10
tub
C
% peptide in pellet
80
40
0
R1
R2
wild type
D65A
D65A/ D79A
E94A
E94A/ E109A
D
% of MTs in pellet
60
40
20
0
R1
R2
MTs alone
wild type
D65A
D65A/ D79A
E94A
E94A/ E109A
E
β–tub
CTT
R1
R2
61
113
R1
R2
61
113
β–tub
CTT
F
GST-SEPT9-N
GST-SEPT9-G
His-SEPT2
His-SEPT9_i1
–
His-SEPT2
His-SEPT9_i1
–
His-SEPT2
His-SEPT9_i1
KDa
75
50
37
His-SEPT9_i1
GST-SEPT9-N
GST-SEPT9-G
His-SEPT2
G
GST-SEPT9-N
GST-SEPT9-G
His-SEPT9-N
–
His-SEPT9-N
His-SEPT9-N
KDa
75
50
37
GST-SEPT9-N
GST-SEPT9-G
SEPT9-N

Figure 2.10. Specific negatively charged amino acids in charged repeats are involved in MT binding and bundling.

(A and B) Gels show the supernatant and pellet fractions from high speed (A) and low speed (B) MT-pelleting assays with the 61–113 peptide and mutant versions with the indicated substitutions of acidic residues with alanine.

(C and D) Graphs show percentage of total 61–113 peptide (wild-type and acidic residue mutants) pelleted with MTs at 39,000 g (C), and percentage of total tubulin pelleted at 8,000 g (D) in three independent experiments.

(E) Schematic shows a model of electrostatic interactions between the acidic (red) CTTs of tubulin and the basic (blue) residues of the SEPT9 repeat motifs. MT cross-linking is achieved by interactions between the acidic and basic residues of the K/R-x-x-E/D and R/K-R-x-E motifs, respectively.

(F) Coomassie-stained gels show the results of in vitro binding assays between recombinant GST-tagged SEPT9-N or SEPT9-G and His-tagged full-length SEPT2 or SEPT9_i1.

(G) Coomassie-stained gels show the results of in vitro binding assays between GST-tagged SEPT9-N or SEPT9-G with His-tagged SEPT9-N.

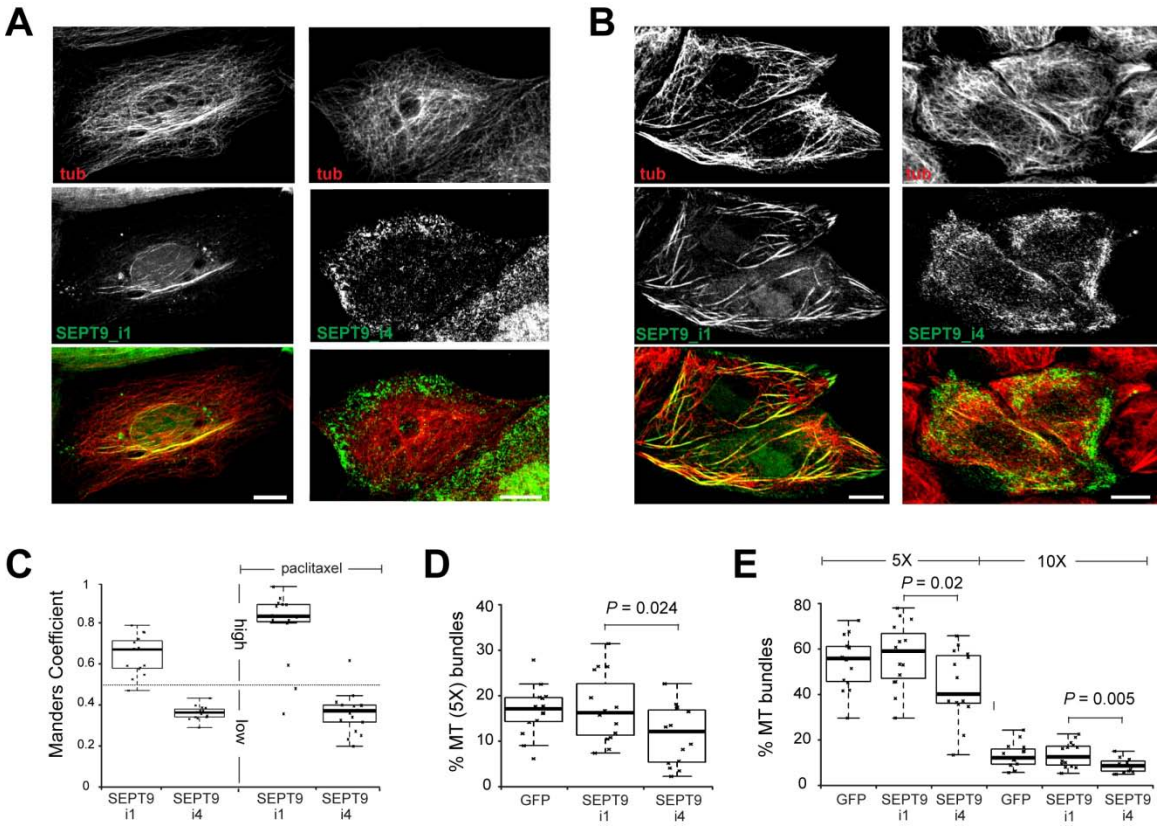
A
tub
tub
SEPT9_i1
SEPT9_i4
B
tub
tub
SEPT9_i1
SEPT9_i4
C
paclitaxel
Manders Coefficient
high
low
SEPT9 i1
SEPT9 i4
SEPT9 i1
SEPT9 i4
D
P = 0.024
% MT (5X) bundles
GFP
SEPT9 i1
SEPT9 i4
E
5X
10X
P = 0.02
P = 0.005
% MT bundles
GFP
SEPT9 i1
SEPT9 i4
GFP
SEPT9 i1
SEPT9 i4

Figure 2.11. Charged repeats in SEPT9_i1 are important for MT bundling.

(A and B) Maximal projections of 3D confocal microscopy images of MDCK cells expressing GFP-tagged SEPT9_i1 and SEPT9_i4 before (A) and after (B) treatment with 5 μM paclitaxel for 1.5 h.

(C) Manders coefficients for the colocalization of GFP-tagged SEPT9_i1 and SEPT9_i4 with MTs in MDCK cells (n = 15). High and low colocalization are indicated by coefficients > 0.5 and < 0.5, respectively.

(D and E) Plots show the fluorescence intensity of putative MT bundles with 5 × and 10 × the mean intensity of single MTs as percentage of total MT intensity in MDCK cells (n = 15) before (D) or after (E) treatment with paclitaxel.

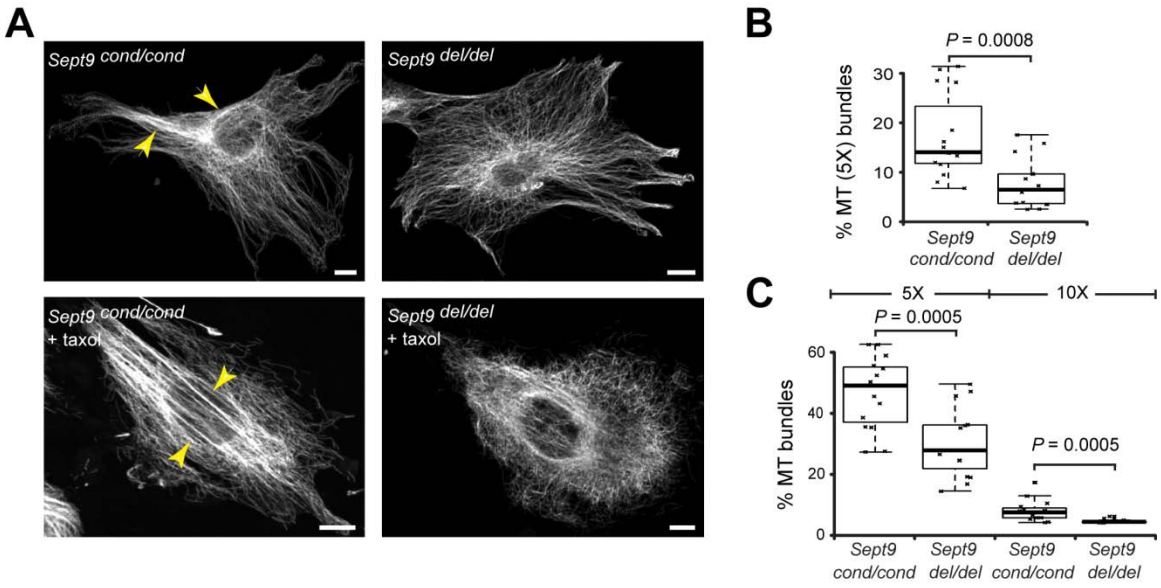

Figure 2.12. SEPT9 knockout decreases MT bundles in embryonic fibroblasts.

(A) Maximal projection of 3D confocal microscopy images of embryonic fibroblasts from *Sept9*$^{cond/cond}$ and *Sept9*$^{del/del}$ mice stained for α-tubulin before and after treatment with paclitaxel (15 μM) for 2 h.

(B and C) Quantification of the sum fluorescence intensity of putative MT bundles with five fold (5 ×) or tenfold (10 ×) the mean intensity of single MTs as a fraction of total MT intensity in *Sept9*$^{cond/cond}$ and *Sept9*$^{del/del}$ fibroblasts (n = 15) before (B) or after (C) treatment with paclitaxel.

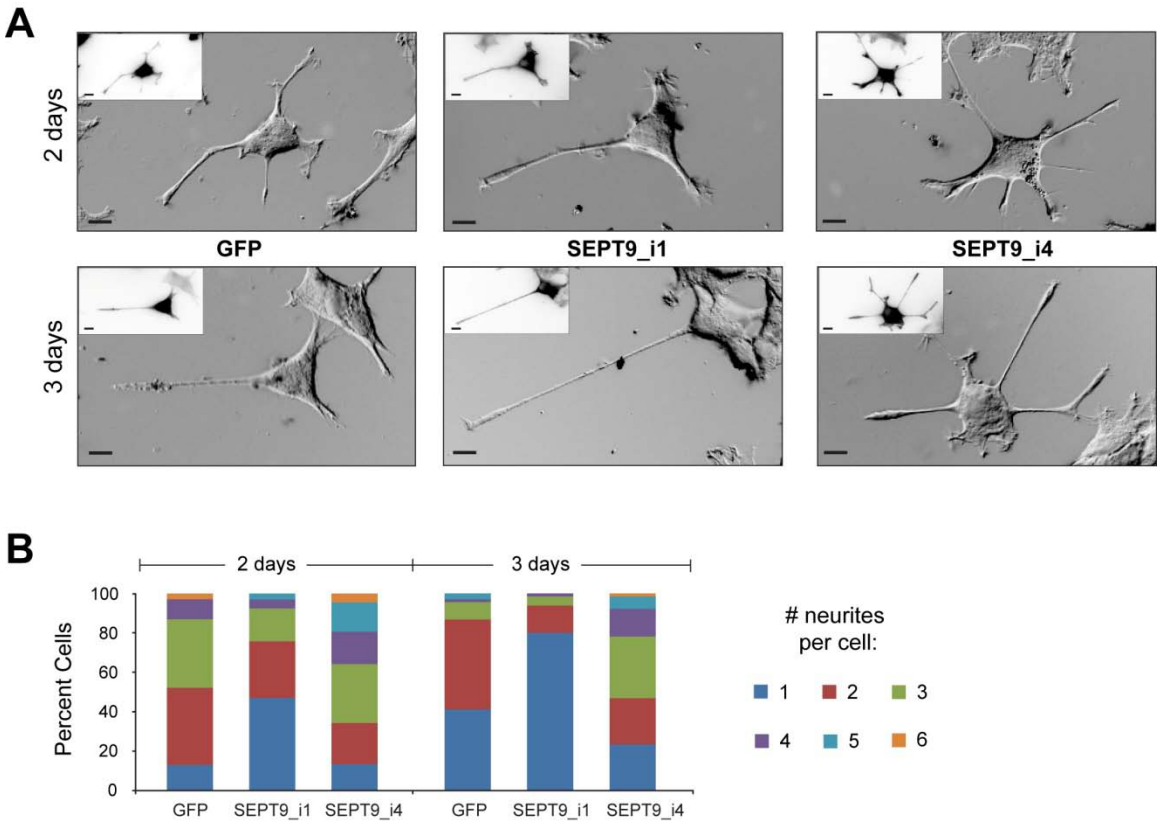

Figure 2.13. Charged repeats in SEPT9_i1 are important in asymmetric neurite development.

(A) Phase-contrast images show PC12 cells transfected with GFP and GFP-tagged SEPT9_i1 and SEPT9_i4 after a 2- and 3-days NGF treatment. Insets show GFP fluorescence in inverted monochrome. Scale bars, 10 µm.

(B) Graph shows percentage of PC12 cells (n = 90) with one or more neurites. Pooled data from three independent experiments are shown.

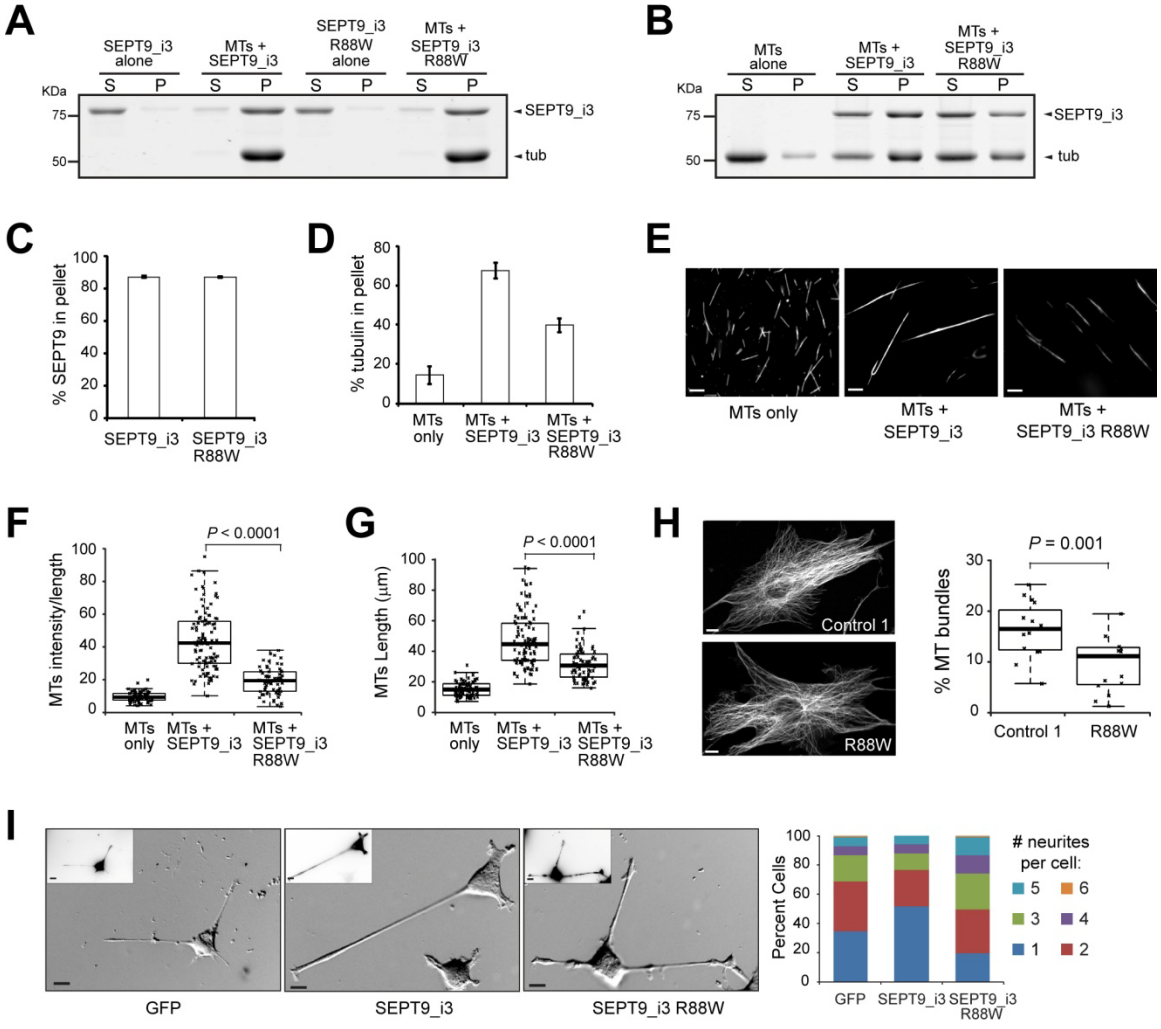
A
SEPT9_i3 alone
MTs + SEPT9_i3
SEPT9_i3 R88W alone
MTs + SEPT9_i3 R88W
S P S P S P S P
KDa
75
50
SEPT9_i3
tub
B
MTs alone
MTs + SEPT9_i3
MTs + SEPT9_i3 R88W
S P S P S P
KDa
75
50
SEPT9_i3
tub
C
% SEPT9 in pellet
100
80
60
40
20
0
SEPT9_i3
SEPT9_i3 R88W
D
% tubulin in pellet
80
60
40
20
0
MTs only
MTs + SEPT9_i3
MTs + SEPT9_i3 R88W
E
MTs only
MTs + SEPT9_i3
MTs + SEPT9_i3 R88W
F
MTs intensity/length
P < 0.0001
100
80
60
40
20
0
MTs only
MTs + SEPT9_i3
MTs + SEPT9_i3 R88W
G
MTs Length (μm)
P < 0.0001
100
80
60
40
20
0
MTs only
MTs + SEPT9_i3
MTs + SEPT9_i3 R88W
H
Control 1
R88W
% MT bundles
P = 0.001
30
20
10
0
Control 1
R88W
I
GFP
SEPT9_i3
SEPT9_i3 R88W
Percent Cells
100
80
60
40
20
0
GFP
SEPT9_i3
SEPT9_i3 R88W
neurites per cell:
5
6
3
4
1
2

Figure 2.14. HNA associated mutation R88W decreases MT bundling and asymmetric neurite development.

(A and B) Gels show supernatant (S) and pellet (P) fractions from high (A; 39,000 g) and low (B; 8,000 g) speed MT-pelleting assays.

(C and D) Graphs show percentages of total protein co-pelleted with MTs (C) and percentage of total tubulin pelleted (D) in three independent experiments.

(E) Images show X-rhodamine–labeled MTs after mixing with recombinant SEPT9_i3 and SEPT9_i3 (R88W). Scale bars, 10 µm.

(F and G) Plots show the intensity of X-rhodamine fluorescence per micron of MT (F; n = 100) and the length of MTs (G; n = 100) per condition.

(H) Images of dermal cells from healthy individual (control 1) and HNA patient with the R88W genotype stained for α-tubulin. Scale bars, 10 µm. Plot shows intensity of putative MT bundles with 5 × the mean intensity of single MTs as percentage of total MT intensity (n = 15).

(I) Phase-contrast images show PC12 cells transfected with GFP and GFP-tagged wild type and R88W SEPT9_i3. Insets show GFP fluorescence in inverted monochrome. Graph shows percentage of cells (n = 90) with one or more neurites. Pooled data from three independent experiments are shown. Scale bars, 10 µm.

CHAPTER III: Septin 9 interacts with kinesin KIF17 and interferes with the mechanism of NMDA receptor cargo binding and transport

Abstract

Intracellular transport involves the regulation of microtubule motor interactions with cargo, but the underlying mechanisms are not well understood. Septins are membrane- and microtubule-binding proteins that assemble into filamentous, scaffold-like structures. Septins are implicated in microtubule-dependent transport, but their roles are unknown. Here, we have uncovered a novel interaction between KIF17, a kinesin 2 family motor, and septin 9 (SEPT9). We show that SEPT9 associates directly with the C-terminal tail of KIF17, and interacts preferentially with the extended cargo-binding conformation of KIF17. In developing rat hippocampal neurons, SEPT9 partially colocalizes and co-migrates with KIF17. We show that SEPT9 interacts with the KIF17 tail domain that associates with mLin-10/Mint1, a cargo adaptor/scaffold protein, which underlies the mechanism of KIF17 binding to the NMDA receptor subunit 2B (NR2B). Significantly, SEPT9 interferes with binding of the PDZ1 domain of mLin-10/Mint1 to KIF17, and thereby, down-regulates NR2B transport into the dendrites of hippocampal neurons. Measurements of KIF17 motility in live neurons show that SEPT9 does not affect the microtubule-dependent motility of KIF17. These results provide the first evidence of an interaction between septins and a non-mitotic kinesin, and suggest that SEPT9 modulates the interactions of KIF17 with membrane cargo.

Introduction

Microtubule (MT) motors of the kinesin family are essential for the long-range intracellular transport of membrane organelles, proteins and mRNA (Hirokawa et al., 2009). Spatio-temporal control and specificity in kinesin-mediated transport is achieved through regulation of kinesin interactions with cargo and MTs (Verhey and Hammond, 2009). Scaffolding and adaptor proteins mediate the interaction of kinesins with specific cargo, and modulate motor activity in coordination with regulatory molecules (Akhmanova and Steinmetz, 2010; Fu and Holzbaur, 2014). On MTs, kinesin motility is regulated by tubulin isoforms and post-translational modifications, and MT-associated proteins (MAPs), which affect the directionality, velocity and processivity of transport (Atherton et al., 2013; Sirajuddin et al., 2014; Verhey and Gaertig, 2007).

The kinesin 2 family motor KIF17 is a homo-dimeric plus-end directed motor that mediates the transport of synaptic receptors, channels and mRNA in neuronal dendrites (Chu et al., 2006; Kayadjanian et al., 2007; Takano, 2007; Yin et al., 2012; Yin et al., 2011). KIF17 is also involved in the nucleocytoplasmic and intraflagellar transport of transcriptional factors and ciliary proteins (Dishinger et al., 2010; Jenkins et al., 2006; Macho et al., 2002). KIF17 consists of an N-terminal motor head domain, a neck and stalk region with coiled-coil domains and a cargo-binding C-terminal tail (Wong-Riley and Besharse, 2012). In the absence of cargo, the motor domain of KIF17 is autoinhibited by the stalk and C-terminal tail, which interfere with MT binding and processive motility (Hammond et al., 2010a). In addition, the C-terminal tail of KIF17 inhibits the catalytic activity of the motor domain and interacts directly with MTs (Acharya et al., 2013). Among the known cargo of KIF17, the NMDA receptor subunit B (NR2B) associates with KIF17 by a mechanism that involves the mLin scaffolding complex. The C-terminal tail of KIF17 interacts directly with the PDZ-1 domain of mLin-10 (Mint1/X11), which

in turn binds NR2B via the mLin-7 subunit of the mLin-10/mLin-2/mLin-7 complex (Jo et al., 1999; Setou et al., 2000).

Septins are a family of G-proteins, which form hetero-oligomeric and polymeric structures that function as scaffolds and diffusion barriers, controlling the localization of membrane and cytoplasmic proteins (Caudron and Barral, 2009; Kinoshita, 2006; Mostowy and Cossart, 2012; Spiliotis and Gladfelter, 2012). Mammalian septins interact with MTs and are involved in Golgi-to-plasma membrane vesicle transport and chromosome alignment (Bai et al., 2013; Nagata et al., 2003; Sellin et al., 2012; Spiliotis et al., 2008; Spiliotis et al., 2005). Septins have been shown to interact with the centromere associated protein E (CENP-E), a mitotic kinesin-like motor that links kinetochores to the ends of spindle MTs (Zhu et al., 2008). However, the role of septins in MT-dependent transport of membrane cargo is unknown.

Materials and Methods

Cells and transfections

MDCKII/G, N2a and HEK293 cells were grown in DMEM with 10% FBS and transfected with Lipofectamine 2000 (Invitrogen) (Dolat et al., 2014b). Primary rat embryonic (E18) hippocampal neurons were obtained from the MINS Neuron Culture Service Center (University of Pennsylvania), cultured in Neurobasal medium supplemented with B27 (GIBCO) and cytosine d-D-arabinofuranoside, and transfected with Lipofectamine LTX (Invitrogen).

Plasmids

GST-tagged fragments of KIF17 were made by PCR amplification from a plasmid encoding for myc-KIF17 (gift from Dr Geri Kreitzer) (Jaulin and Kreitzer, 2010) and cloning into pGEX-KT-ext vector. GFP-KIF17 was made by inserting the full length KIF17 sequence into pEGFP-C1. His-KIF17(850-1029) was created by inserting the PCR-amplified fragment into pET-28a(+). All mutations and truncations were made with the QuikChange II Site-Directed Mutagenesis kit (Agilent Technologies). The plasmids encoding for His-Mint1/mLin-10(653-839) was a gift from Dr. Angela Ho (Matos et al., 2012). C-terminal fusions of SEPT2 and SEPT9_i1 with GFP or mCherry were made by PCR amplifying each gene and cloning into pEGFP- or pmCherry-N1 plasmids. Plasmids encoding for His-tagged SEPT9_i1, SEPT2 and SEPT6-His-SEPT7 were previously described (Bai et al., 2013). His-SEPT9-mCherry was made by PCR amplifying SEPT9_i1_mCherry from the mammalian vector pmCherry-N1-SEPT9 and inserting it into the NdeI and SalI sites of pET-28a(+); pmCherry-N1-SEPT9 was made by inserting SEPT9_i1 in the XhoI and HindIII sites of pmCherry-N1. Myc-SEPT9 was made by PCR amplifying SEPT9_i1 using the primers 5'-CGTAAGCTTGCATGAAGAAGTCTTACTC-3' and

5'-GTACTCGAGCATCTCTGGGGCTTC-3' and inserting the amplified fragment into pcDNA™3.1/myc-His A. pCI-EGFP-NR2b wt (Addgene plasmid # 45447) was a gift from Andress Barria and Robert Malinow (Barria and Malinow, 2002).

Protein purification and binding assays

Bacterial expression and purification of recombinant proteins were performed as previously (Bai et al., 2013). In protein binding assays, GST-tagged proteins (10 µg) were first coupled to GSH agarose 4B beads (Macherey Nagel), which were subsequently incubated for 30 min with His-tagged proteins in GST pull-down buffer (50 mM HEPES, 150 mM NaCl, 2 mM EGTA, 0.1% Triton X-100, 1 mM PMSF, 5 mM DTT, pH 7.4). For competitions assays, beads were incubated for 10 min with His-SEPT9, and then mixed and incubated for 30 min with mLin-10(653-839). After washing (5X) with GST pull-down buffer, beads were resuspended in SDS loading buffer, boiled and loaded onto SDS-PAGE gels, which were stained with Coomassie Brilliant Blue.

GST pull-downs & immunoprecipitations

MDCK cells ($3x10^6$) and an embryonic (E18) rat brain (BrainBits) were homogenized in GST pull down buffer for 1 h at 4 °C. Cell debris was pelleted by centrifugation and supernatants were incubated for 30 min with GST-KIF17(850-1029)-bound beads. After washing, beads were resuspended in SDS loading buffer, boiled and loaded onto SDS-PAGE gels, which were transferred to nitrocellulose membranes and blotted with a SEPT9 antibody (proteintech). Co-immunoprecipitations of KIF17 and SEPT9 were performed by lysing E18 rat brains, MDCK and HEK293 cells for 4 h at 4 °C in buffer containing 10 mM HEPES, pH 7.5, 150 mM NaCl, 0.25%

Triton X-100 and protease inhibitors (EMD Millipore). After spinning at 14,000xg for 3 min, supernatants were pre-cleared overnight at 4 °C with protein A beads (ThermoFisher Scientific) and subsequently, incubated for 12 h at 4 °C with 4 µg of rabbit anti-SEPT9 (proteintech) or pre-immune rabbit IgG. Complexes were captured by incubating overnight with 50 µl of protein A beads, which were pre-blocked in lysis buffer containing 5% BSA. Beads were washed (5X) in lysis buffer, boiled in SDS loading buffer and run on 10% SDS-PAGE. Gels were western blotted with goat anti-KIF17 (1:500, Santa Cruz Biotechnology) and rabbit anti-SEPT9 (1:1000, proteintech). Co-immunoprecipitation of endogenous SEPT9 with myc-KIF17 was similarly performed after transfection of HEK293 cells with myc-KIF17 constructs. Co-immunoprecipitations of myc-KIF17 and GFP-tagged SEPT9 were performed after transfecting HEK293 cells with plasmids encoding for myc-KIF17 (wild-type or G754E) and GFP or SEPT9-GFP. Cells were lysed in buffer containing 25 mM Tris-HCl (pH 7.5), 150 mM NaCl, 1 mM EDTA, 0.5% Trition X-100 and protease inhibitors (EMD Millipore). Lysates were pre-cleared with protein A beads (Thermo Fisher) and incubated overnight with rabbit anti-GFP (A6455; Invitrogen) and subsequently, with protein A beads for 6 h at 4 °C. Beads were washed (5X) with lysis buffer, boiled in SDS loading buffer and run on 10% SDS-PAGE. Western blots were performed with mouse anti-myc (Roche) and anti-GFP (A11120; Invitrogen), and secondary antibodies conjugated to infrared dyes. Membranes were scanned and protein bands were quantified with the Odyssey system (LI-COR).

Co-immunoprecipitation of endogenous KIF17 with GFP-mLin-10 (Figure 3.4 F) was performed by transfecting N2a with plasmids encoding for GFP-mLin10 and myc-SEPT9_i1. Cells were lysed in ice-cold RIPA buffer (50 mM Tris, 1% Triton X-100, 0.1% SDS, 150 mM NaCl, pH 8.0) and protease inhibitors (EMD Millipore). Lysates were pre-cleared with protein A beads (Thermo Fisher) and incubated with rabbit IgG or anti-GFP (A6455; Invitrogen) and

protein A beads overnight at 4 °C. Beads were washed with TBST (0.05% Tween-20, Tris-buffered saline pH 7.4), boiled in SDS loading buffer and run on 10% SDS-PAGE. Western blots were performed with mouse anti rat Mint1/mLin-10 (clone 23; BD Biosciences), goat anti-KIF17 (M-20, Santa Cruz Biotech) and secondary antibodies conjugated to infrared dyes. Membranes were scanned with the Odyssey system (LI-COR).

Fluorescence microscopy and image analysis

Rat hippocampal neurons were incubated in fixation buffer (PBS, 4% PFA, 4% sucrose) for 10 min, and blocked and permeabilized for 20 min with GDB (30mM sodium phosphate pH 7.4, 0.2% gelatin, 450 mM NaCl) and 0.05% Triton X-100. Cells were stained with the goat anti-KIF17 (1:100; M-20; Santa Cruz Biotech), rabbit anti-SEPT9 (1:200, Proteintech group) for 4 h at room temperature and secondary donkey Alexa 594 F(ab')2 anti-goat IgG and donkey Alexa 647 F(ab')2 anti-rabbit IgG (1:200; Jackson Immunolabs) for 1 h at room temperature. Additional staining with mouse antibodies against PSD95 (1:1000; NeuroMAb, Antibodies Incorporated) and Mint1/mLin-10 (1:200; BD Biosciences) were performed with donkey Alexa 488 F(ab')2 anti-mouse IgG. In Figure 3.5A and B, GFP and SEPT9-GFP expressing neurons were stained for endogenous NR2B by fixing (10 min) with PBS containing 4% PFA and 4% sucrose. Cells were washed with PBS and then blocked and permeabilized with GDB buffer containing 0.05% Triton X-100 for 40 min. Subsequently, cells were stained with mouse antibody to NR2B (1:200; NeuroMab) and secondary donkey Alexa 594-conjugated F(ab)2 to mouse IgG (Jackson ImmunoResearch) in GDB buffer. In Figure 3.5E, neurons that were co-transfected with GFP-NR2B and mCherry or SEPT9-mCherry were stained live with rabbit anti-GFP (5 µg/ml; Invitrogen) for 10 min at 37 °C. After rinsing with cold media, cells were incubated with fixation buffer and stained with donkey Alexa 649-conjugated secondary antibody, which was diluted in

GDB buffer. In Figure 3.5D, the same protocol was used for the staining of endogenous surface Kv4.2 with an antibody from NeuroMab (75-016, Antibodies Incorporated). Samples were mounted in FluorSave hard mounting medium (EMD Millipore) and imaged on a Zeiss AxioObserver Z1 with a Plan Apo 63x/1.4 oil objective, a Hamamatsu Orca-R2 CCD camera and the Slidebook 6.0 software. Alternatively, samples were imaged with the SIM and TIRF modules of the OMX V4 microscope (GE Healthcare). Super-resolution SIM imaging was performed with a 60X 1.42 NA objective. A z-step size of 0.125 µm was used and images were acquired with sCMOS pco.edge cameras (PCO) and reconstructed with softWoRx software (Applied Precision).

Fluorescence quantifications per surface area of neuronal cell and neurite length were performed using a custom semi-automated MATLAB script that generated masks for neuronal cell bodies and processes by thresholding GFP, mCherry, SEPT9-GFP or SEPT9-mCherry intensities. Fluorescence intensities per surface area unit were automatically calculated for each mask. Line scans of fluorescence (Figure 3.1F) were performed with Slidebook 6.0 software. Analysis of SEPT9, mLin-10 or PSD95 presence in KIF17 and measurements of NR2B-GFP clusters per 10 µM of dendrite were done by manual inspections of randomized dendrite regions and samples.

Live cell imaging of hippocampal neurons was performed after co-transfection with GFP-KIF17 or GFP-KIF17(G754E) and mCherry or SEPT9-mCherry. After 48 h, coverslips were mounted on a 35 mm dish with a 7 mm diameter bottomless hole using vacuum grease silicone. Phenol red-free Neurobasal media supplemented with B27 (Invitrogen) and 10 mM HEPES was added and dishes were covered and sealed with parafilm. Samples were imaged at 37 °C with TIRF microscopy on a DeltaVision OMX V4 inverted microscope (GE Healthcare) equipped with an Olympus 60x/1.49 objective and a temperature controlled stage-top incubator. Images were acquired with the softWoRx software and movies were imported into the Fiji software,

which was used for kymograph and particle tracking analysis for the quantification of instantaneous velocities, run lengths and percentage motility (Figure 3.5 H and I).

Statistical analysis

Data sets were plotted in box-and-whisker diagrams or bar graphs with the R software. The whisker ends of each plot correspond to minimum and maximum values, and the top and bottom lines of each box represent the 25^{th} (Q1) and 75^{th} (Q3) percentile of the data range. The median value is designated with a bold horizontal line. Statistical outliers were defined as values that were 1.5 times more the Q3 and less the Q1 values, and were shown outside the whiskers of each plot. Bar graphs show mean values plus/minus standard error of the mean (error bars). Each data set was tested for normal distribution using the Kolmogorov-Smirnof test. Mean, standard error of the mean and *p* values were derived using a student's t-test for normally distributed data and the Mann Whitney U test for non-normally data in the GraphPad Prism software.

Results

SEPT9 interacts directly with the C-terminal tail of KIF17 in its cargo-binding conformation

Previous work showed that septins associate with the C-terminal tail of a mitotic kinesin (Zhu *et al*., 2008). Given the role of the C-terminal tail of KIF17 in cargo binding and in the regulation of KIF17 motor activity and localization (Acharya et al., 2013; Dishinger et al., 2010; Guillaud et al., 2003; Hammond et al., 2010a; Setou et al., 2000), we used a GST-tagged KIF17 tail (amino acids 850-1029) as bait to probe for potential interactions with septins. In embryonic (E18) rat brain homogenates (Figure 3.1 A) and Madin-Darby canine kidney (MDCK) cell lysates (Figure 3.1 C), we found that GST-KIF17(850-1029) pulls down SEPT9. Consistent with this finding, endogenous KIF17 and SEPT9 co-immunoprecipitated in lysates from whole rat brains, and MDCK cells (Figure 3.1 B and D).

Next, we examined the localization of SEPT9 and KIF17 in primary rat embryonic (E18) hippocampal neurons using Abs. KIF17 had a punctate and diffuse distribution (Figure 3.1 E). SEPT9 was similarly punctate and diffusive (Figure 3.1 E). Wide-field and super-resolution structured illumination microscopy (SIM) showed that SEPT9 colocalizes with a fraction of KIF17 puncta (~10% of total KIF17), which are found in dendritic shafts and branch points (Figure 3.1 E and F), and occasionally at post-synaptic densities; 16 ± 3% (n = 17 cells) of SEPT9/KIF17-containing puncta colocalized with PSD95.

To test whether SEPT9 associates directly and specifically with KIF17, we performed *in vitro* binding assays with recombinant septins and KIF17 domains (Figure 3.2 A). The C-terminal tail of KIF17 pulled down recombinant SEPT9, but not SEPT2 (Figure 3.2 B) or SEPT6/7 (Figure 3.2 C), which are known to heteromerize with SEPT9 (Kim et al., 2011; Sellin et al., 2011). In

vitro binding assays with the motor head domain KIF17(1-339) and KIF17(1-490), which consists of the head and neck domains (Figure 3.2 A), as well as KIF17(340-849), which contains the neck and stalk domains, showed that SEPT9 interacts preferentially with the C-terminal tail of KIF17 (Figure 3.2 D-G). Thus, SEPT9 interacts directly with KIF17 via its C-terminal cargo-binding domain.

Because the C-terminal tail of KIF17 exists in an extended cargo-binding or a "closed" auto-inhibitory conformation (Hammond et al., 2010a), we tested whether SEPT9 binding is affected by the conformation of the KIF17 tail. We performed co-immunoprecipitations with myc-tagged wild type KIF17 or the mutant KIF17(G754E), which maintains an extended cargo-binding conformation (Hammond et al., 2010a). We found that the amount of endogenous SEPT9 that co-immunoprecipitated with KIF17(G754E) was 1.5-2.5-fold more relative to wild type KIF17 (Figure 3.3 A). A similar difference was also observed in the amount of SEPT9-GFP that co-immunoprecipitated with myc-KIF17(G754E) vs. myc-KIF17 (Figure 3.3 B). In agreement with SEPT9 binding to the extended conformation of KIF17, SEPT9-mCherry co-migrated with GFP-KIF17(G754E) in hippocampal neurons (Figure 3.3 C). Taken together, these data indicate that SEPT9 interacts directly and preferentially with the C-terminal tail of KIF17 in its cargo-binding conformation, raising the possibility that SEPT9 is involved in the interactions of KIF17 with membrane cargo.

SEPT9 competes with mLin-10/Mint1 for binding to the tail of KIF17

KIF17 was first discovered as a kinesin motor that mediates the transport of NR2B cargo. Mechanistically, KIF17 associates with NR2B-carrying vesicles through the mLin-2/mLin-7/mLin-10 complex. While mLin-7 binds the cytoplasmic tail of NR2B, mLin-10 interacts with

the C-terminal half of the KIF17 tail through its PDZ1 domain (Jo et al., 1999; Setou et al., 2000). Given that SEPT9 associates with the tail of KIF17 and is highly expressed in rodent brains during mid-to-late gestation (E15 - E18), which marks the onset of NR2B, KIF17 and mLin2/7/10 expression (Setou et al., 2000; Tsang et al., 2011), we sought to examine whether SEPT9 affects the mechanism of interaction between KIF17 and NR2B.

To determine the binding site of SEPT9 with respect to mLin-10, we performed *in vitro* binding assays with the C-terminal tail fragments KIF17(850-980) and KIF17(981-1029). We found that SEPT9 interacts preferentially with KIF17(981-1029) (Figure 3.4 A), which contains the binding site of mLin-10. Because the KIF17-mLin-10 interaction involves the last three amino acids (EPL) of the C-terminal tail of KIF17 (Setou et al., 2000), we tested whether the EPL sequence is also required for SEPT9-KIF17 binding. Mutating the EPL sequence into AAA resulted in 2- to 3-fold reduction in the binding of full length SEPT9 to KIF17(981-1029) (Figure 3.4 B). Thus, SEPT9 and the PDZ1 domain of mLin-10 interact with the C-terminal tail of KIF17 through overlapping binding sites, and hence, may compete for KIF17. Indeed, binding of the PDZ1-containing mLin-10(653-839) to KIF17(981-1029) was reduced by 50% in the presence of SEPT9 (Figure 3.4 C and D). In N2a cells, co-immunoprecipitation of endogenous KIF17 with GFP-mLin-10 was also reduced in the presence of SEPT9 (Figure 3.4 E and F).

To test whether SEPT9 has a similar effect on the interaction of KIF17 with mLin-10 in hippocampal neurons, we over-expressed SEPT9-GFP in hippocampal neurons and analyzed the localization of endogenous KIF17 with respect to mLin-10. Expression of SEPT9-GFP decreased the punctate distribution of KIF17 in dendritic processes (Figure 3.4 H and I), and reduced the percentage of KIF17-positive mLin-10 puncta from 37.6 ± 2.7% to 18.7 ± 1.8% per 10 μm of dendritic process (Figure 3.4 G). Super-resolution SIM imaging of endogenous KIF17, SEPT9 and mLin-10 showed that only 9 ± 3% (n = 17 cells) of KIF17/SEPT9 puncta contained mLin-10

(Figure 3.4 J) and SEPT9 was similarly absent from KIF17/mLin-10 puncta (Figure 3.4 K). Taken together with the biochemical evidence of a physical interference, these data indicate that SEPT9 competes with mLin-10 for binding to KIF17.

SEPT9 down-regulates the transport of NR2B cargo without interfering with the motility of KIF17

Given that SEPT9 interferes with the binding of mLin-10 to KIF17, we asked whether SEPT9 affects the intracellular transport of NR2B. We tested how SEPT9 affects first, the localization of endogenous NR2B, and second, the transport of newly synthesized GFP-NR2B. Hippocampal neurons were transfected with SEPT9-GFP or GFP, and cells were stained for endogenous NR2B using a gentle permeabilization protocol that preserved the localization of NR2B in both surface and intracellular membranes. In contrast to control cells, where NR2B outlined each dendrite, NR2B was weakly present in the dendrites of SEPT9-GFP-expressing cells (Figure 3.5 A and B; insets) and the mean intensity of NR2B was reduced by 42% (Figure 3.5 C). This effect was specific to NR2B, as SEPT9-GFP over-expression did not affect the surface levels of the potassium channel Kv4.2 (Figure 3.5 D), which is also transported by KIF17 (Chu *et al.*, 2006).

Next, we transfected hippocampal neurons with GFP-NR2B and SEPT9-mCherry or mCherry, and analyzed the distribution of surface and total GFP-NR2B. Staining of live neurons with an anti-GFP antibody prior to fixation showed that GFP-NR2B is properly transported and incorporated into the surface membranes of dendrites, forming an array of clusters that outline each dendrite (Figure 3.5 E). Compared to control cells, surface levels of GFP-NR2B decreased by 30% (Figure 3.5 F). This reduction in surface NR2B was not due to a local defect in

membrane targeting within individual dendrites, because total GFP-NR2B fluorescence was reduced in all dendrites (Figure 3.5 G) and GFP-NR2B clusters decreased by 40% from 5.6 ± 0.4 to 3.3 ± 0.3 ($p < 0.0001$) per 10 μm of dendrite. Moreover, this quantitative effect was not due to variations in GFP-NR2B expression, which was similar between cell populations that expressed mCherry and SEPT9-mCherry (66 ± 8 vs. 71 ± 8 AU/μm^2, $p = 0.6$). Thus, SEPT9 appears to down-regulate the long-range transport of NR2B.

Taken together with the diminished binding of mLin-10 to KIF17, our results suggest that SEPT9 affects the mechanism of KIF17-mediated transport of NR2B at the level of cargo-motor binding. Down-regulation of NR2B transport, however, could also stem from alterations in the motility of KIF17. To address this possibility, we used TIRF microscopy to image the motility of GFP-KIF17 in rat hippocampal neurons that expressed SEPT9-mCherry or mCherry. Quantification of GFP-KIF17 motility showed that SEPT9 over-expression had no statistically significant effect on the velocity and run lengths of KIF17 (Figure 3.5 H). Moreover, SEPT9 over-expression did not affect the percentage of KIF17 puncta that were mobile (Figure 3.5 I). Therefore, the activity and motile properties of KIF17 are not altered by SEPT9.

Discussion

Our results provide the first evidence of septin involvement in kinesin-cargo interactions, and raise the possibility that septins may act as regulators of cargo-motor binding. Similar to other scaffolding proteins (e.g., Hook-1) that bind kinesins (Bielska, 2014; Walenta et al., 2001), septins interact with both MTs and cell membranes (Spiliotis and Gladfelter, 2012). Interestingly, SEPT9 has been reported to associate with the c-Jun-N-terminal kinase (JNK), which is reminiscent of the JNK-interacting proteins (JIP) that interact with kinesin 1 and the dynein/dynactin complex (Fu and Holzbaur, 2013; Gonzalez et al., 2009; Sun et al., 2011; Verhey and Rapoport, 2001). In contrast to JIP1, which regulates motor activity by relieving the autoinhibition of kinesin 1 (Blasius et al., 2007; Fu and Holzbaur, 2013), SEPT9 is not likely to affect the autoinhibition of KIF17, because first, SEPT9 interacts preferentially with the C-terminal tail of KIF17 in its extended cargo-binding conformation, and second, SEPT9 does not affect the motility of KIF17 in living neurons.

Our results suggest that SEPT9 could affect the loading of cargo to KIF17 or trigger the release of cargo from KIF17. To date, it is unknown whether SEPT9 associates with specific organelles or membrane cargo, but SEPT2 and SEPT7 have been reported to interact respectively with the cytoplasmic tail of the GLAST glutamate receptor and the adaptor protein AP3 (Baust et al., 2008; Kinoshita et al., 2004). Thus, SEPT9 could link KIF17 to specific cargo directly or indirectly through hetero-oligomerization with other membrane-bound septin subunits. Alternatively, septins could influence cargo selection by rendering the tail of KIF17 unavailable to other cargo adaptor/scaffold proteins (e.g., mLin-10). In the context of brain development, high levels of SEPT9 expression may inhibit the transport of NR2B in late gestation when KIF17, NR2B and the mLin10 complex are initially expressed (Setou et al., 2000; Tsang et al., 2011).

The inhibition of KIF17-mLin10 binding by SEPT9, which interacts preferentially with the cargo-binding conformation of KIF17, and the partial colocalization of SEPT9 with KIF17 suggest that SEPT9 triggers the release of cargo by binding KIF17 selectively and/or transiently. Thus, SEPT9 may provide a new mechanism for the unloading of KIF17 cargo under the control of spatial and temporal cues. Given that septins localize to dendritic branch points and at the base of protrusive structures including dendritic spines, axonal filopodia and primary cilia (Hu et al., 2012; Hu et al., 2010; Tada et al., 2007; Xie et al., 2007), septins could mediate the release of cargo at these intracellular sites and compartments. Future studies will further explore a septin-mediated regulation of cargo-motor interactions and its significance for the spatiotemporal control of intracellular transport.

Figures:

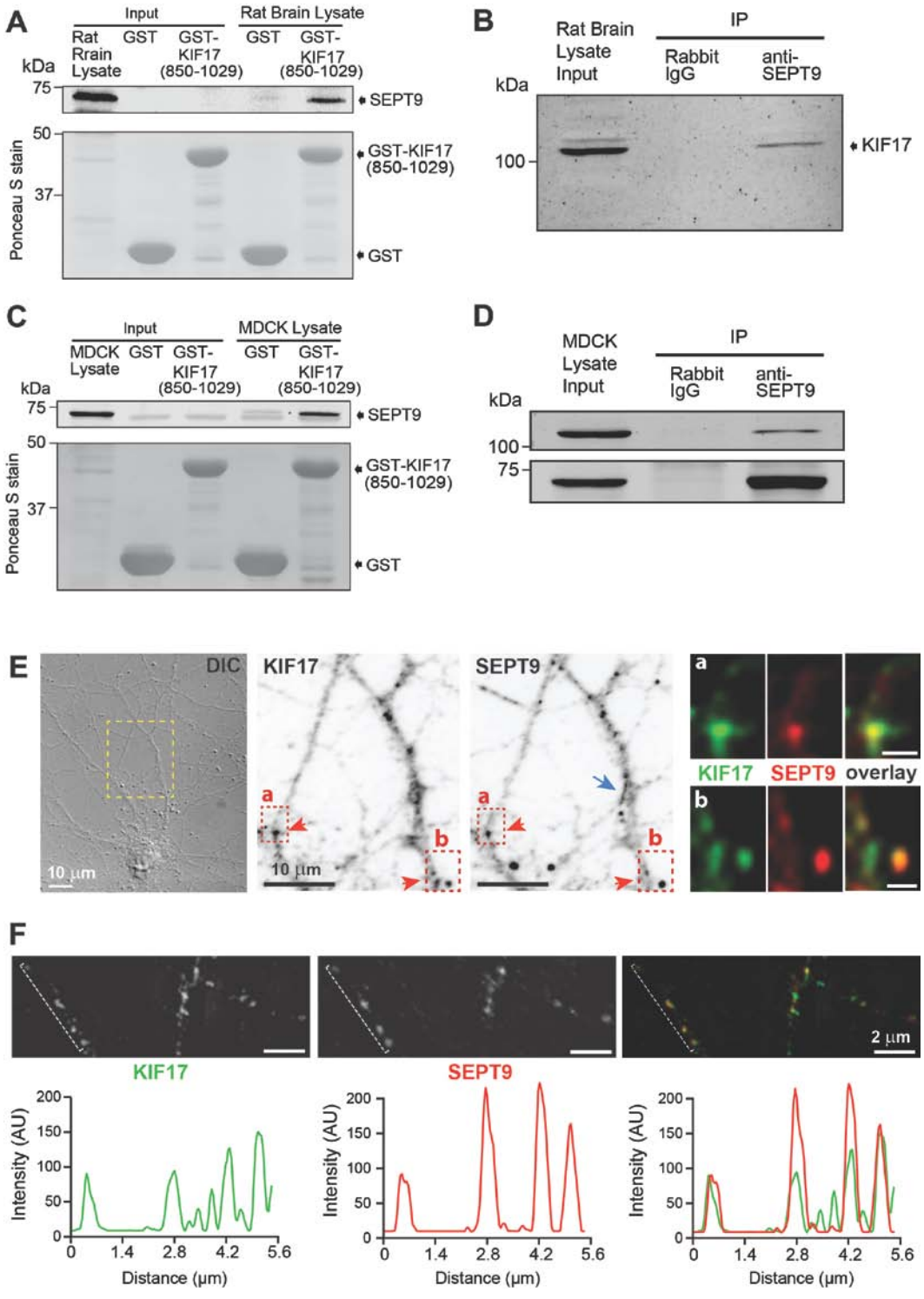
A
Input
Rat Brain Lysate
Rat Rrain Lysate
GST
GST-KIF17 (850-1029)
GST
GST-KIF17 (850-1029)
kDa
75
SEPT9
50
37
Ponceau S stain
GST-KIF17 (850-1029)
GST
B
Rat Brain Lysate Input
IP
Rabbit IgG
anti-SEPT9
kDa
100
KIF17
C
Input
MDCK Lysate
MDCK Lysate
GST
GST-KIF17 (850-1029)
GST
GST-KIF17 (850-1029)
kDa
75
SEPT9
50
37
Ponceau S stain
GST-KIF17 (850-1029)
GST
D
MDCK Lysate Input
IP
Rabbit IgG
anti-SEPT9
kDa
100
75
E
DIC
KIF17
SEPT9
a
b
10 μm
KIF17
SEPT9
overlay
F
2 μm
KIF17
SEPT9
Intensity (AU)
200
150
100
50
0
0
1.4
2.8
4.2
5.6
Distance (μm)

Figure 3.1. SEPT9 interacts and partially colocalizes with KIF17.

(A) Western blot (top) of GST pull-downs from embryonic (E18) rat brain homogenate. Ponceau S-stained membrane (bottom) shows the presence of GST proteins. Input is 2% of total lysate.

(B) Western blot of immunoprecipitates from rat brain homogenates. Input is 2% of total lysate.

(C) Western blot (top) of GST pull-downs from MDCK lysate. Ponceau S-stained membrane (bottom) shows the presence of GST proteins. Input is 2% of total lysate.

(D) Western blot of immunoprecipitates from MDCK lysate. Input is 2% of total lysate.

(E) DIC and fluorescence microscopy images of a rat hippocampal neuron (DIV14) stained for KIF17 and SEPT9. Red arrows point to colocalizing SEPT9 and KIF17 puncta. Regions (a, b) outlined by dotted lines are shown in higher magnification (scale bars, ~2 μm). Blue arrow points to filamentous SEPT9.

(F) Super-resolution SIM imaging of KIF17 and SEPT9 puncta in hippocampal neurons. Line scans show the fluorescence intensity profiles of KIF17 and SEPT9 along the outlined region.

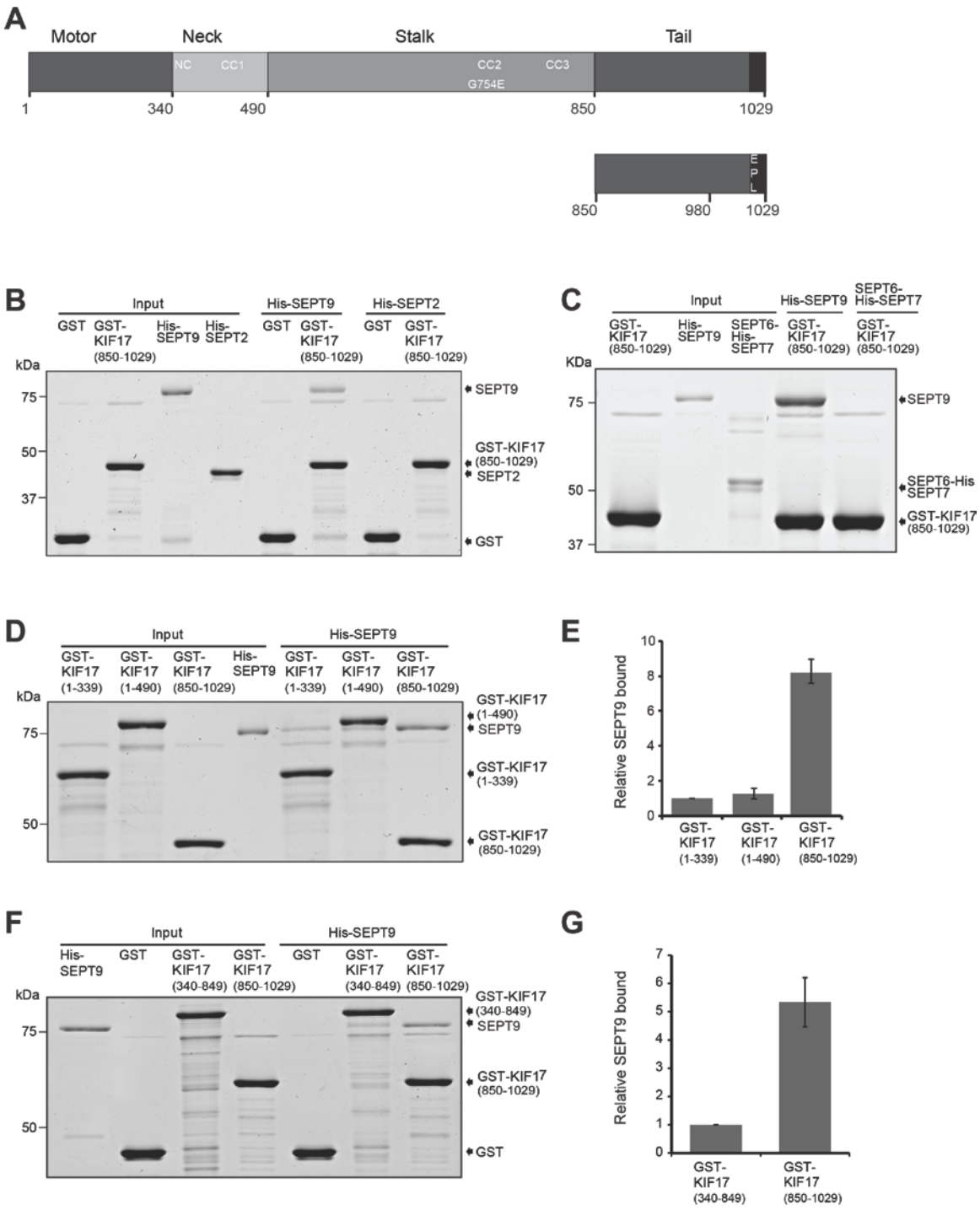
A
Motor
Neck
Stalk
Tail
NC
CC1
CC2
CC3
G754E
1
340
490
850
1029
E
P
L
980
B
Input
His-SEPT9
His-SEPT2
GST
GST-KIF17 (850-1029)
His-SEPT9
His-SEPT2
kDa
75
50
37
SEPT9
GST-KIF17 (850-1029)
SEPT2
GST
C
Input
His-SEPT9
SEPT6-His-SEPT7
GST-KIF17 (850-1029)
His-SEPT9
SEPT6-His-SEPT7
KDa
SEPT9
SEPT6-His SEPT7
GST-KIF17 (850-1029)
D
Input
His-SEPT9
GST-KIF17 (1-339)
GST-KIF17 (1-490)
GST-KIF17 (850-1029)
His-SEPT9
kDa
GST-KIF17 (1-490)
SEPT9
GST-KIF17 (1-339)
GST-KIF17 (850-1029)
E
Relative SEPT9 bound
GST-KIF17 (1-339)
GST-KIF17 (1-490)
GST-KIF17 (850-1029)
F
Input
His-SEPT9
His-SEPT9
GST
GST-KIF17 (340-849)
GST-KIF17 (850-1029)
kDa
GST-KIF17 (340-849)
SEPT9
GST-KIF17 (850-1029)
GST
G
Relative SEPT9 bound
GST-KIF17 (340-849)
GST-KIF17 (850-1029)

Figure 3.2. SEPT9 associates directly with the C-terminal tail of KIF17.

(A) Schematic shows the boundaries of the motor, neck, stalk and tail domains of KIF17. The position of the G754E mutation, neck coil (NC) and coiled coil (CC) domains, and the EPL site involved in the binding of the PDZ domain of mLin-10/Mint1 are shown.

(B) Coomassie-stained SDS-PAGE gel shows the cosedimentation of His-SEPT9 or His-SEPT2 with GST or GST-KIF17(850-1029).

(C) Coomassie-stained SDS-PAGE gel shows that His-SEPT9 cosediments with GST-KIF17(850-1029), but SEPT6/His-SEPT7 does not.

(D) Coomassie-stained gel shows the co-sedimentation of His-SEPT9 with GST-tagged KIF17(1-339), KIF17(1-490) or KIF17(850-1029).

(E) Bar graph shows relative His-SEPT9 binding after quantification of His-SEPT9 band intensities and normalization to GST-tagged protein bands. The amount of His-SEPT9 cosedimented with GST-KIF17(1-339) was set to 1. Error bars correspond to the highest and lowest values from three independent experiments.

(F) Coomassie-stained SDS-PAGE gel shows that His-SEPT9 cosediments preferentially with GST-KIF17-TAIL (amino acids 850-1029) compared to GST-KIF17(340-849), which contains the neck and stalk domains of KIF17. Dotted rectangle outlines that position of the SEPT9 protein band.

(G) Bar graph shows the amount of His-SEPT9 bound to GST-KIF17-TAIL relative to GST-KIF17(340-849) after quantification of SEPT9 band intensities and normalization to GST-tagged protein bands. The amount of His-SEPT9 cosedimented with GST-KIF17(340-849) was set to 1. Error bars correspond to the highest and lowest values from three independent experiments.

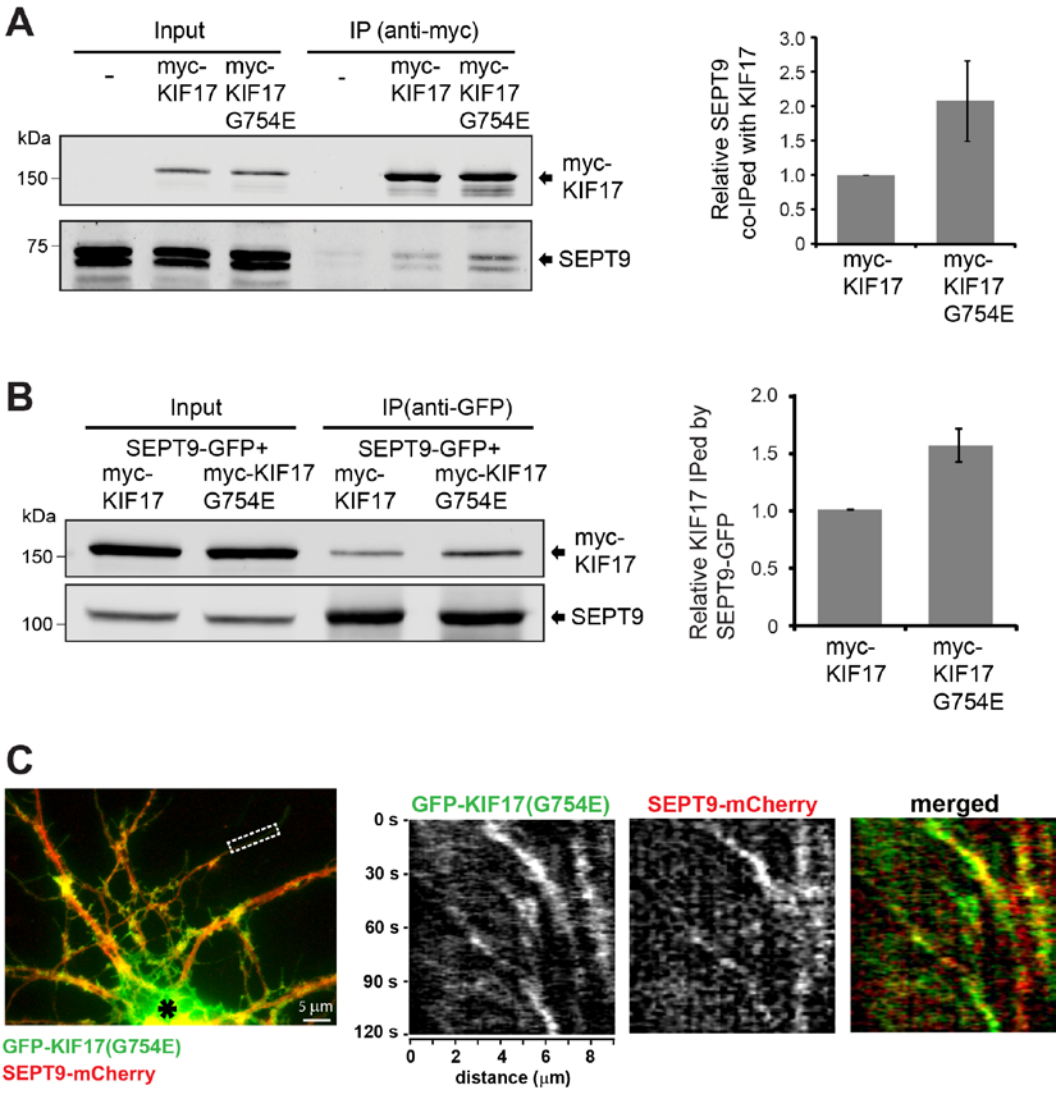
A
Input
IP (anti-myc)
-
myc-KIF17
myc-KIF17 G754E
kDa
150
75
myc-KIF17
SEPT9
Relative SEPT9 co-IPed with KIF17
3.0
2.5
2.0
1.5
1.0
0.5
0
myc-KIF17
myc-KIF17 G754E
B
Input
IP(anti-GFP)
SEPT9-GFP+
myc-KIF17
myc-KIF17 G754E
kDa
150
100
myc-KIF17
SEPT9
Relative KIF17 IPed by SEPT9-GFP
2.0
1.5
1.0
0.5
0
myc-KIF17
myc-KIF17 G754E
C
5 µm
GFP-KIF17(G754E)
SEPT9-mCherry
GFP-KIF17(G754E)
SEPT9-mCherry
merged
0 s
30 s
60 s
90 s
120 s
0
2
4
6
8
distance (µm)

Figure 3.3. SEPT9 interacts preferentially and comigrates with the extended cargo-binding conformation of KIF17(G754E).

(A) Western blots of co-immunoprecipitations of endogenous SEPT9 with myc-tagged KIF17 or KIF17(G754E) from HEK293 lysates. Input is 2% of total lysate. Bar graph shows the relative difference in the amount of SEPT9 that co-immunoprecipitated with myc-KIF17 vs. myc-KIF17(G754E). After background subtraction, protein band intensities were quantified and the ratio of SEPT9 to KIF17 was calculated; the ratio of SEPT9 to myc-KIF17 was set to 1. Error bars show the minimum and maximum values from three independent experiments.

(B) HEK293 cells were co-transfected with SEPT9-GFP and myc-tagged KIF17 or KIF17(G754E), and immunoprecipitations were performed with anti-GFP. Precipitates were run on SDS-PAGE gels and immunoblotted with antibodies against myc and GFP. Input is 4% of total lysate. Bar graph shows the relative difference in the amount of SEPT9-GFP that co-immunoprecipitated with myc-KIF17 versus myc-KIF17(G754E). After background subtraction, protein band intensities were quantified and the ratio of SEPT9-GFP to myc-KIF17 was calculated; the ratio of SEPT9-GFP to myc-KIF17 was set to 1. Error bars show the minimum and maximum values from three independent experiments.

(C) Rat hippocampal neurons were transfected with GFP-KIF17(G754E) (green) and SEPT9-mCherry (red), and imaged by TIRF microscopy. Image shows the dendritic processes of a hippocampal neuron; cell body is denoted with a black asterisk. Kymographs show the comigration of GFP-KIF17(G754E) and SEPT9-mCherry in the region outlined with a dotted rectangle.

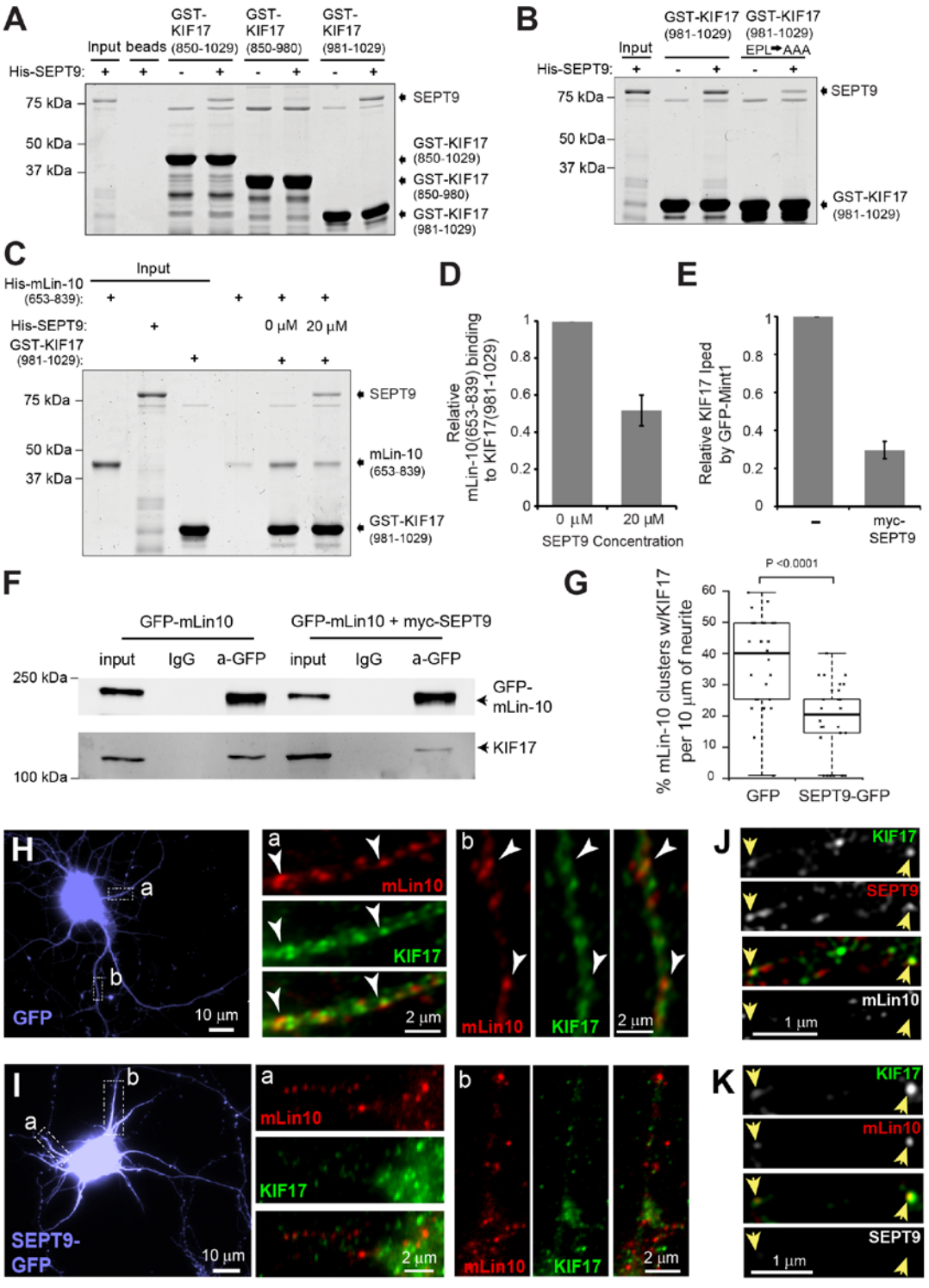
A
Input
beads
GST-KIF17 (850-1029)
GST-KIF17 (850-980)
GST-KIF17 (981-1029)
His-SEPT9:
75 kDa
50 kDa
37 kDa
SEPT9
GST-KIF17 (850-1029)
GST-KIF17 (850-980)
GST-KIF17 (981-1029)
B
Input
GST-KIF17 (981-1029)
GST-KIF17 (981-1029) EPL➡AAA
His-SEPT9:
75 kDa
50 kDa
37 kDa
SEPT9
GST-KIF17 (981-1029)
C
Input
His-mLin-10 (653-839):
His-SEPT9:
0 μM
20 μM
GST-KIF17 (981-1029):
75 kDa
50 kDa
37 kDa
SEPT9
mLin-10 (653-839)
GST-KIF17 (981-1029)
D
Relative mLin-10(653-839) binding to KIF17(981-1029)
0 μM
20 μM
SEPT9 Concentration
E
Relative KIF17 Iped by GFP-Mint1
–
myc-SEPT9
F
GFP-mLin10
GFP-mLin10 + myc-SEPT9
input
IgG
a-GFP
input
IgG
a-GFP
250 kDa
100 kDa
GFP-mLin-10
KIF17
G
P <0.0001
% mLin-10 clusters w/KIF17 per 10 μm of neurite
GFP
SEPT9-GFP
H
GFP
10 μm
mLin10
KIF17
2 μm
J
KIF17
SEPT9
mLin10
1 μm
I
SEPT9-GFP
10 μm
K
KIF17
mLin10
SEPT9
1 μm

Figure 3.4. SEPT9 interferes with the binding of mLin-10/Mint1 to the C-terminal tail of KIF17.

(A) Coomassie-stained gels show His-SEPT9 pull-down with GST-tagged KIF17(850-1029), KIF17(850-980) or KIF17(981-1029).

(B) Coomassie-stained gel shows decreased binding of SEPT9 to the mutant KIF17(981-1029)EPLAAA compared to the wild type KIF17(981-1029).

(C, D) Coomassie-stained gel (C) shows that mLin-10/Mint1(653-839) binding to KIF17(981-1029) decreases in the presence of SEPT9. Bar graph (D) shows relative binding of mLin-10/Mint1(653-839) to KIF17(981-1029); in the absence of SEPT9, binding was set to 1. Error bars correspond to the highest and lowest values from three independent experiments.

(E, F) Western blots (F) show that co-immunoprecipitation of GFP-mLin10 with KIF17 decreases in N2a cells that express myc-SEPT9. Input is 1% of total lysate. Bar graph (E) shows the relative amount of KIF17 that co-immunoprecipitates with myc-SEPT9. Error bars correspond to the highest and lowest values from three independent experiments.

(G – I) Box-and-whisker plot (G) shows the percentage of mLin-10/Mint-1 clusters, which colocalized with KIF17, per 10 µm dendrite in neurons expressing GFP (n = 28) or SEPT9-GFP (n = 35). Images show hippocampal neurons (DIV10) transfected with GFP (H) or SEPT9-GFP (I) and stained for mLin-10/Mint1 (red) and KIF17 (green). High magnification images show the localization of mLin-10/Mint-1 clusters with respect to KIF17 from dendrite regions (a, b) outlined with dotted rectangles. Arrowheads point to colocalizing KIF17 and mLin-10 puncta.

(J, K) Super-resolution SIM imaging of endogenous SEPT9, KIF17 and mLin-10. Arrowheads point to KIF17/SEPT9-positive puncta that lack mLin-10 (J), and KIF17/mLin-10-positive puncta that lack SEPT9 (K).

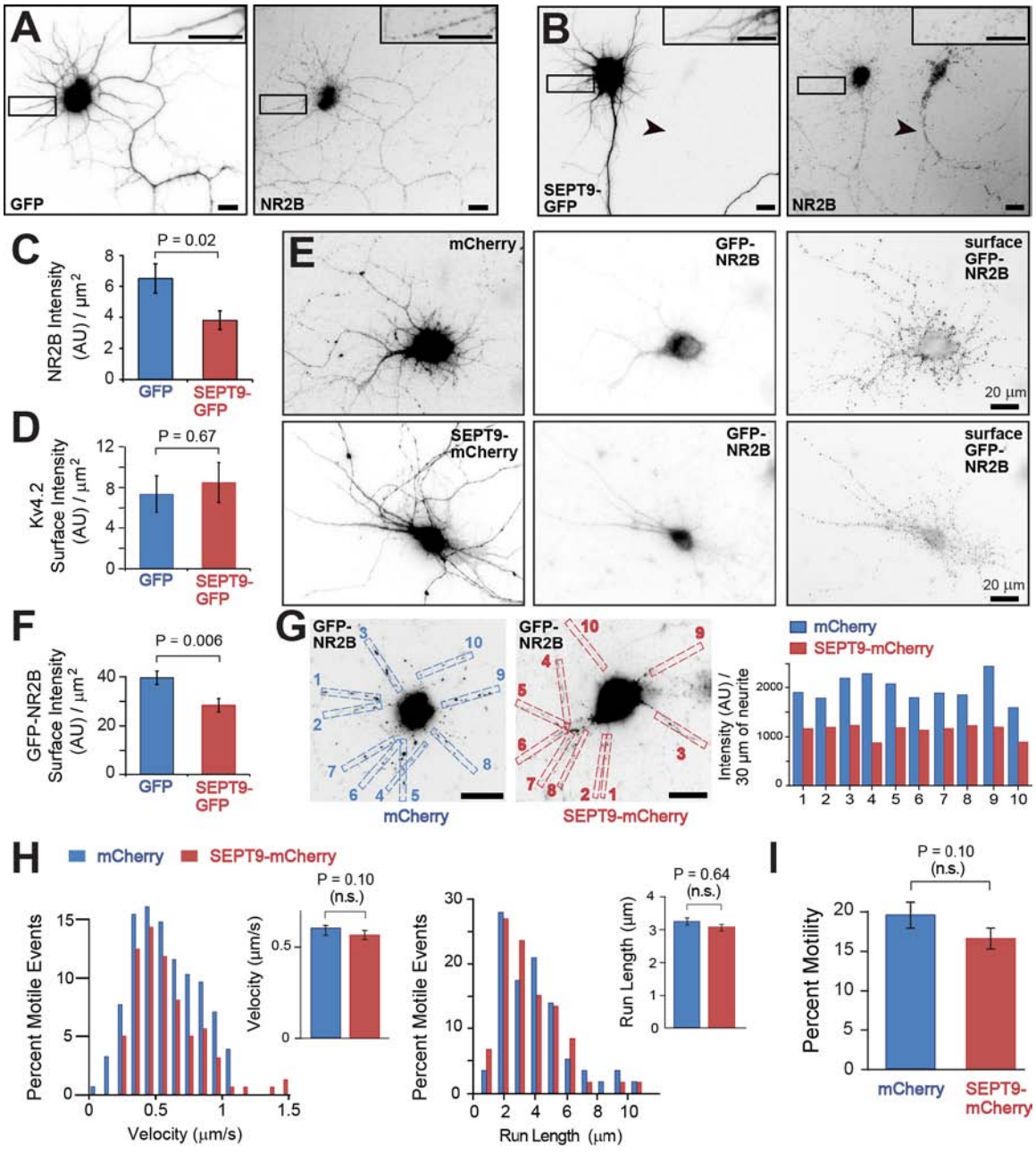
A
GFP
NR2B
B
SEPT9-GFP
NR2B
C
P = 0.02
NR2B Intensity (AU) / µm²
GFP
SEPT9-GFP
D
P = 0.67
Kv4.2 Surface Intensity (AU) / µm²
GFP
SEPT9-GFP
E
mCherry
GFP-NR2B
surface GFP-NR2B
20 µm
SEPT9-mCherry
GFP-NR2B
surface GFP-NR2B
20 µm
F
P = 0.006
GFP-NR2B Surface Intensity (AU) / µm²
GFP
SEPT9-GFP
G
GFP-NR2B
mCherry
SEPT9-mCherry
Intensity (AU) / 30 µm of neurite
H
mCherry
SEPT9-mCherry
Percent Motile Events
Velocity (µm/s)
P = 0.10 (n.s.)
Velocity (µm/s)
Percent Motile Events
Run Length (µm)
P = 0.64 (n.s.)
Run Length (µm)
I
P = 0.10 (n.s.)
Percent Motility
mCherry
SEPT9-mCherry

Figure 3.5. SEPT9 down-regulates NR2B transport without affecting KIF17 motility.

(A - C) Images show rat hippocampal neurons (DIV10) transfected with GFP (A) or SEPT9-GFP (B) and stained for endogenous NR2B using gentle permeabilization and fixation conditions. Insets show selected dendrite regions in high magnification (scale bars, 10 μm). Arrowhead points to an untransfected neuron. Bar graph (C) shows the mean (± s.e.m.) fluorescence intensity of endogenous NR2B per μm^2 for the total area of neuronal processes (n = 18 cells).

(D) Hippocampal neurons were stained live with an antibody against Kv4.2. Bar graph shows the mean (± s.e.m.) fluorescence intensity of surface Kv4.2 per μm^2 (n = 20 cells).

(E) Images show hippocampal neurons (DIV12) co-transfected with GFP-NR2B and mCherry or SEPT9-mCherry, and stained live with anti-GFP to label surface GFP-NR2B. Note that mCherry and GFP channels were equally adjusted, so dendritic processes are more visible. Surface GFP-NR2B images correspond to the raw unadjusted data, which were acquired with the same exposure.

(F) Bar graph shows the mean (± s.e.m.) intensity of surface GFP-NR2B per μm^2 for total neurite surface area (n = 25 cells).

(G) Images show total GFP-NR2B fluorescence in cells that express mCherry or SEPT9-mCherry (not shown). Histogram shows the sum fluorescence intensity of GFP-NR2B in the 30 μm-long regions of neurites, which are individually numbered and outlined with dotted rectangles.

(H) Histograms show the distribution of the velocities (n = 158) and total run lengths (n = 58) of GFP-KIF17 in live hippocampal neurons (DIV12, n = 8) that express mCherry and SEPT9-mCherry. Bar graphs show the mean (± s.e.m.) velocity and run lengths.

(I) Bar graph shows the mean (± s.e.m.) percentage of GFP-KIF17 particles that were motile in eight different neurons that express mCherry (n = 646 particles) and SEPT9-mCherry (n = 576 particles).

CHAPTER IV: Conclusions and future directions

In this thesis, I showed that the mechanism of septin interaction with microtubules (MTs) involves a novel charged repeat motif in the N-terminus of SEPT9, which is mutated in the HNA neuropathy. In addition, I found that SEPT9 affects the transport of kinesin KIF17 cargo by competing with a cargo adaptor/scaffold protein for binding to the C-terminal tail of KIF17.

Mechanism of SEPT9 interaction with MTs

A major conclusion from this PhD dissertation is that the charged repeat motifs K/R-x-x-D/E and K/R-R-x-D/E of SEPT9 bind and crosslink MTs through direct interactions with the acidic C-terminal tails of β-tubulin. The interaction between MTs and septins is electrostatic, similar to the interaction between MTs and some motor proteins and MAPs (Kotani et al., 1990; Vonmassow et al., 1989). The repeat motifs of SEPT9 most closely resemble the KKE repeat motifs of the microtubule-binding domain of MAP1A/B (Cravchik et al., 1994). However, the K/R-R/x-x-D/E repeats of SEPT9 cannot be identified in other MAPs or motor proteins, suggesting that SEPT9 interacts with MTs through a novel mechanism. These repeats appear to mediate trans-interactions between SEPT9 molecules through electrostatic binding between the extra arginines in dibasic repeats (K/R-R-x-D/E) and acidic residues in the monobasic repeats (K/R-x-x-D/E), leading to the cross linking and bundling of MTs. This mechanism resembles the electrostatic zippering between the basic and acidic repeat motifs of tau that links two MTs together (Rosenberg et al., 2008). Sequence blast suggested that the novel repeats that we identified in SEPT9 N-terminus are present in other septins, especially for these in SEPT6 group (Figure 4.1). In many of these septins, these repeats cluster in their C-terminus, suggesting that the mechanism for MT binding might vary among septins.

As suggested by the data in Chapter II, septin heteromers SEPT6/7/9 bundle MTs more efficiently than SEPT9 alone or the heteromeric SEPT2/6/7. This finding indicates that SEPT9-containing complexes have stronger MT-binding affinities and are more potent MT crosslinkers than SEPT9 alone. Septins are a family of multiple proteins. Septin heteromeric complexes with different combinations of septin monomers have been identified (Sellin et al., 2014; Weirich et al., 2008). Thus it would be very helpful to understand how septin heteromers with different subunits perform a specific function such as MT binding and bundling.

My results indicate that SEPT9 interacts preferentially with the C-terminal tails of βII tubulin. β tubulin-isotypes exhibit more complex and variable tissue distributions than α-isotypes, and the expression of specific isotypes is important in many cell activities (Janke, 2014). For example, βII tubulin transcripts increase in differentiating normal human epidermal keratinocytes (NHEK) cells, the predominant cell type in the epidermis, and the distribution of βII tubulin expression varies in different epidermal tissues (Lee et al., 2005). In addition, the intracellular distribution of βII tubulin changes during differentiation of NHEK cells (Lee et al., 2005). In future work, it would be interesting to test whether the specific distribution pattern of septins could be determined by the expression of βII tubulin in NHEK cells. Expression of βII tubulin isotype occurs mostly in neurites after differentiation and is crucial for neurite outgrowth (Guo et al., 2010). This is consistent with the preferential interaction of SEPT9 with βII tubulin and the effects of SEPT9 on asymmetric neurite growth, which in turn is dependent on the MT-binding and bundling domain of SEPT9. MT bundling by SEPT9 might also be involved in Alzheimer's disease and Pick's disease as βII aggregates in the brain of these patients with phospho-tau (Puig et al., 2005). βII mRNA expression in chronically injured neurons increases after a second spinal cord injury (Storer and Houle, 2003), which might increase SEPT9 mediated MT bundling and asymmetric neurite development to promote neuronal repair. Mutation of βII tubulin associates

with Simplified Gyral Patterning, Infantile-Onset Epilepsy and abnormalities of brain morphology (Jaglin et al., 2009), and can also lead to asymmetrical polymicrogyria (Cushion et al., 2014). These mutations impair formation of tubulin heterodimers, which might decrease SEPT9 mediated MT bundling and asymmetric neurite growth; therefore contribute to the pathogenesis of these diseases.

Previous and recent work show that septins associate with polyglutamylated microtubules and contribute to epithelial polarity and resistance of cancer cell to microtubule-targeting drugs (Froidevaux-Klipfel et al., 2015; Spiliotis et al., 2008). The MTs used in this thesis research were made with bovine brain tubulin, which is highly glutamylated (Audebert et al., 1993). Glutamylation increases the negative charge of tubulin C-terminal tail, therefore, polyglutamylation of MTs might be involved in regulation of septin-MTs association. The length of MT polyglutamylation side chain might also affect SEPT9-MT interaction, as MAP1B, MAP2 and tau binds to moderately-glutamylated tubulin, while MAP1A binds to MTs with longer polyglutamyl chains (Bonnet et al., 2001). Interestingly, a new study shows that septins can scaffold polyglutamylation enzymes to fine tune the length of glutamate side chain, and in turn, MT polyglutamylation promotes septin binding to MTs. (Froidevaux-Klipfel et al., 2015).

In future work, it is also important to understand how the interaction between septins and MTs is regulated besides polyglutamylation. The interaction between MAPs and MTs can be regulated in multiple ways. For example, tubulin isoform polymorphism has been shown to affect the binding of tau to MTs (Bonnet et al., 2001; Larcher et al., 1996) and phosphorylation/dephosphorylation of specific residues in MAP2 and tau have been found to affect their MT affinity (Trinczek et al., 1995). Multiple tubulin PTMs also affect MAP-MTs association. For example, tyrosination/ detyrosination alters MT binding by the CAP-Gly domain of certain MAPs (Bieling et al., 2008) and acetylation increases KIF5 binding (Konishi and Setou,

2009). Finally, some MAPs can regulate MT binding of other MAPs. For instance, MAP1B can sequester EBs in the cytosol of extending neurites/axons of developing neuronal cells, and MAP2 can recruits EB3 to MT bundles in dendrites of mature neurons (Sayas and Avila, 2014). Since the direct interaction between SEPT9 and MTs is now determined, and the regulation of the interaction is unknown, it would be helpful to study whether this interaction is regulated by other MAPs.

PTMs of septins have been studied in the past years. SUMOylation, acetylation and phosphorylation of septins have been identified and shown to affect their membrane association, polymerization, subcellular localization and nucleotide binding/hydrolysis (Hernandez-Rodriguez and Momany, 2012; Mostowy and Cossart, 2012). Phosphorylation of yeast septins has been reported and found to regulate filaments formation of septins and affect cell viability (Meseroll et al., 2013). In human septins, we also found some sites in SEPT9 that might be phosphorylated by kinases such as PKA/PKC and GSK-3 in between the novel charged repeats (Figure 4.2 A). Visual binding assays showed the phosphomimetic mutations of these residues decrease the MT bundling by SEPT9 (Figure 4.2 B). Therefore, the phosporylation of these residues and other PTMs are likely to regulate MT binding and bundling properties of SEPT9. In addition, septin PTMs might affect the dynamics of septin structures, which would further impact the association between SEPT9 and MTs. It is therefore necessary to identify the post-translational modifications in septins, and test their role in MT binding and bundling.

Function of MT-SEPT9 interactions

The direct interaction between SEPT9 and MTs enables the formation of MT bundles and induces MT bundling, which is important for the development of asymmetric neurite growth. Similar to the effects of tau on asymmetric neurite development (Caceres et al., 1991), neurite

asymmetry is affected by the basic region of N-terminal domain of SEPT9, which contains the MT-binding and bundling repeat motifs. Because SEPT9 has multiple isoforms, most of which differ in the length and sequence of the N-terminus, changes in the expression level of different SEPT9 isoforms would affect the process of neurite development. Septin PTMs, which might regulate the MT bundling property of SEPT9, would therefore also affect asymmetric neurite development. Finally, since the SEPT9 mutation associated with HNA has been found to decrease MT bundling and asymmetric neurite development, it might be possible to reverse the disease development process by enhancing MT bundling with SEPT9 or other MT-bundling MAPs. This approach could be potentially useful for the regeneration of injured neurons of the spinal cord.

MT-associated SEPT9 might affect the interaction of kinesin motors with MTs, similar to the effects of tau, which can reverse the direction of dynein and/or result in the detachment of kinesins from MTs (Dixit et al., 2008). As shown in this thesis, MT-bound SEPT9 does not affect the motility or run length of the kinesin 2 motor KIF17. However, on-going work in the lab indicates that MT-associated SEPT9 affects the motility of kinesin 1 and kinesin 3 motors. The detailed mechanism is still not clear but preliminary data have shown that SEPT9 directly interacts with the motor domain of KIF1A, suggesting that SEPT9 might increase the MT attachment of some motor proteins like KIF1A. The differential effects of SEPT9 on kinesin motors indicate that other septins might also regulate the motility of motor proteins. Since the septin family has many members and each one has multiple isoforms, septins might control the activities of motor proteins in a very precise manner through different members. In addition, since PTMs of MTs affect the motility of motor proteins, for example, polyglutamylation of β-tubulin increases the motility of kinesin-1 and detyrosination of α-tubulin increases the motility of kinesin-2 (Sirajuddin et al., 2014), the effect of septins on intracellular transport might also be related to the PTM status of MTs.

Septins promote persistent MT growth and suppress MT catastrophe (Bowen et al., 2011). They also regulate plus end dynamics of MTs in polarizing epithelia, and guide the directionality of MT plus end movement (Bowen et al., 2011). The navigation of MTs by septins is essential for the maintenance of perinuclear MT bundles and the orientation of peripheral MTs as well as for the apicobasal positioning of MTs (Bowen et al., 2011). These functions of septins are likely due to the indirect interaction with MTs and SEPT9. In addition to SEPT9, other subunits within septin complexes might mediate septin-MT interactions. For example, SEPT7 can also bind to MTs directly. In axons of sensory neurons, SEPT7 accumulates at incipient sites of filopodia formation, promoting the entry of axonal MTs into filopodia and thus, enabling the formation of collateral branches (Hu et al., 2012).

Although septin filaments are less dynamic than MTs (Bowen et al., 2011), septin dynamics are functionally important for exocytosis (Tokhtaeva et al., 2015). The GTPase activity has been shown to be involved in regulation of septin filaments formation. The binding of GDP to septins seems to stabilize septin filaments, similar to the effect of GTP to MTs (Mendoza et al., 2002), however, the details are still elusive and more work is needed to understand the role of GTP/GDP in how septins function. PTMs might also provide additional regulation of the dynamics of septin filaments.

Septins and actin are interdependent in some cell types (Schmidt and Nichols, 2004). SEPT9 can directly bundle actin filaments (Dolat et al., 2014b), and the direct interaction between septins and actin enables septins to stabilize nascent focal adhesions and affect the organization of the lamellar stress fiber network (Dolat et al., 2014b). In the axons of sensory neurons, SEPT6 also accumulates at incipient sites of filopodia formation similar to SEPT7, but it has distinct distribution pattern compared with SEPT7 (Hu et al., 2012). SEPT6 localizes to

axonal patches of F-actin and increases the recruitment of cortactin, a regulator of Arp2/3-mediated actin polymerization, triggering the emergence of filopodia (Hu et al., 2012).

The ability of septins to associate with both microtubules and actin suggests that septins can mediate a cross talk between these two cytoskeletons. In sensory neurons, immunodepletion of SEPT6 leads to partial depletion of SEPT7 (Hu et al., 2012), suggesting that SEPT6 and SEPT7 can function together but also independently in coordinating the activities of microtubule and actin during the axon branching process.

In the Chapter II of this thesis, I found that SEPT9_i4, which lacks the MT-binding/bundling repeat motifs, increases the percentage of cells with multiple neurites, compared with the control cells. Besides the possibility that SEPT9_i4 may compete with the endogenous SEPT9_i1 for incorporating into septin complexes, decreasing MT bundling and affecting neurite development, it is also possible that SEPT9_i4 may affect actin organization and promote the generation of multiple neurites.

Since septins function mostly as a complex, it is possible that incorporation of different septin proteins into a complex may change the distribution and function of septins with respect to the MT and actin cytoskeletons. Individual septin subunits might be responsible for interacting with different cytoskeletal systems, facilitating the cross talk between different structures. This effect can be further enhanced through the dynamic property of septin filaments, which allows the exchange of subunits in a septin complex. In addition, post-translational modifications (PTMs) may also affect septin assembly and distribution. Future work is necessary to explore these possibilities.

Regulation of kinesin-cargo interactions

In addition to their interaction with microtubule and actin, septins associate with membranes and are also found in the cytoplasm. Through their polybasic region, septins interact directly with phospholipids (Zhang et al., 1999) and can assemble into oligomeric structures on membranes (Bridges et al., 2014), affecting membrane structures and dynamics (Gilden et al., 2012; Tanaka-Takiguchi et al., 2009). Septin-membrane interactions also enable septins to form a diffusion barrier at the base of cilia, dendritic spines and the sperm annulus (Helge Ewers 2014; Hu et al., 2010; Kwitny et al., 2010).

Here, we found that SEPT9 regulates the KIF17-mediated transport of the NR2B protein by competing with the cargo adaptor/scaffold protein Mint1/mLin-10. This might be an alternative mechanism for NR2B-containing cargo to unload from KIF17, besides the known unloading mechanism, which involves phosphorylation of the C-terminal tail of KIF17 by the CamKII kinase (Guillaud et al., 2008). Interestingly, SEPT9 can dissociate mLin-10 from a KIF17 mutant, which cannot be phosphorylated by CamKII (Figure 4.3). The intracellular location at which SEPT9 triggers the unloading of cargo from KIF17 is unknown. However, since septins have been found to concentrate at the base of spines and neurite branch points (Helge Ewers 2014; Tada et al., 2007), it is possible that SEPT9 promotes the unloading of KIF17 cargo at these destinations.

Alternatively, SEPT9 may function as a cargo adaptor/scaffold for KIF17, similar to other scaffolding proteins (e.g., Hook-1) that bind kinesins (Bielska, 2014; Walenta et al., 2001). To date, it is unknown whether SEPT9 associates with specific organelles or membrane cargo, but SEPT2 and SEPT7 have been reported to interact respectively with the cytoplasmic tail of the GLAST glutamate receptor and the adaptor protein AP3 (Baust et al., 2008; Kinoshita et al., 2004). Thus, SEPT9 could link KIF17 to specific cargo directly or indirectly through hetero-

oligomerization with other membrane-bound septin subunits. Alternatively, septins could influence cargo selection by rendering the tail of KIF17 unavailable to other cargo adaptor/scaffold proteins (e.g., mLin-10). In addition, preliminary data have suggested that SEPT9 might increase the interaction between KIF17 and CamkII (Data not shown), which might result to increased phosphorylation of KIF17 and further promote the release of NR2B containing cargo. Therefore, it is possible that SEPT9 and other septins can scaffold the interaction between motor proteins with their regulators and cargo. Further studies will help us to better understand the related roles of septins.

Recent work has shown that KIF17 interacts with the MT plus end protein EB1 and contributes to the MT stabilization in epithelial cells (Acharya et al., 2013; Jaulin and Kreitzer, 2010). Work from our lab has shown that septins can affect the directionality of MT growth, providing directional guidance cues necessary for the establishment of the apical microtubule network in polarizing epithelia (Bowen et al., 2011). Since SEPT9 interacts directly with the tail of KIF17, it is possible that MT-associated SEPT9 can interact with MT plus ends that contain KIF17 and EB1. This may provide a mechanism for the capture of MT plus ends by septin coated MT bundles. Alternatively, SEPT9 could be transported to the MT plus ends by KIF17. Future studies will address these possibilities.

Figures:

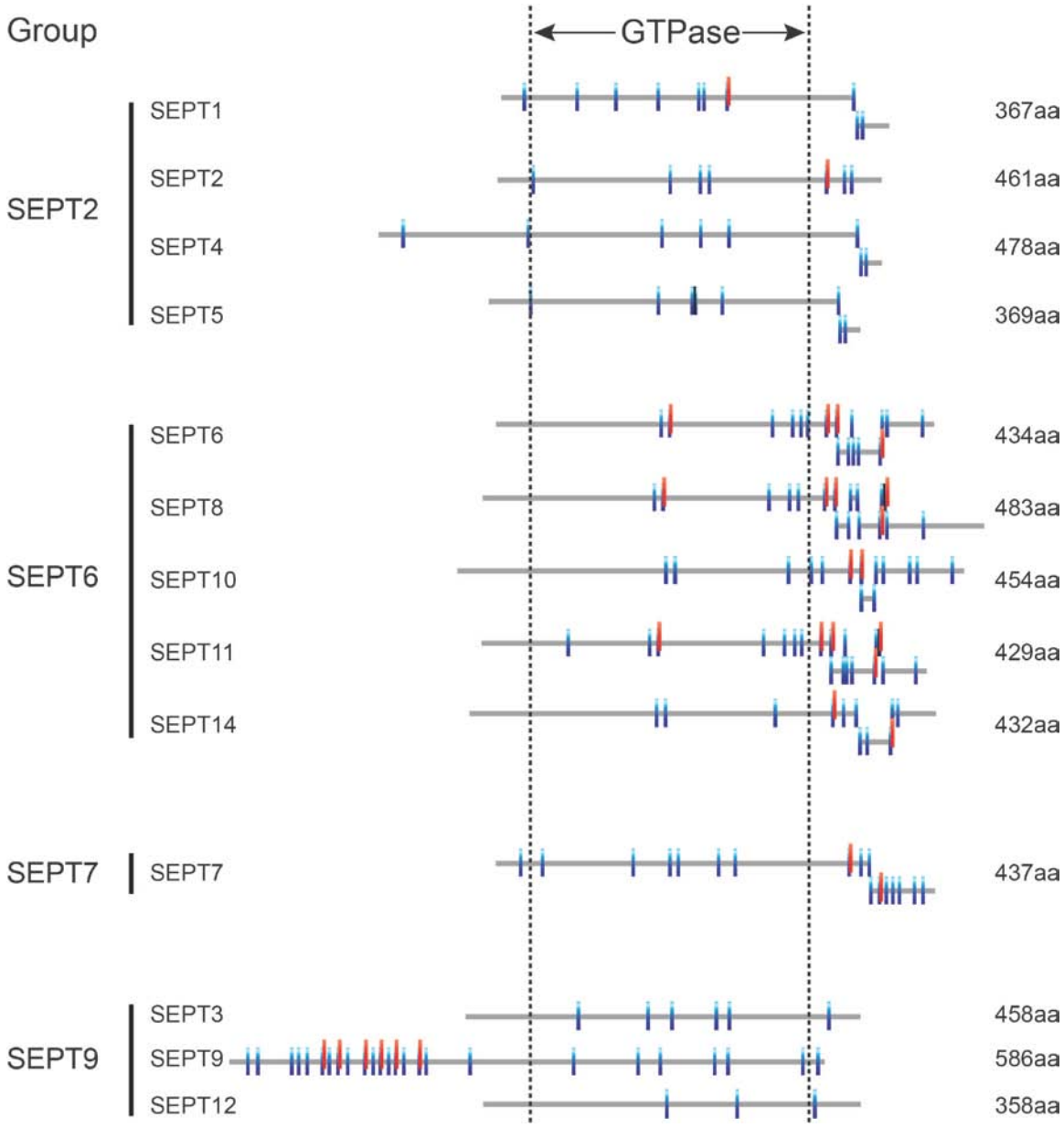
Group
GTPase
SEPT2
SEPT1
SEPT2
SEPT4
SEPT5
367aa
461aa
478aa
369aa
SEPT6
SEPT6
SEPT8
SEPT10
SEPT11
SEPT14
434aa
483aa
454aa
429aa
432aa
SEPT7
SEPT7
437aa
SEPT9
SEPT3
SEPT9
SEPT12
458aa
586aa
358aa

Figure 4.1. Charged repeat motifs in human septins

A protein sequence blast for [R/K]-x-x-[D/E] and [R/K]-[R/K]-x-[D/E] motif in human septins was performed. The distribution of charged repeat motifs relative to their GTPase domains in each septin is shown. Each blue vertical bar represents a [R/K]-x-x-[D/E] motif, and each red vertical bar represents a [R/K]-[R/K]-x-[D/E] motif.

A

MKKSYSGGTRTSSGRLRRLGDSSGPALKRSFEVEEVETPNSTPPRRVQTPLLRATVASSTQ

KFQDLGVKNSEPSARHVDSLSQRSPKASLRRVELSGPKAAEPVSRRTELSIDISSKQVENA

GAIGPSRFGLKRAEVLGHKTPEPAPRRTEITIVKPQESAHRRMEPPASKVPEVPTAPATDA

APKRVEIQMPKPAEAPTAPSPAQTLENSEPAPVSQLQSRLEPKPQPPVAEATPRSQEATEA

APSCVGDMADTPRDAGLKQAPASRNEKAPVDFGYVGIDS

(30) (80) (82) (85) (111) (115, 116)

*: putitive PKA/PKC kinase phosphorylation site

^: putitive GSK-3 kinase phosphorylation site

B

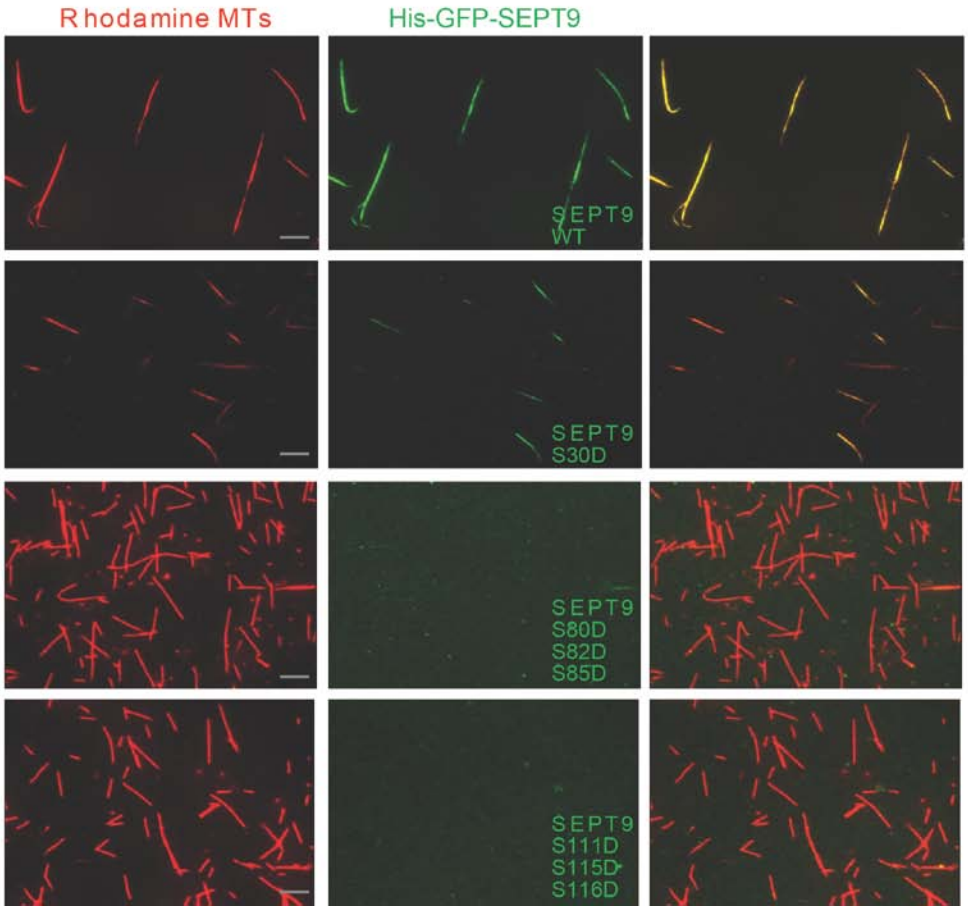

Figure 4.2. Phosphomimetic mutations of SEPT9 affect MT binding and bundling by SEPT9

(A) *PhosphoMotif Finder* of Human Protein Reference Database (HPRD) was used to predict the potential phosphorylation sites in SEPT9 N-terminus. Putative phosphorylation sites of PKA/PKC kinase or GSK-3 kinase were labeled with stars and arrowheads, respectively. Repeat motifs were underlined. Serines labeled with numbers were mutated in B. (B) His-GFP tagged SEPT9 wild type (WT) or with the indicated phosphomimetic mutations were expressed and purified from bacteria, and mixed with Rhodamine labeled MTs. Images show that phosphomimetic mutations reduce the binding and bundling of MTs by SEPT9. Scale bars: 10μm.

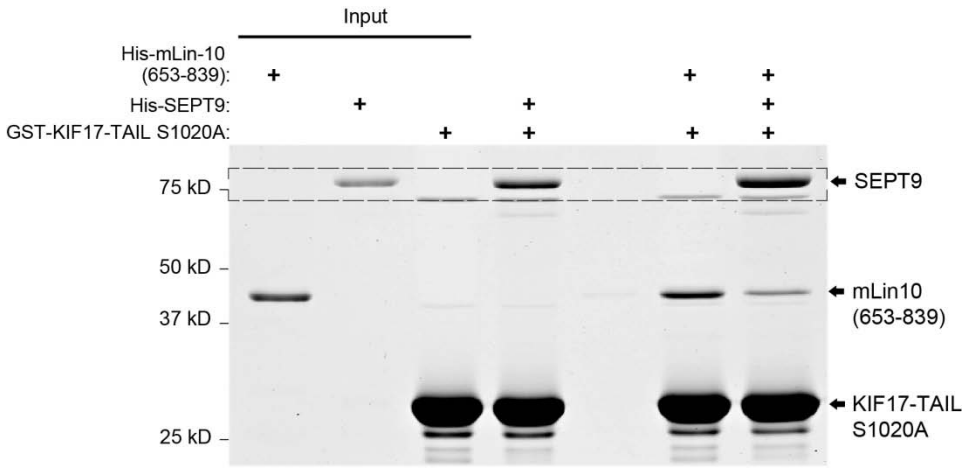

Figure 4.3. SEPT9 interferes with the binding of mLin-10/Mint1 to KIF17(850-1029) S1020A.

In vitro binding assay was performed with bacteria expressed and purified GST-KIF17 (981-1029) S1020A, His-SEPT9_i1 and His-mLin-10/Mint1(653-839). Samples were separated in SDS-PAGE gel and stained with Coomassie blue.

BIBLIOGRAPHY

Acharya, B.R., Espenel, C., and Kreitzer, G. (2013). Direct regulation of microtubule dynamics by KIF17 motor and tail domains. J Biol Chem *288*, 32302-32313.

Ackmann, M., Wiech, H., and Mandelkow, E. (2000). Nonsaturable binding indicates clustering of Tau on the microtubule surface in a paired helical filament-like conformation. Journal of Biological Chemistry *275*, 30335-30343.

Akhmanova, A., and Steinmetz, M.O. (2008). Tracking the ends: a dynamic protein network controls the fate of microtubule tips. Nat Rev Mol Cell Biol *9*, 309-322.

Akhmanova, A., and Steinmetz, M.O. (2010). Microtubule +TIPs at a glance. J Cell Sci *123*, 3415-3419.

Amir, S., Wang, R.X., Simons, J.W., and Mabjeesh, N.J. (2009). SEPT9_v1 Up-regulates Hypoxia-inducible Factor 1 by Preventing Its RACK1-mediated Degradation. Journal of Biological Chemistry *284*, 11142-11151.

Amos, L.A., and Schlieper, D. (2005). Microtubules and maps. Adv Protein Chem *71*, 257-298.

Arimura, N., Kimura, T., Nakamuta, S., Taya, S., Funahashi, Y., Hattori, A., Shimada, A., Menager, C., Kawabata, S., Fujii, K., *et al.* (2009). Anterograde Transport of TrkB in Axons Is Mediated by Direct Interaction with Slp1 and Rab27. Developmental Cell *16*, 675-686.

Atherton, J., Houdusse, A., and Moores, C. (2013). MAPping out distribution routes for kinesin couriers. Biol Cell *105*, 465-487.

Audebert, S., Desbruyeres, E., Gruszczynski, C., Koulakoff, A., Gros, F., Denoulet, P., and Edde, B. (1993). Reversible polyglutamylation of alpha- and beta-tubulin and microtubule dynamics in mouse brain neurons. Mol Biol Cell *4*, 615-626.

Audebert, S., Koulakoff, A., Berwaldnetter, Y., Gros, F., Denoulet, P., and Edde, B. (1994). Developmental Regulation of Polyglutamylated Alpha-Tubulin and Beta-Tubulin in Mouse-Brain Neurons. Journal of Cell Science *107*, 2313-2322.

Baas, P.W., Black, M.M., and Banker, G.A. (1989). Changes in microtubule polarity orientation during the development of hippocampal neurons in culture. J Cell Biol *109*, 3085-3094.

Bai, X., Bowen, J.R., Knox, T.K., Zhou, K., Pendziwiat, M., Kuhlenbaumer, G., Sindelar, C.V., and Spiliotis, E.T. (2013). Novel septin 9 repeat motifs altered in neuralgic amyotrophy bind and bundle microtubules. J Cell Biol *203*, 895-905.

Bananis, E., Nath, S., Gordon, K., Satir, P., Stockert, R.J., Murray, J.W., and Wolkoff, A.W. (2004). Microtubule-dependent movement of late endocytic vesicles in vitro: requirements for Dynein and Kinesin. Mol Biol Cell *15*, 3688-3697.

Barlan, K., Lu, W., and Gelfand, V.I. (2013). The microtubule-binding protein ensconsin is an essential cofactor of kinesin-1. Curr Biol *23*, 317-322.

Barria, A., and Malinow, R. (2002). Subunit-specific NMDA receptor trafficking to synapses. Neuron *35*, 345-353.

Basu, J., and Siegelbaum, S.A. (2015). The Corticohippocampal Circuit, Synaptic Plasticity, and Memory. Cold Spring Harb Perspect Biol *7*.

Baust, T., Anitei, M., Czupalla, C., Parshyna, I., Bourel, L., Thiele, C., Krause, E., and Hoflack, B. (2008). Protein networks supporting AP-3 function in targeting lysosomal membrane proteins. Mol Biol Cell *19*, 1942-1951.

Beise, N., and Trimble, W. (2011). Septins at a glance. Journal of Cell Science *124*, 4141-4146.

Bieling, P., Kandels-Lewis, S., Telley, I.A., van Dijk, J., Janke, C., and Surrey, T. (2008). CLIP-170 tracks growing microtubule ends by dynamically recognizing composite EB1/tubulin-binding sites. J Cell Biol *183*, 1223-1233.

Bieling, P., Laan, L., Schek, H., Munteanu, E.L., Sandblad, L., Dogterom, M., Brunner, D., and Surrey, T. (2007). Reconstitution of a microtubule plus-end tracking system in vitro. Nature *450*, 1100-1105.

Bielska, E., Schuster, M., Roger, Y., Berepiki, A., Soanes, D.M., Talbot, N.J., and Steinberg, G. (2014). Hook is an adapter that coordinates kinesin-3 and dynein cargo attachment on early endosomes. The Journal of cell biology *204*, 989-1007.

Blasius, T.L., Cai, D., Jih, G.T., Toret, C.P., and Verhey, K.J. (2007). Two binding partners cooperate to activate the molecular motor Kinesin-1. Journal of Cell Biology *176*, 11-17.

Bobinnec, Y., Moudjou, M., Fouquet, J.P., Desbruyeres, E., Edde, B., and Bornens, M. (1998). Glutamylation of centriole and cytoplasmic tubulin in proliferating non-neuronal cells. Cell Motil Cytoskel *39*, 223-232.

Bond, J.F., Fridovich-Keil, J.L., Pillus, L., Mulligan, R.C., and Solomon, F. (1986). A chicken-yeast chimeric beta-tubulin protein is incorporated into mouse microtubules in vivo. Cell *44*, 461-468.

Bongiovanni, L., Pirozzi, F., Guidi, F., Orsini, M., Chiurazzi, P., Bassi, P.F., and Racioppi, M. (2012). Bradeion (SEPT4) as a Urinary Marker of Transitional Cell Bladder Cancer: A Real-Time Polymerase Chain Reaction Study of Gene Expression. J Urology *187*, 2223-2227.

Bonnet, C., Boucher, D., Lazereg, S., Pedrotti, B., Islam, K., Denoulet, P., and Larcher, J.C. (2001). Differential binding regulation of microtubule-associated proteins MAP1A, MAP1B, and MAP2 by tubulin polyglutamylation. Journal of Biological Chemistry *276*, 12839-12848.

Borkhardt, A., Teigler-Schlegel, A., Fuchs, U., Keller, C., Konig, M., Harbott, J., and Haas, O.A. (2001). An ins(X;11)(q24;q23) fuses the MLL and the Septin 6/KIAA0128 gene in an infant with AML-M2. Genes Chromosomes Cancer *32*, 82-88.

Bosc, C., Oenarier, E., Andrieux, A., and Job, D. (1999). STOP proteins. Cell Structure and Function *24*, 393-399.

Bowen, J.R., Hwang, D., Bai, X.B., Roy, D., and Spiliotis, E.T. (2011). Septin GTPases spatially guide microtubule organization and plus end dynamics in polarizing epithelia. Journal of Cell Biology *194*, 187-197.

Bre, M.H., Redeker, V., Vinh, J., Rossier, J., and Levilliers, N. (1998). Tubulin polyglycylation: Differential posttranslational modification of dynamic cytoplasmic and stable axonemal microtubules in Paramecium. Molecular Biology of the Cell *9*, 2655-2665.

Bridges, A.A., Zhang, H., Mehta, S.B., Occhipinti, P., Tani, T., and Gladfelter, A.S. (2014). Septin assemblies form by diffusion-driven annealing on membranes. Proc Natl Acad Sci U S A *111*, 2146-2151.

Brouhard, G.J., Stear, J.H., Noetzel, T.L., Al-Bassam, J., Kinoshita, K., Harrison, S.C., Howard, J., and Hyman, A.A. (2008). XMAP215 is a processive microtubule polymerase. Cell *132*, 79-88.

Brown, C.L., Maier, K.C., Stauber, T., Ginkel, L.M., Wordeman, L., Vernos, I., and Schroer, T.A. (2005). Kinesin-2 is a motor for late endosomes and lysosomes. Traffic *6*, 1114-1124.

Bulinski, J.C., McGraw, T.E., Gruber, D., Nguyen, H.L., and Sheetz, M.P. (1997). Overexpression of MAP4 inhibits organelle motility and trafficking in vivo. J Cell Sci *110 (Pt 24)*, 3055-3064.

Burmeister, T., Meyer, C., Schwartz, S., Hofmann, J., Molkentin, M., Kowarz, E., Schneider, B., Raff, T., Reinhardt, R., Gokbuget, N., *et al.* (2009). The MLL recombinome of adult CD10-negative B-cell precursor acute lymphoblastic leukemia: results from the GMALL study group. Blood *113*, 4011-4015.

Buser, A.M., Erne, B., Werner, H.B., Nave, K.A., and Schaeren-Wiemers, N. (2009). The septin cytoskeleton in myelinating glia. Mol Cell Neurosci *40*, 156-166.

Caceres, A., Potrebic, S., and Kosik, K.S. (1991). The effect of tau antisense oligonucleotides on neurite formation of cultured cerebellar macroneurons. J Neurosci *11*, 1515-1523.

Cai, D., McEwen, D.P., Martens, J.R., Meyhofer, E., and Verhey, K.J. (2009). Single molecule imaging reveals differences in microtubule track selection between Kinesin motors. PLoS Biol *7*, e1000216.

Cai, D.W., Hoppe, A.D., Swanson, J.A., and Verhey, K.J. (2007). Kinesin-1 structural organization and conformational changes revealed by FRET stoichiometry in live cells. Journal of Cell Biology *176*, 51-63.

Cai, Q., Gerwin, C., and Sheng, Z.H. (2005). Syntabulin-mediated anterograde transport of mitochondria along neuronal processes. J Cell Biol *170*, 959-969.

Cao, L., Ding, X., Yu, W., Yang, X., Shen, S., and Yu, L. (2007). Phylogenetic and evolutionary analysis of the septin protein family in metazoan. FEBS Lett *581*, 5526-5532.

Carvalho, P., Gupta, M.L., Hoyt, M.A., and Pellman, D. (2004). Cell cycle control of kinesin-mediated transport of Bik1 (CLIP-170) regulates microtubule stability and dynein activation. Developmental Cell *6*, 815-829.

Carvalho, P., Tirnauer, J.S., and Pellman, D. (2003). Surfing on microtubule ends. Trends in Cell Biology *13*, 229-237.

Cassimeris, L. (2002). The oncoprotein 18/stathmin family of microtubule destabilizers. Current Opinion in Cell Biology *14*, 18-24.

Caudron, F., and Barral, Y. (2009). Septins and the lateral compartmentalization of eukaryotic membranes. Dev Cell *16*, 493-506.

Cerveira, N., Bizarro, S., and Teixeira, M.R. (2011). MLL-SEPTIN gene fusions in hematological malignancies. Biological Chemistry *392*, 713-724.

Cerveira, N., Correia, C., Bizarro, S., Pinto, C., Lisboa, S., Mariz, J.M., Marques, M., and Teixeira, M.R. (2006). SEPT2 is a new fusion partner of MLL in acute myeloid leukemia with t(2 ; 11)(q37 ; q23). Oncogene *25*, 6147-6152.

Chacko, A.D., McDade, S.S., Chanduloy, S., Church, S.W., Kennedy, R., Price, J., Hall, P.A., and Russell, S.E.H. (2012). Expression of the SEPT9_i4 isoform confers resistance to microtubule-interacting drugs. Cell Oncol *35*, 85-93.

Chance, P.F., and Windebank, A.J. (1996). Hereditary neuralgic amyotrophy. Curr Opin Neurol *9*, 343-347.

Chang, D.T., Honick, A.S., and Reynolds, I.J. (2006). Mitochondrial trafficking to synapses in cultured primary cortical neurons. J Neurosci *26*, 7035-7045.

Chen, J., Kanai, Y., Cowan, N.J., and Hirokawa, N. (1992). Projection Domains of Map2 and Tau Determine Spacings between Microtubules in Dendrites and Axons. Nature *360*, 674-676.

Chih, B., Liu, P., Chinn, Y., Chalouni, C., Komuves, L.G., Hass, P.E., Sandoval, W., and Peterson, A.S. (2012). A ciliopathy complex at the transition zone protects the cilia as a privileged membrane domain. Nature Cell Biology *14*, 61-U97.

Cho, K.I., Cai, Y., Yi, H., Yeh, A., Aslanukov, A., and Ferreira, P.A. (2007). Association of the kinesin-binding domain of RanBP2 to KIF5B and KIF5C determines mitochondria localization and function. Traffic *8*, 1722-1735.

Choi, P., Snyder, H., Petrucelli, L., Theisler, C., Chong, M., Zhang, Y., Lim, K., Chung, K.K.K., Kehoe, K., D'Adamio, L., *et al.* (2003). SEPT5_v2 is a parkin-binding protein. Mol Brain Res *117*, 179-189.

Chu, P.J., Rivera, J.F., and Arnold, D.B. (2006). A role for Kif17 in transport of Kv4.2. J Biol Chem *281*, 365-373.

Cleveland, D.W., Mao, Y., and Sullivan, K.F. (2003). Centromeres and kinetochores: from epigenetics to mitotic checkpoint signaling. Cell *112*, 407-421.

Cole, D.G., Diener, D.R., Himelblau, A.L., Beech, P.L., Fuster, J.C., and Rosenbaum, J.L. (1998). Chlamydomonas kinesin-II-dependent intraflagellar transport (IFT): IFT particles contain proteins required for ciliary assembly in Caenorhabditis elegans sensory neurons. J Cell Biol *141*, 993-1008.

Conacci-Sorrell, M., Ngouenet, C., and Eisenman, R.N. (2010). Myc-nick: a cytoplasmic cleavage product of Myc that promotes alpha-tubulin acetylation and cell differentiation. Cell *142*, 480-493.

Conde, C., and Caceres, A. (2009). Microtubule assembly, organization and dynamics in axons and dendrites. Nat Rev Neurosci *10*, 319-332.

Connell, J.W., Lindon, C., Luzio, J.P., and Reid, E. (2009). Spastin Couples Microtubule Severing to Membrane Traffic in Completion of Cytokinesis and Secretion. Traffic *10*, 42-56.

Connolly, D., Yang, Z., Castaldi, M., Simmons, N., Oktay, M.H., Coniglio, S., Fazzari, M.J., Verdier-Pinard, P., and Montagna, C. (2011). Septin 9 isoform expression, localization and epigenetic changes during human and mouse breast cancer progression. Breast Cancer Res *13*, R76.

Cravchik, A., Reddy, D., and Matus, A. (1994). Identification of a novel microtubule-binding domain in microtubule-associated protein 1A (MAP1A). J Cell Sci *107 (Pt 3)*, 661-672.

Craven, R.A., Hanrahan, S., Totty, N., Harnden, P., Stanley, A.J., Maher, E.R., Harris, A.L., Trimble, W.S., Selby, P.J., and Banks, R.E. (2006). Proteomic identification of a role for the von Hippel Lindau tumour suppressor in changes in the expression of mitochondrial proteins and septin 2 in renal cell carcinoma. Proteomics *6*, 3880-3893.

Creppe, C., Malinouskaya, L., Volvert, M.L., Gillard, M., Close, P., Malaise, O., Laguesse, S., Cornez, I., Rahmouni, S., Ormenese, S., *et al.* (2009). Elongator controls the migration and differentiation of cortical neurons through acetylation of alpha-tubulin. Cell *136*, 551-564.

Culver-Hanlon, T.L., Lex, S.A., Stephens, A.D., Quintyne, N.J., and King, S.J. (2006). A microtubule-binding domain in dynactin increases dynein processivity by skating along microtubules. Nature Cell Biology *8*, 264-270.

Cushion, T.D., Paciorkowski, A.R., Pilz, D.T., Mullins, J.G., Seltzer, L.E., Marion, R.W., Tuttle, E., Ghoneim, D., Christian, S.L., Chung, S.K., *et al.* (2014). De novo mutations in the beta-tubulin gene TUBB2A cause simplified gyral patterning and infantile-onset epilepsy. Am J Hum Genet *94*, 634-641.

Dehmelt, L., and Halpain, S. (2005). The MAP2/Tau family of microtubule-associated proteins. Genome Biol *6*, 204.

Dekker, C., Stirling, P.C., McCormack, E.A., Filmore, H., Paul, A., Brost, R.L., Costanzo, M., Boone, C., Leroux, M.R., and Willison, K.R. (2008). The interaction network of the chaperonin CCT. EMBO J *27*, 1827-1839.

des Portes, V., Pinard, J.M., Billuart, P., Vinet, M.C., Koulakoff, A., Carrie, A., Gelot, A., Dupuis, E., Motte, J., Berwald-Netter, Y., *et al.* (1998). A novel CNS gene required for neuronal migration and involved in X-linked subcortical laminar heterotopia and lissencephaly syndrome. Cell *92*, 51-61.

Deuel, T.A.S., Liu, J.S., Corbo, J.C., Yoo, S.Y., Rorke-Adams, L.B., and Walsh, C.A. (2006). Genetic interactions between doublecortin and doublecortin-like kinase in neuronal migration and axon outgrowth. Neuron *49*, 41-53.

Diefenbach, R.J., Diefenbach, E., Douglas, M.W., and Cunningham, A.L. (2002). The heavy chain of conventional kinesin interacts with the SNARE proteins SNAP25 and SNAP23. Biochemistry-Us *41*, 14906-14915.

Dishinger, J.F., Kee, H.L., Jenkins, P.M., Fan, S.L., Hurd, T.W., Hammond, J.W., Truong, Y.N.T., Margolis, B., Martens, J.R., and Verhey, K.J. (2010). Ciliary entry of the kinesin-2 motor KIF17 is regulated by importin-beta 2 and RanGTP. Nature Cell Biology *12*, 703-U164.

Dixit, R., Ross, J.L., Goldman, Y.E., and Holzbaur, E.L. (2008). Differential regulation of dynein and kinesin motor proteins by tau. Science *319*, 1086-1089.

Dolat, L., Hu, Q., and Spiliotis, E.T. (2014a). Septin functions in organ system physiology and pathology. Biol Chem *395*, 123-141.

Dolat, L., Hunyara, J.L., Bowen, J.R., Karasmanis, E.P., Elgawly, M., Galkin, V.E., and Spiliotis, E.T. (2014b). Septins promote stress fiber-mediated maturation of focal adhesions and renal epithelial motility. J Cell Biol *207*, 225-235.

Dougherty, G.W., Adler, H.J., Rzadzinska, A., Gimona, M., Tomita, Y., Lattig, M.C., Merritt, R.C., Jr., and Kachar, B. (2005). CLAMP, a novel microtubule-associated protein with EB-type calponin homology. Cell Motil Cytoskeleton *62*, 141-156.

Dubey, M., Chaudhury, P., Kabiru, H., and Shea, T.B. (2008). Tau inhibits anterograde axonal transport and perturbs stability in growing axonal neurites in part by displacing kinesin cargo: neurofilaments attenuate tau-mediated neurite instability. Cell Motil Cytoskeleton *65*, 89-99.

Dunn, S., Morrison, E.E., Liverpool, T.B., Molina-Paris, C., Cross, R.A., Alonso, M.C., and Peckham, M. (2008). Differential trafficking of Kif5c on tyrosinated and detyrosinated microtubules in live cells. J Cell Sci *121*, 1085-1095.

Echard, A., Jollivet, F., Martinez, O., Lacapere, J.J., Rousselet, A., Janoueix-Lerosey, I., and Goud, B. (1998). Interaction of a Golgi-associated kinesin-like protein with Rab6. Science *279*, 580-585.

Ersfeld, K., Wehland, J., Plessmann, U., Dodemont, H., Gerke, V., and Weber, K. (1993). Characterization of the tubulin-tyrosine ligase. J Cell Biol *120*, 725-732.

Espeut, J., Gaussen, A., Bieling, P., Morin, V., Prieto, S., Fesquet, D., Surrey, T., and Abrieu, A. (2008). Phosphorylation relieves autoinhibition of the kinetochore motor Cenp-E. Mol Cell *29*, 637-643.

Evans, L., Mitchison, T., and Kirschner, M. (1985). Influence of the centrosome on the structure of nucleated microtubules. J Cell Biol *100*, 1185-1191.

Fackenthal, J.D., Turner, F.R., and Raff, E.C. (1993). Tissue-specific microtubule functions in Drosophila spermatogenesis require the beta 2-tubulin isotype-specific carboxy terminus. Dev Biol *158*, 213-227.

Folker, E.S., Baker, B.M., and Goodson, H.V. (2005). Interactions between CLIP-170, tubulin, and microtubules: Implications for the mechanism of CLIP-170 plus-end tracking behavior. Molecular Biology of the Cell *16*, 5373-5384.

Ford, S.K., and Pringle, J.R. (1991). Cellular morphogenesis in the Saccharomyces cerevisiae cell cycle: localization of the CDC11 gene product and the timing of events at the budding site. Dev Genet *12*, 281-292.

Froidevaux-Klipfel, L., Targa, B., Cantaloube, I., Ahmed-Zaid, H., Pous, C., and Baillet, A. (2015). Septin cooperation with tubulin polyglutamylation contributes to cancer cell adaptation to taxanes. Oncotarget *6*, 36063-36080.

Fu, M.M., and Holzbaur, E.L. (2013). JIP1 regulates the directionality of APP axonal transport by coordinating kinesin and dynein motors. J Cell Biol *202*, 495-508.

Fu, M.M., and Holzbaur, E.L. (2014). Integrated regulation of motor-driven organelle transport by scaffolding proteins. Trends Cell Biol *24*, 564-574.

Fuchs, Y., Brown, S., Gorenc, T., Rodriguez, J., Fuchs, E., and Steller, H. (2013). Sept4/ARTS regulates stem cell apoptosis and skin regeneration. Science *341*, 286-289.

Fuchtbauer, A., Lassen, L.B., Jensen, A.B., Howard, J., Quiroga, A.D., Warming, S., Sorensen, A.B., Pedersen, F.S., and Fuchtbauer, E.M. (2011). Septin9 is involved in septin filament formation and cellular stability. Biological Chemistry *392*, 769-777.

Fujishima, K., Kiyonari, H., Kurisu, J., Hirano, T., and Kengaku, M. (2007). Targeted disruption of Sept3, a heteromeric assembly partner of Sept5 and Sept7 in axons, has no effect on developing CNS neurons. J Neurochem *102*, 77-92.

Galjart, N. (2005). CLIPs and CLASPs and cellular dynamics. Nat Rev Mol Cell Biol *6*, 487-498.

Gamblin, T.C., Nachmanoff, K., Halpain, S., and Williams, R.C. (1996). Recombinant microtubule-associated protein 2c reduces the dynamic instability of individual microtubules. Biochemistry-Us *35*, 12576-12586.

Garcia-Fernandez, M., Kissel, H., Brown, S., Gorenc, T., Schile, A.J., Rafii, S., Larisch, S., and Steller, H. (2010). Sept4/ARTS is required for stem cell apoptosis and tumor suppression. Genes Dev *24*, 2282-2293.

Gasper, R., Meyer, S., Gotthardt, K., Sirajuddin, M., and Wittinghofer, A. (2009). It takes two to tango: regulation of G proteins by dimerization. Nat Rev Mol Cell Biol *10*, 423-429.

Geeraert, C., Ratier, A., Pfisterer, S.G., Perdiz, D., Cantaloube, I., Rouault, A., Pattingre, S., Proikas-Cezanne, T., Codogno, P., and Pous, C. (2010). Starvation-induced Hyperacetylation of Tubulin Is Required for the Stimulation of Autophagy by Nutrient Deprivation. Journal of Biological Chemistry *285*, 24184-24194.

Gilden, J.K., Peck, S., Chen, Y.C., and Krummel, M.F. (2012). The septin cytoskeleton facilitates membrane retraction during motility and blebbing. J Cell Biol *196*, 103-114.

Gimona, M., Djinovic-Carugo, K., Kranewitter, W.J., and Winder, S.J. (2002). Functional plasticity of CH domains. FEBS Lett *513*, 98-106.

Gindhart, J.G., Chen, J., Faulkner, M., Gandhi, R., Doerner, K., Wisniewski, T., and Nandlestadt, A. (2003). The kinesin-associated protein UNC-76 is required for axonal transport in the Drosophila nervous system. Mol Biol Cell *14*, 3356-3365.

Glater, E.E., Megeath, L.J., Stowers, R.S., and Schwarz, T.L. (2006). Axonal transport of mitochondria requires milton to recruit kinesin heavy chain and is light chain independent. J Cell Biol *173*, 545-557.

Gleeson, J.G., Lin, P.T., Flanagan, L.A., and Walsh, C.A. (1999). Doublecortin is a microtubule-associated protein and is expressed widely by migrating neurons. Neuron *23*, 257-271.

Gonzalez, M.E., Makarova, O., Peterson, E.A., Privette, L.M., and Petty, E.M. (2009). Up-regulation of SEPT9_v1 stabilizes c-Jun-N-terminal kinase and contributes to its pro-proliferative activity in mammary epithelial cells. Cell Signal *21*, 477-487.

Gonzalez, M.E., Peterson, E.A., Privette, L.M., Loffreda-Wren, J.L., Kalikin, L.M., and Petty, E.M. (2007). High SEPT9_v1 expression in human breast cancer cells is associated with oncogenic phenotypes. Cancer Research *67*, 8554-8564.

Greer, C.A., and Shepherd, G.M. (1982). Mitral cell degeneration and sensory function in the neurological mutant mouse Purkinje cell degeneration (PCD). Brain Res *235*, 156-161.

Grigoriev, I., Gouveia, S., Van der Vaart, B., Demmers, J., Smyth, J.T., Honnappa, S., Splinter, D., Steinmetz, M.O., Putney, J.W., Hoogenraad, C.C., *et al.* (2008). STIM1 is a MT-plus-end-tracking protein involved in remodeling of the ER. Current Biology *18*, 177-182.

Grigoriev, I., Splinter, D., Keijzer, N., Wulf, P.S., Demmers, J., Ohtsuka, T., Modesti, M., Maly, I.V., Grosveld, F., Hoogenraad, C.C., *et al.* (2007). Rab6 regulates transport and targeting of exocytotic carriers. Developmental Cell *13*, 305-314.

Gross, S.P., Welte, M.A., Block, S.M., and Wieschaus, E.F. (2002). Coordination of opposite-polarity microtubule motors. J Cell Biol *156*, 715-724.

Guillaud, L., Setou, M., and Hirokawa, N. (2003). KIF17 dynamics and regulation of NR2B trafficking in hippocampal neurons. J Neurosci *23*, 131-140.

Guillaud, L., Wong, R., and Hirokawa, N. (2008). Disruption of KIF17-Mint1 interaction by CaMKII-dependent phosphorylation: a molecular model of kinesin-cargo release. Nat Cell Biol *10*, 19-29.

Gundersen, G.G., Gomes, E.R., and Wen, Y. (2004). Cortical control of microtubule stability and polarization. Current Opinion in Cell Biology *16*, 106-112.

Gundersen, G.G., Khawaja, S., and Bulinski, J.C. (1987). Postpolymerization detyrosination of alpha-tubulin: a mechanism for subcellular differentiation of microtubules. J Cell Biol *105*, 251-264.

Guo, J., Walss-Bass, C., and Luduena, R.F. (2010). The beta isotypes of tubulin in neuronal differentiation. Cytoskeleton (Hoboken) *67*, 431-441.

Guo, X., Macleod, G.T., Wellington, A., Hu, F., Panchumarthi, S., Schoenfield, M., Marin, L., Charlton, M.P., Atwood, H.L., and Zinsmaier, K.E. (2005). The GTPase dMiro is required for axonal transport of mitochondria to Drosophila synapses. Neuron *47*, 379-393.

Hagiwara, A., Tanaka, Y., Hikawa, R., Morone, N., Kusumi, A., Kimura, H., and Kinoshita, M. (2011). Submembranous Septins as Relatively Stable Components of Actin-Based Membrane Skeleton. Cytoskeleton *68*, 512-525.

Hall, P.A., Jung, K., Hillan, K.J., and Russell, S.E. (2005). Expression profiling the human septin gene family. J Pathol *206*, 269-278.

Hall, P.A., and Russell, S.E. (2004). The pathobiology of the septin gene family. J Pathol *204*, 489-505.

Hall, S.R.a.P. (2005). Do septins have a role in cancer? British Journal of Cancer *93*, 5.

Hammond, J.W., Blasius, T.L., Soppina, V., Cai, D., and Verhey, K.J. (2010a). Autoinhibition of the kinesin-2 motor KIF17 via dual intramolecular mechanisms. J Cell Biol *189*, 1013-1025.

Hammond, J.W., Cai, D.W., Blasius, T.L., Li, Z., Jiang, Y.Y., Jih, G.T., Meyhofer, E., and Verhey, K.J. (2009). Mammalian Kinesin-3 Motors Are Dimeric In Vivo and Move by Processive Motility upon Release of Autoinhibition. Plos Biology *7*, 650-663.

Hammond, J.W., Huang, C.F., Kaech, S., Jacobson, C., Banker, G., and Verhey, K.J. (2010b). Posttranslational modifications of tubulin and the polarized transport of kinesin-1 in neurons. Mol Biol Cell *21*, 572-583.

Harada, A., Oguchi, K., Okabe, S., Kuno, J., Terada, S., Ohshima, T., Satoyoshitake, R., Takei, Y., Noda, T., and Hirokawa, N. (1994). Altered Microtubule Organization in Small-Caliber Axons of Mice Lacking Tau-Protein. Nature *369*, 488-491.

Harada, A., Teng, J., Takei, Y., Oguchi, K., and Hirokawa, N. (2002). MAP2 is required for dendrite elongation, PKA anchoring in dendrites, and proper PKA signal transduction. Molecular Biology of the Cell *13*, 325a-325a.

Harper, K.M., Hiramoto, T., Tanigaki, K., Kang, G., Suzuki, G., Trimble, W., and Hiroi, N. (2012). Alterations of social interaction through genetic and environmental manipulation of the 22q11.2 gene Sept5 in the mouse brain. Hum Mol Genet *21*, 3489-3499.

Hartwell, L.H. (1971). Genetic control of the cell division cycle in yeast. IV. Genes controlling bud emergence and cytokinesis. Exp Cell Res *69*, 265-276.

Helenius, J., Brouhard, G., Kalaidzidis, Y., Diez, S., and Howard, J. (2006). The depolymerizing kinesin MCAK uses lattice diffusion to rapidly target microtubule ends. Nature *441*, 115-119.

Helge Ewers , T.T., Jennifer D. Petersen, Bence Racz, Morgan Sheng, Daniel Choquet (2014). A Septin-Dependent Diffusion Barrier at Dendritic Spine Necks. Plos One *9*.

Hernandez-Rodriguez, Y., and Momany, M. (2012). Posttranslational modifications and assembly of septin heteropolymers and higher-order structures. Curr Opin Microbiol *15*, 660-668.

Hirokawa, N., Noda, Y., Tanaka, Y., and Niwa, S. (2009). Kinesin superfamily motor proteins and intracellular transport. Nat Rev Mol Cell Biol *10*, 682-696.

Hoepfner, S., Severin, F., Cabezas, A., Habermann, B., Runge, A., Gillooly, D., Stenmark, H., and Zerial, M. (2005). Modulation of receptor recycling and degradation by the endosomal kinesin KIF16B. Cell *121*, 437-450.

Holtbernd, F., Zehnhoff-Dinnesen, A.A., Duning, T., Kemmling, A., and Ringelstein, E.B. (2011). An unusual case of neuralgic amyotrophy presenting with bilateral phrenic nerve and vocal cord paresis. Case Rep Neurol *3*, 69-74.

Homma, N., Takei, Y., Tanaka, Y., Nakata, T., Terada, S., Kikkawa, M., Noda, Y., and Hirokawa, N. (2004). Kinesin superfamily protein 2A (KIF2A) functions in suppression of collateral branch extension. Cell Structure and Function *29*, 55-55.

Honnappa, S., John, C.M., Kostrewa, D., Winkler, F.K., and Steinmetz, M.O. (2005). Structural insights into the EB1-APC interaction. EMBO J *24*, 261-269.

Honnappa, S., Okhrimenko, O., Jaussi, R., Jawhari, H., Jelesarov, I., Winkler, F.K., and Steinmetz, M.O. (2006). Key interaction modes of dynamic +TIP networks. Mol Cell *23*, 663-671.

Horiguchi, K., Hanada, T., Fukui, Y., and Chishti, A.H. (2006). Transport of PIP3 by GAKIN, a kinesin-3 family protein, regulates neuronal cell polarity. J Cell Biol *174*, 425-436.

Hu, J., Bai, X., Bowen, J.R., Dolat, L., Korobova, F., Yu, W., Baas, P.W., Svitkina, T., Gallo, G., and Spiliotis, E.T. (2012). Septin-driven coordination of actin and microtubule remodeling regulates the collateral branching of axons. Curr Biol *22*, 1109-1115.

Hu, Q.C., Milenkovic, L., Jin, H., Scott, M.P., Nachury, M.V., Spiliotis, E.T., and Nelson, W.J. (2010). A Septin Diffusion Barrier at the Base of the Primary Cilium Maintains Ciliary Membrane Protein Distribution. Science *329*, 436-439.

Hu, Q.C., Nelson, W.J., and Spiliotis, E.T. (2008). Forchlorfenuron Alters Mammalian Septin Assembly, Organization, and Dynamics. Journal of Biological Chemistry *283*, 29563-29571.

Hubbert, C., Guardiola, A., Shao, R., Kawaguchi, Y., Ito, A., Nixon, A., Yoshida, M., Wang, X.F., and Yao, T.P. (2002). HDAC6 is a microtubule-associated deacetylase. Nature *417*, 455-458.

Huijbregts, R.P., Svitin, A., Stinnett, M.W., Renfrow, M.B., and Chesnokov, I. (2009). Drosophila Orc6 facilitates GTPase activity and filament formation of the septin complex. Mol Biol Cell *20*, 270-281.

Huisman, S.M., and Segal, M. (2005). Cortical capture of microtubules and spindle polarity in budding yeast - where's the catch? Journal of Cell Science *118*, 463-471.

Ichihara, K., Kitazawa, H., Iguchi, Y., Hotani, H., and Itoh, T.J. (2001). Visualization of the stop of microtubule depolymerization that occurs at the high-density region of microtubule-associated protein 2 (MAP2). Journal of Molecular Biology *312*, 107-118.

Ihara, M., Kinoshita, A., Yamada, S., Tanaka, H., Tanigaki, A., Kitano, A., Goto, M., Okubo, K., Nishiyama, H., Ogawa, O., *et al.* (2005). Cortical organization by the septin cytoskeleton is essential for structural and mechanical integrity of mammalian spermatozoa. Developmental Cell *8*, 343-352.

Ihara, M., Tomimoto, H., Kitayama, H., Morioka, Y., Akiguchi, I., Shibasaki, H., Noda, M., and Kinoshita, M. (2003). Association of the cytoskeletal GTP-binding protein Sept4/H5 with cytoplasmic inclusions found in Parkinson's disease and other synucleinopathies. Journal of Biological Chemistry *278*, 24095-24102.

Ikegami, K., Heier, R.L., Taruishi, M., Takagi, H., Mukai, M., Shimma, S., Taira, S., Hatanaka, K., Morone, N., Yao, I., *et al.* (2007). Loss of alpha-tubulin polyglutamylation in ROSA22 mice is associated with abnormal targeting of KIF1A and modulated synaptic function. P Natl Acad Sci USA *104*, 3213-3218.

Imamura, T., Huang, J., Usui, I., Satoh, H., Bever, J., and Olefsky, J.M. (2003). Insulin-induced GLUT4 translocation involves protein kinase C-lambda-mediated functional coupling between Rab4 and the motor protein kinesin. Mol Cell Biol *23*, 4892-4900.

Ito, H., Atsuzawa, K., Morishita, R., Usuda, N., Sudo, K., Iwamoto, I., Mizutani, K., Katoh-Semba, R., Nozawa, Y., Asano, T., *et al.* (2009). Sept8 controls the binding of vesicle-associated membrane protein 2 to synaptophysin. J Neurochem *108*, 867-880.

Iwaisako, K., Hatano, E., Taura, K., Nakajima, A., Tada, M., Seo, S., Tamaki, N., Sato, F., Ikai, I., Uemoto, S., *et al.* (2008). Loss of Sept4 exacerbates liver fibrosis through the dysregulation of hepatic stellate cells. J Hepatol *49*, 768-778.

Jaglin, X.H., Poirier, K., Saillour, Y., Buhler, E., Tian, G., Bahi-Buisson, N., Fallet-Bianco, C., Phan-Dinh-Tuy, F., Kong, X.P., Bomont, P., *et al.* (2009). Mutations in the beta-tubulin gene TUBB2B result in asymmetrical polymicrogyria. Nat Genet *41*, 746-752.

Janke, C. (2014). The tubulin code: molecular components, readout mechanisms, and functions. J Cell Biol *206*, 461-472.

Janke, C., and Bulinski, J.C. (2011). Post-translational regulation of the microtubule cytoskeleton: mechanisms and functions. Nat Rev Mol Cell Bio *12*, 773-786.

Janke, C., Rogowski, K., Wloga, D., Regnard, C., Kajava, A.V., Strub, J.M., Temurak, N., van Dijk, J., Boucher, D., van Dorsselaer, A., *et al.* (2005). Tubulin polyglutamylase enzymes are members of the TTL domain protein family. Science *308*, 1758-1762.

Jaulin, F., and Kreitzer, G. (2010). KIF17 stabilizes microtubules and contributes to epithelial morphogenesis by acting at MT plus ends with EB1 and APC. J Cell Biol *190*, 443-460.

Jenkins, P.M., Hurd, T.W., Zhang, L., McEwen, D.P., Brown, R.L., Margolis, B., Verhey, K.J., and Martens, J.R. (2006). Ciliary targeting of olfactory CNG channels requires the CNGB1b subunit and the kinesin-2 motor protein, KIF17. Curr Biol *16*, 1211-1216.

Jimbo, T., Kawasaki, Y., Koyama, R., Sato, R., Takada, S., Haraguchi, K., and Akiyama, T. (2002). Identification of a link between the tumour suppressor APC and the kinesin superfamily. Nature Cell Biology *4*, 323-327.

Jo, K., Derin, R., Li, M., and Bredt, D.S. (1999). Characterization of MALS/Velis-1, -2, and -3: a family of mammalian LIN-7 homologs enriched at brain synapses in association with the postsynaptic density-95/NMDA receptor postsynaptic complex. J Neurosci *19*, 4189-4199.

Joberty, G., Perlungher, R.R., Sheffield, P.J., Kinoshita, M., Noda, M., Haystead, T., and Macara, I.G. (2001). Borg proteins control septin organization and are negatively regulated by Cdc42. Nat Cell Biol *3*, 861-866.

Johansson, M., Rocha, N., Zwart, W., Jordens, I., Janssen, L., Kuijl, C., Olkkonen, V.M., and Neefjes, J. (2007). Activation of endosomal dynein motors by stepwise assembly of Rab7-RILP-p150(Glued), ORP1L, and the receptor beta III spectrin. Journal of Cell Biology *176*, 459-471.

John, C.M., Hite, R.K., Weirich, C.S., Fitzgerald, D.J., Jawhari, H., Faty, M., Schlapfer, D., Kroschewski, R., Winkler, F.K., Walz, T., *et al.* (2007). The Caenorhabditis elegans septin complex is nonpolar. Embo Journal *26*, 3296-3307.

Johnson, K.A. (1998). The axonemal microtubules of the Chlamydomonas flagellum differ in tubulin isoform content. J Cell Sci *111 (Pt 3)*, 313-320.

Joo, E., Tsang, C.W., and Trimble, W.S. (2005). Septins: Traffic control at the cytokinesis intersection. Traffic *6*, 626-634.

Joshi, H.C., and Cleveland, D.W. (1989). Differential utilization of beta-tubulin isotypes in differentiating neurites. J Cell Biol *109*, 663-673.

Kamal, A., Stokin, G.B., Xia, C.H., and Goldstein, L.S.B. (2000). Axonal transport of amyloid precursor protein is mediated by direct binding to the kinesin light chain subunit of kinesin-I. Molecular Biology of the Cell *11*, 78a-78a.

Kanai, Y., Dohmae, N., and Hirokawa, N. (2004). Kinesin transports RNA: isolation and characterization of an RNA-transporting granule. Neuron *43*, 513-525.

Kardon, J.R., and Vale, R.D. (2009). Regulators of the cytoplasmic dynein motor. Nat Rev Mol Cell Biol *10*, 854-865.

Kartmann, B., and Roth, D. (2001). Novel roles for mammalian septins: from vesicle trafficking to oncogenesis. J Cell Sci *114*, 839-844.

Kayadjanian, N., Lee, H.S., Pina-Crespo, J., and Heinemann, S.F. (2007). Localization of glutamate receptors to distal dendrites depends on subunit composition and the kinesin motor protein KIF17. Mol Cell Neurosci *34*, 219-230.

Kim, M.S., Froese, C.D., Estey, M.P., and Trimble, W.S. (2011). SEPT9 occupies the terminal positions in septin octamers and mediates polymerization-dependent functions in abscission. J Cell Biol *195*, 815-826.

Kim, S.K., Shindo, A., Park, T.J., Oh, E.C., Ghosh, S., Gray, R.S., Lewis, R.A., Johnson, C.A., Attie-Bittach, T., Katsanis, N., *et al.* (2010). Planar Cell Polarity Acts Through Septins to Control Collective Cell Movement and Ciliogenesis. Science *329*, 1337-1340.

Kimura, Y., Kurabe, N., Ikegami, K., Tsutsumi, K., Konishi, Y., Kaplan, O.I., Kunitomo, H., Iino, Y., Blacque, O.E., and Setou, M. (2010). Identification of Tubulin Deglutamylase among Caenorhabditis elegans and Mammalian Cytosolic Carboxypeptidases (CCPs). Journal of Biological Chemistry *285*, 22934-22939.

Kinoshita, A., Kinoshita, M., Akiyama, H., Tomimoto, H., Akiguchi, I., Kumar, S., Noda, M., and Kimura, J. (1998). Identification of septins in neurofibrillary tangles in Alzheimer's disease. Am J Pathol *153*, 1551-1560.

Kinoshita, M. (2003). The septins. Genome Biol *4*, 236.

Kinoshita, M. (2006). Diversity of septin scaffolds. Curr Opin Cell Biol *18*, 54-60.

Kinoshita, M. (2008). Insight into Septin Functions from Mouse Models. In The septins, S.E.H.R.a.J.R.P. Peter A. Hall, ed. (West Sussex, UK, Wiley-Blackwell).

Kinoshita, M., and Noda, M. (2001). Roles of septins in the mammalian cytokinesis machinery. Cell Structure and Function *26*, 667-670.

Kinoshita, N., Kimura, K., Matsumoto, N., Watanabe, M., Fukaya, M., and Ide, C. (2004). Mammalian septin Sept2 modulates the activity of GLAST, a glutamate transporter in astrocytes. Genes Cells *9*, 1-14.

Kissel, H., Georgescu, M.M., Larisch, S., Manova, K., Hunnicutt, G.R., and Steller, H. (2005). The Sept4 septin locus is required for sperm terminal differentiation in mice. Developmental Cell *8*, 353-364.

Klopfenstein, D.R., Tomishige, M., Stuurman, N., and Vale, R.D. (2002). Role of phosphatidylinositol(4,5)bisphosphate organization in membrane transport by the Unc104 kinesin motor. Cell *109*, 347-358.

Kojima, K., Sakai, I., Hasegawa, A., Niiya, H., Azuma, T., Matsuo, Y., Fujii, N., Tanimoto, M., and Fujita, S. (2004). FLJ10849, a septin family gene, fuses MLL in a novel leukemia cell line CNLBC1 derived from chronic neutrophilic leukemia in transformation with t(4;11)(q21;q23). Leukemia *18*, 998-1005.

Kollman, J.M., Merdes, A., Mourey, L., and Agard, D.A. (2011). Microtubule nucleation by gamma-tubulin complexes. Nat Rev Mol Cell Biol *12*, 709-721.

Komarova, Y.A., Akhmanova, A.S., Kojima, S., Galjart, N., and Borisy, G.G. (2002). Cytoplasmic linker proteins promote microtubule rescue in vivo. J Cell Biol *159*, 589-599.

Konishi, Y., and Setou, M. (2009). Tubulin tyrosination navigates the kinesin-1 motor domain to axons. Nat Neurosci *12*, 559-567.

Kotani, S., Kawai, G., Yokoyama, S., and Murofushi, H. (1990). Interaction Mechanism between Microtubule-Associated Proteins and Microtubules - a Proton Nuclear-Magnetic-Resonance Analysis on the Binding of Synthetic Peptide to Tubulin. Biochemistry-Us *29*, 10049-10054.

Krauhs, E., Little, M., Kempf, T., Hofer-Warbinek, R., Ade, W., and Ponstingl, H. (1981). Complete amino acid sequence of beta-tubulin from porcine brain. Proc Natl Acad Sci U S A *78*, 4156-4160.

Kremer, B.E., Haystead, T., and Macara, I.G. (2005). Mammalian septins regulate microtubule stability through interaction with the microtubule-binding protein MAPP-1. Molecular Biology of the Cell *16*, 4648-4659.

Kubo, T., Yanagisawa, H.A., Yagi, T., Hirono, M., and Kamiya, R. (2010). Tubulin polyglutamylation regulates axonemal motility by modulating activities of inner-arm dyneins. Curr Biol *20*, 441-445.

Kueh, H.Y., and Mitchison, T.J. (2009). Structural plasticity in actin and tubulin polymer dynamics. Science *325*, 960-963.

Kuhlenbaumer, G., Hannibal, M.C., Nelis, E., Schirmacher, A., Verpoorten, N., Meuleman, J., Watts, G.D., De Vriendt, E., Young, P., Stogbauer, F., *et al.* (2005). Mutations in SEPT9 cause hereditary neuralgic amyotrophy. Nat Genet *37*, 1044-1046.

Kuhlenbaumer, G., Meuleman, J., De Jonghe, P., Falck, B., Young, P., Hunermund, G., Van Broeckhoven, C., Timmerman, V., and Stogbauer, F. (2001). Hereditary neuralgic amyotrophy (HNA) is genetically heterogeneous. Journal of Neurology *248*, 861-865.

Kull, F.J., and Sloboda, R.D. (2014). A slow dance for microtubule acetylation. Cell *157*, 1255-1256.

Kumar, N., and Flavin, M. (1981). Preferential action of a brain detyrosinolating carboxypeptidase on polymerized tubulin. J Biol Chem *256*, 7678-7686.

Kuo, Y.C., Lin, Y.H., Chen, H.I., Wang, Y.Y., Chiou, Y.W., Lin, H.H., Pan, H.A., Wu, C.M., Su, S.M., Hsu, C.C., *et al.* (2012). SEPT12 mutations cause male infertility with defective sperm annulus. Human Mutation *33*, 710-719.

Kusch, J., Meyer, A., Snyder, M.P., and Barral, Y. (2002). Microtubule capture by the cleavage apparatus is required for proper spindle positioning in yeast. Gene Dev *16*, 1627-1639.

Kwitny, S., Klaus, A.V., and Hunnicutt, G.R. (2010). The Annulus of the Mouse Sperm Tail Is Required to Establish a Membrane Diffusion Barrier That Is Engaged During the Late Steps of Spermiogenesis. Biol Reprod *82*, 669-678.

Lacroix, B., van Dijk, J., Gold, N.D., Guizetti, J., Aldrian-Herrada, G., Rogowski, K., Gerlich, D.W., and Janke, C. (2010). Tubulin polyglutamylation stimulates spastin-mediated microtubule severing. Journal of Cell Biology *189*, 945-954.

Landsverk, M.L., Ruzzo, E.K., Mefford, H.C., Buysse, K., Buchan, J.G., Eichler, E.E., Petty, E.M., Peterson, E.A., Knutzen, D.M., Barnett, K., *et al.* (2009). Duplication within the SEPT9 gene associated with a founder effect in North American families with hereditary neuralgic amyotrophy. Hum Mol Genet *18*, 1200-1208.

Lansbergen, G., and Akhmanova, A. (2006). Microtubule plus end: a hub of cellular activities. Traffic *7*, 499-507.

Larcher, J.C., Boucher, D., Lazereg, S., Gros, F., and Denoulet, P. (1996). Interaction of kinesin motor domains with alpha- and beta-tubulin subunits at a tau-independent binding site. Regulation by polyglutamylation. J Biol Chem *271*, 22117-22124.

Larisch, S., Yi, Y., Lotan, R., Kerner, H., Eimerl, S., Tony Parks, W., Gottfried, Y., Birkey Reffey, S., de Caestecker, M.P., Danielpour, D., *et al.* (2000). A novel mitochondrial septin-like protein, ARTS, mediates apoptosis dependent on its P-loop motif. Nat Cell Biol *2*, 915-921.

Lechtreck, K.F., and Geimer, S. (2000). Distribution of polyglutamylated tubulin in the flagellar apparatus of green flagellates. Cell Motil Cytoskeleton *47*, 219-235.

Lee, T., Langford, K.J., Askham, J.M., Bruning-Richardson, A., and Morrison, E.E. (2008). MCAK associates with EB1. Oncogene *27*, 2494-2500.

Lee, W.H., Kim, J.Y., Kim, Y.S., Song, H.J., Song, K.J., Song, J.W., Baek, L.J., Seo, E.Y., Kim, C.D., Lee, J.H., *et al.* (2005). Upregulation of class II beta-tubulin expression in differentiating keratinocytes. J Invest Dermatol *124*, 291-297.

Leipe, D.D., Wolf, Y.I., Koonin, E.V., and Aravind, L. (2002). Classification and evolution of P-loop GTPases and related ATPases. J Mol Biol *317*, 41-72.

Lewis, S.A., Gu, W., and Cowan, N.J. (1987). Free Intermingling of Mammalian Beta-Tubulin Isotypes among Functionally Distinct Microtubules. Cell *49*, 539-548.

Lhernault, S.W., and Rosenbaum, J.L. (1985). Chlamydomonas Alpha-Tubulin Is Posttranslationally Modified by Acetylation on the Epsilon-Amino Group of a Lysine. Biochemistry-Us *24*, 473-478.

Ligon, L.A., Shelly, S.S., Tokito, M.K., and Holzbaur, E.L. (2006). Microtubule binding proteins CLIP-170, EB1, and p150Glued form distinct plus-end complexes. FEBS Lett *580*, 1327-1332.

Lin, D., and Clarkson, W.A. (2015). Polarization-dependent transverse mode selection in an Yb-doped fiber laser. Opt Lett *40*, 498-501.

Lin, M.Y., and Sheng, Z.H. (2015). Regulation of mitochondrial transport in neurons. Exp Cell Res *334*, 35-44.

Longtine, M.S., DeMarini, D.J., Valencik, M.L., Al-Awar, O.S., Fares, H., De Virgilio, C., and Pringle, J.R. (1996). The septins: roles in cytokinesis and other processes. Curr Opin Cell Biol *8*, 106-119.

Lopez, L.A., and Sheetz, M.P. (1993). Steric Inhibition of Cytoplasmic Dynein and Kinesin Motility by Map2. Cell Motil Cytoskel *24*, 1-16.

Luduena, R.F. (1993). Are tubulin isotypes functionally significant. Mol Biol Cell *4*, 445-457.

Maas, C., Belgardt, D., Lee, H.K., Heisler, F.F., Lappe-Siefke, C., Magiera, M.M., van Dijk, J., Hausrat, T.J., Janke, C., and Kneussel, M. (2009). Synaptic activation modifies microtubules underlying transport of postsynaptic cargo. P Natl Acad Sci USA *106*, 8731-8736.

Macara, I.G., Baldarelli, R., Field, C.M., Glotzer, M., Hayashi, Y., Hsu, S.C., Kennedy, M.B., Kinoshita, M., Longtine, M., Low, C., *et al.* (2002). Mammalian septins nomenclature. Mol Biol Cell *13*, 4111-4113.

Macho, B., Brancorsini, S., Fimia, G.M., Setou, M., Hirokawa, N., and Sassone-Corsi, P. (2002). CREM-dependent transcription in male germ cells controlled by a kinesin. Science *298*, 2388-2390.

Mandelkow, E.M., Stamer, K., Ebneth, A., Godemann, R., Trinczek, B., Illenberger, S., and Mandelkow, E. (1999). Overexpression of tau protein inhibits kinesin-dependent outward flow of vesicles ind organelles along microtubules. Molecular Biology of the Cell *10*, 372a-372a.

Martinez, C., Corral, J., Dent, J.A., Sesma, L., Vicente, V., and Ware, J. (2006). Platelet septin complexes form rings and associate with the microtubular network. J Thromb Haemost *4*, 1388-1395.

Marx, A., Muller, J., Mandelkow, E.M., Hoenger, A., and Mandelkow, E. (2006). Interaction of kinesin motors, microtubules, and MAPs. J Muscle Res Cell Motil *27*, 125-137.

Mary, J., Redeker, V., Lecaer, J.P., Prome, J.C., and Rossier, J. (1994). Class-I and Iva Beta-Tubulin Isotypes Expressed in Adult-Mouse Brain Are Glutamylated. Febs Letters *353*, 89-94.

Matos, M.F., Xu, Y., Dulubova, I., Otwinowski, Z., Richardson, J.M., Tomchick, D.R., Rizo, J., and Ho, A. (2012). Autoinhibition of Mint1 adaptor protein regulates amyloid precursor protein binding and processing. Proc Natl Acad Sci U S A *109*, 3802-3807.

Mayr, M., Hummer, S., Bormann, J., and Mayer, T. (2007). The human kinesin Kif18A is a motile microtubule depolymerase essential for chromosome congression. Febs J *274*, 294-294.

McDade, S.S., Hall, P.A., and Russell, S.E.H. (2007). Translational control of SEPT9 isoforms is perturbed in disease. Hum Mol Genet *16*, 742-752.

McIlhatton, M.A., Burrows, J.F., Donaghy, P.G., Chanduloy, S., Johnston, P.G., and Russell, S.E. (2001). Genomic organization, complex splicing pattern and expression of a human septin gene on chromosome 17q25.3. Oncogene *20*, 5930-5939.

McMurray, M.A., and Thorner, J. (2009). Septins: molecular partitioning and the generation of cellular asymmetry. Cell Div *4*, 18.

McVicker, D.P., Chrin, L.R., and Berger, C.L. (2011). The nucleotide-binding state of microtubules modulates kinesin processivity and the ability of Tau to inhibit kinesin-mediated transport. J Biol Chem *286*, 42873-42880.

Megonigal, M.D., Rappaport, E.F., Jones, D.H., Williams, T.M., Lovett, B.D., Kelly, K.M., Lerou, P.H., Moulton, T., Budarf, M.L., and Felix, C.A. (1998). t(11;22)(q23;q11.2) In acute myeloid leukemia of infant twins fuses MLL with hCDCrel, a cell division cycle gene in the genomic region of deletion in DiGeorge and velocardiofacial syndromes. Proc Natl Acad Sci U S A *95*, 6413-6418.

Mejillano, M.R., and Himes, R.H. (1991). Assembly properties of tubulin after carboxyl group modification. J Biol Chem *266*, 657-664.

Mendoza, M., Hyman, A.A., and Glotzer, M. (2002). GTP binding induces filament assembly of a recombinant septin. Curr Biol *12*, 1858-1863.

Meseroll, R.A., Occhipinti, P., and Gladfelter, A.S. (2013). Septin phosphorylation and coiled-coil domains function in cell and septin ring morphology in the filamentous fungus Ashbya gossypii. Eukaryot Cell *12*, 182-193.

Meulemann, J., Kuhlenbaumer, G., Schirmacher, A., Wehnert, M., De Jonghe, P., De Vriendt, E., Young, P., Airaksinen, E., Pou-Serradell, A., Prats, J.M., *et al.* (1999). Genetic refinement of the hereditary neuralgic amyotrophy (HNA) locus at chromosome 17q25. Eur J Hum Genet *7*, 920-927.

Midorikawa, R., Takei, Y., and Hirokawa, N. (2006). KIF4 motor regulates activity-dependent neuronal survival by suppressing PARP-1 enzymatic activity. Cell *125*, 371-383.

Mimori-Kiyosue, Y., Grigoriev, I., Lansbergen, G., Sasaki, H., Matsui, C., Severin, F., Galjart, N., Grosveld, F., Vorobjev, I., Tsukita, S., *et al.* (2005). CLASP1 and CLASP2 bind to EB1 and regulate microtubule plus-end dynamics at the cell cortex. J Cell Biol *168*, 141-153.

Mitchison, T., and Kirschner, M. (1984). Dynamic instability of microtubule growth. Nature *312*, 237-242.

Mogessie, B., Roth, D., Rahil, Z., and Straube, A. (2015). A novel isoform of MAP4 organises the paraxial microtubule array required for muscle cell differentiation. Elife *4*, e05697.

Molnar, B., Toth, K., Bartak, B.K., and Tulassay, Z. (2015). Plasma methylated septin 9: a colorectal cancer screening marker. Expert Rev Mol Diagn *15*, 171-184.

Moores, C.A., and Milligan, R.A. (2006). Lucky 13-microtubule depolymerisation by kinesin-13 motors. J Cell Sci *119*, 3905-3913.

Moores, C.A., Perderiset, M., Kappeler, C., Kain, S., Drummond, D., Perkins, S.J., Chelly, J., Cross, R., Houdusse, A., and Francis, F. (2006). Distinct roles of doublecortin modulating the microtubule cytoskeleton. Embo Journal *25*, 4448-4457.

Morfini, G., Szebenyi, G., Elluru, R., Ratner, N., and Brady, S.T. (2002). Glycogen synthase kinase 3 phosphorylates kinesin light chains and negatively regulates kinesin-based motility. EMBO J *21*, 281-293.

Moseley, J.B., Bartolini, F., Okada, K., Wen, Y., Gundersen, G.G., and Goode, B.L. (2007). Regulated binding of adenomatous polyposis coli protein to actin. Journal of Biological Chemistry *282*, 12661-12668.

Mostowy, S., Bonazzi, M., Hamon, M.A., Tham, T.N., Mallet, A., Lelek, M., Gouin, E., Demangel, C., Brosch, R., Zimmer, C., *et al.* (2010). Entrapment of intracytosolic bacteria by septin cage-like structures. Cell Host Microbe *8*, 433-444.

Mostowy, S., and Cossart, P. (2012). Septins: the fourth component of the cytoskeleton. Nat Rev Mol Cell Biol *13*, 183-194.

Mostowy, S., Janel, S., Forestier, C., Roduit, C., Kasas, S., Pizarro-Cerda, J., Cossart, P., and Lafont, F. (2011). A role for septins in the interaction between the Listeria monocytogenes INVASION PROTEIN InlB and the Met receptor. Biophys J *100*, 1949-1959.

Mostowy, S., Tham, T.N., Danckaert, A., Guadagnini, S., Boisson-Dupuis, S., Pizarro-Cerda, J., and Cossart, P. (2009). Septins Regulate Bacterial Entry into Host Cells. Plos One *4*.

Mullen, R.J., Eicher, E.M., and Sidman, R.L. (1976). Purkinje cell degeneration, a new neurological mutation in the mouse. Proc Natl Acad Sci U S A *73*, 208-212.

Muntean, A.G., and Hess, J.L. (2012). The pathogenesis of mixed-lineage leukemia. Annu Rev Pathol *7*, 283-301.

Nagata, K., Kawajiri, A., Matsui, S., Takagishi, M., Shiromizu, T., Saitoh, N., Izawa, I., Kiyono, T., Itoh, T.J., Hotani, H., *et al.* (2003). Filament formation of MSF-A, a mammalian septin, in human mammary epithelial cells depends on interactions with microtubules. Journal of Biological Chemistry *278*, 18538-18543.

Nakagawa, T., Tanaka, Y., Matsuoka, E., Kondo, S., Okada, Y., Noda, Y., Kanai, Y., and Hirokawa, N. (1997). Identification and classification of 16 new kinesin superfamily (KIF) proteins in mouse genome. Proc Natl Acad Sci U S A *94*, 9654-9659.

Nakata, T., and Hirokawa, N. (1995). Point mutation of adenosine triphosphate-binding motif generated rigor kinesin that selectively blocks anterograde lysosome membrane transport. J Cell Biol *131*, 1039-1053.

Nangaku, M., Sato-Yoshitake, R., Okada, Y., Noda, Y., Takemura, R., Yamazaki, H., and Hirokawa, N. (1994). KIF1B, a novel microtubule plus end-directed monomeric motor protein for transport of mitochondria. Cell *79*, 1209-1220.

Nathke, I.S. (2004). The adenomatous polyposis coli protein: the Achilles heel of the gut epithelium. Annu Rev Cell Dev Biol *20*, 337-366.

Nielsen, E., Severin, F., Backer, J.M., Hyman, A.A., and Zerial, M. (1999). Rab5 regulates motility of early endosomes on microtubules. Nat Cell Biol *1*, 376-382.

Niethammer, P., Kronja, I., Kandels-Lewis, S., Rybina, S., Bastiaens, P., and Karsenti, E. (2007). Discrete states of a protein interaction network govern interphase and mitotic microtubule dynamics. PLoS Biol *5*, e29.

Niwa, S., Tanaka, Y., and Hirokawa, N. (2008). KIF1Bbeta- and KIF1A-mediated axonal transport of presynaptic regulator Rab3 occurs in a GTP-dependent manner through DENN/MADD. Nat Cell Biol *10*, 1269-1279.

Nonaka, S., Tanaka, Y., Okada, Y., Takeda, S., Harada, A., Kanai, Y., Kido, M., and Hirokawa, N. (1999). Randomization of left-right asymmetry due to loss of nodal cilia generating leftward flow of extraembryonic fluid in mice lacking KIF3B motor protein (vol 95, pg 829, 95). Cell *99*.

North, B.J., Marshall, B.L., Borra, M.T., Denu, J.M., and Verdin, E. (2003). The human Sir2 ortholog, SIRT2, is an NAD(+)-dependent tubulin deacetylase. Mol Cell *11*, 437-444.

Ohkawa, N., Sugisaki, S., Tokunaga, E., Fujitani, K., Hayasaka, T., Setou, M., and Inokuchi, K. (2008). N-acetyltransferase ARD1-NAT1 regulates neuronal dendritic development. Genes Cells *13*, 1171-1183.

Okada, Y., Yamazaki, H., Sekine-Aizawa, Y., and Hirokawa, N. (1995). The neuron-specific kinesin superfamily protein KIF1A is a unique monomeric motor for anterograde axonal transport of synaptic vesicle precursors. Cell *81*, 769-780.

Ono, R., Ihara, M., Nakajima, H., Ozaki, K., Kataoka-Fujiwara, Y., Taki, T., Nagata, K., Inagaki, M., Yoshida, N., Kitamura, T., *et al.* (2005). Disruption of Sept6, a fusion partner gene of MLL, does not affect ontogeny, leukemogenesis induced by MLL-SEPT6, or phenotype induced by the loss of Sept4. Molecular and Cellular Biology *25*, 10965-10978.

Ookata, K., Hisanaga, S., Bulinski, J.C., Murofushi, H., Aizawa, H., Itoh, T.J., Hotani, H., Okumura, E., Tachibana, K., and Kishimoto, T. (1995). Cyclin-B Interaction with Microtubule-

Associated Protein-4 (Map4) Targets P34(Cdc2) Kinase to Microtubules and Is a Potential Regulator of M-Phase Microtubule Dynamics. Journal of Cell Biology *128*, 849-862.

Orstavik, K., Ro, H., and Orstavik, K.H. (1997). Recurrent brachial plexus neuropathy in a family with subtle dysmorphic features -- a case of hereditary neuralgic amyotrophy. Clin Genet *51*, 421-425.

Osaka, M., Rowley, J.D., and Zeleznik-Le, N.J. (1999). MSF (MLL septin-like fusion), a fusion partner gene of MLL, in a therapy-related acute myeloid leukemia with a t(11;17)(q23;q25). P Natl Acad Sci USA *96*, 6428-6433.

Ou, G., Blacque, O.E., Snow, J.J., Leroux, M.R., and Scholey, J.M. (2005). Functional coordination of intraflagellar transport motors. Nature *436*, 583-587.

Pablo-Hernando, M.E., Arnaiz-Pita, Y., Tachikawa, H., del Rey, F., Neiman, A.M., and de Aldana, C.R.V. (2008). Septins localize to microtubules during nutritional limitation in Saccharomyces cerevisiae. Bmc Cell Biol *9*.

Panda, D., Miller, H.P., Banerjee, A., Luduena, R.F., and Wilson, L. (1994). Microtubule dynamics in vitro are regulated by the tubulin isotype composition. Proc Natl Acad Sci U S A *91*, 11358-11362.

Paturle-Lafanechere, L., Edde, B., Denoulet, P., Van Dorsselaer, A., Mazarguil, H., Le Caer, J.P., Wehland, J., and Job, D. (1991). Characterization of a major brain tubulin variant which cannot be tyrosinated. Biochemistry-Us *30*, 10523-10528.

Paturle-Lafanechere, L., Manier, M., Trigault, N., Pirollet, F., Mazarguil, H., and Job, D. (1994). Accumulation of delta 2-tubulin, a major tubulin variant that cannot be tyrosinated, in neuronal tissues and in stable microtubule assemblies. J Cell Sci *107 (Pt 6)*, 1529-1543.

Patzig, J., Jahn, O., Tenzer, S., Wichert, S.P., de Monasterio-Schrader, P., Rosfa, S., Kuharev, J., Yan, K., Bormuth, I., Bremer, J., *et al.* (2011). Quantitative and Integrative Proteome Analysis of Peripheral Nerve Myelin Identifies Novel Myelin Proteins and Candidate Neuropathy Loci. J Neurosci *31*, 16369-16386.

Pearson, C.G., and Bloom, K. (2004). Dynamic microtubules lead the way for spindle positioning. Nat Rev Mol Cell Bio *5*, 481-492.

Pedrotti, B., and Islam, K. (1994). Purified Native Microtubule-Associated Protein Map1a - Kinetics of Microtubule Assembly and Map1a Tubulin Stoichiometry. Biochemistry-Us *33*, 12463-12470.

Pellegrino, J.E., Rebbeck, T.R., Brown, M.J., Bird, T.D., and Chance, P.F. (1996). Mapping of hereditary neuralgic amyotrophy (familial brachial plexus neuropathy) to distal chromosome 17q. Neurology *46*, 1128-1132.

Pennington, K., Beasley, C.L., Dicker, P., Fagan, A., English, J., Pariante, C.M., Wait, R., Dunn, M.J., and Cotter, D.R. (2008). Prominent synaptic and metabolic abnormalities revealed by

proteomic analysis of the dorsolateral prefrontal cortex in schizophrenia and bipolar disorder. Mol Psychiatry *13*, 1102-1117.

Peris, L., Thery, M., Faure, J., Saoudi, Y., Lafanechere, L., Chilton, J.K., Gordon-Weeks, P., Galjart, N., Bornens, M., Wordeman, L., *et al.* (2006). Tubulin tyrosination is a major factor affecting the recruitment of CAP-Gly proteins at microtubule plus ends. J Cell Biol *174*, 839-849.

Peris, L., Wagenbach, M., Lafanechere, L., Brocard, J., Moore, A.T., Kozielski, F., Job, D., Wordeman, L., and Andrieux, A. (2009). Motor-dependent microtubule disassembly driven by tubulin tyrosination. J Cell Biol *185*, 1159-1166.

Peterman, E.J., and Scholey, J.M. (2009). Mitotic microtubule crosslinkers: insights from mechanistic studies. Curr Biol *19*, R1089-1094.

Peterson, E.A., Kalikin, L.M., Steels, J.D., Estey, M.P., Trimble, W.S., and Petty, E.M. (2007). Characterization of a SEPT9 interacting protein, SEPT14, a novel testis-specific septin. Mamm Genome *18*, 796-807.

Pfister, K.K., Shah, P.R., Hummerich, H., Russ, A., Cotton, J., Annuar, A.A., King, S.M., and Fisher, E.M. (2006). Genetic analysis of the cytoplasmic dynein subunit families. PLoS Genet *2*, e1.

Plessmann, U., and Weber, K. (1997). Mammalian sperm tubulin: an exceptionally large number of variants based on several posttranslational modifications. J Protein Chem *16*, 385-390.

Ponstingl, H., Krauhs, E., Little, M., and Kempf, T. (1981). Complete amino acid sequence of alpha-tubulin from porcine brain. Proc Natl Acad Sci U S A *78*, 2757-2761.

Presley, J.F., Cole, N.B., Schroer, T.A., Hirschberg, K., Zaal, K.J., and Lippincott-Schwartz, J. (1997). ER-to-Golgi transport visualized in living cells. Nature *389*, 81-85.

Puig, B., Ferrer, I., Luduena, R.F., and Avila, J. (2005). BetaII-tubulin and phospho-tau aggregates in Alzheimer's disease and Pick's disease. J Alzheimers Dis *7*, 213-220; discussion 255-262.

Qi, M.Y., Yu, W.B., Liu, S., Jia, H.J., Tang, L.S., Shen, M.J., Yan, X.M., Saiyin, H., Lang, Q.Y., Wan, B., *et al.* (2005). Septin1, a new interaction partner for human serine/threonine kinase aurora-B. Biochem Bioph Res Co *336*, 994-1000.

Raybin, D., and Flavin, M. (1977). Enzyme which specifically adds tyrosine to the alpha chain of tubulin. Biochemistry-Us *16*, 2189-2194.

Redeker, V., Levilliers, N., Schmitter, J.M., Lecaer, J.P., Rossier, J., Adoutte, A., and Bre, M.H. (1994). Polyglycylation of Tubulin - a Posttranslational Modification in Axonemal Microtubules. Science *266*, 1688-1691.

Redeker, V., Rossier, J., and Frankfurter, A. (1998). Posttranslational modifications of the C-terminus of alpha-tubulin in adult rat brain: alpha 4 is glutamylated at two residues. Biochemistry-Us *37*, 14838-14844.

Reed, N.A., Cai, D., Blasius, T.L., Jih, G.T., Meyhofer, E., Gaertig, J., and Verhey, K.J. (2006). Microtubule acetylation promotes kinesin-1 binding and transport. Curr Biol *16*, 2166-2172.

Regnard, C., Desbruyeres, E., Denoulet, P., and Edde, B. (1999). Tubulin polyglutamylase: isozymic variants and regulation during the cell cycle in HeLa cells. Journal of Cell Science *112*, 4281-4289.

Reid, E., Kloos, M., Ashley-Koch, A., Hughes, L., Bevan, S., Svenson, I.K., Graham, F.L., Gaskell, P.C., Dearlove, A., Pericak-Vance, M.A., *et al.* (2002). A kinesin heavy chain (KIF5A) mutation in hereditary spastic paraplegia (SPG10). Am J Hum Genet *71*, 1189-1194.

Reiner, O., Coquelle, F.M., Peter, B., Levy, T., Kaplan, A., Sapir, T., Orr, I., Barkai, N., Eichele, G., and Bergmann, S. (2006). The evolving doublecortin (DCX) superfamily. BMC Genomics *7*, 188.

Roberts, A.J., Kon, T., Knight, P.J., Sutoh, K., and Burgess, S.A. (2013). Functions and mechanics of dynein motor proteins. Nat Rev Mol Cell Biol *14*, 713-726.

Robson, S.J., and Burgoyne, R.D. (1989). Differential localisation of tyrosinated, detyrosinated, and acetylated alpha-tubulins in neurites and growth cones of dorsal root ganglion neurons. Cell Motil Cytoskeleton *12*, 273-282.

Rogowski, K., Juge, F., van Dijk, J., Wloga, D., Strub, J.M., Levilliers, N., Thomas, D., Bre, M.H., Van Dorsselaer, A., Gaertig, J., *et al.* (2009). Evolutionary divergence of enzymatic mechanisms for posttranslational polyglycylation. Cell *137*, 1076-1087.

Rogowski, K., van Dijk, J., Magiera, M.M., Bosc, C., Deloulme, J.C., Bosson, A., Peris, L., Gold, N.D., Lacroix, B., Grau, M.B., *et al.* (2010). A Family of Protein-Deglutamylating Enzymes Associated with Neurodegeneration. Cell *143*, 564-578.

Roll-Mecak, A., and McNally, F.J. (2010). Microtubule-severing enzymes. Curr Opin Cell Biol *22*, 96-103.

Rosenberg, K.J., Ross, J.L., Feinstein, H.E., Feinstein, S.C., and Israelachvili, J. (2008). Complementary dimerization of microtubule-associated tau protein: Implications for microtubule bundling and tau-mediated pathogenesis. Proc Natl Acad Sci U S A *105*, 7445-7450.

Rudiger, M., Plessmann, U., Rudiger, A.H., and Weber, K. (1995). Beta-Tubulin of Bull Sperm Is Polyglycylated. Febs Letters *364*, 147-151.

Russell, S.E.H., McIlhatton, M.A., Burrows, J.F., Donaghy, P.G., Chanduloy, S., Petty, E.M., Kalikin, L.M., Church, S.W., McIlroy, S., Harkin, D.P., *et al.* (2000). Isolation and mapping of a human septin gene to a region on chromosome 17q, commonly deleted in sporadic epithelial ovarian tumors. Cancer Research *60*, 4729-4734.

Sakamoto, T., Uezu, A., Kawauchi, S., Kuramoto, T., Makino, K., Umeda, K., Araki, N., Baba, H., and Nakanishi, H. (2008). Mass spectrometric analysis of microtubule co-sedimented proteins from rat brain. Genes Cells *13*, 295-312.

Sandblad, L., Busch, K.E., Tittmann, P., Gross, H., Brunner, D., and Hoenger, A. (2006). The Schizosaccharomyces pombe EB1 homolog Mal3p binds and stabilizes the microtubule lattice seam. Cell *127*, 1415-1424.

Santama, N., Er, C.P., Ong, L.L., and Yu, H. (2004). Distribution and functions of kinectin isoforms. J Cell Sci *117*, 4537-4549.

Sapir, T., Frotscher, M., Levy, T., Mandelkow, E.M., and Reiner, O. (2012). Tau's role in the developing brain: implications for intellectual disability. Hum Mol Genet *21*, 1681-1692.

Sato-Yoshitake, R., Yorifuji, H., Inagaki, M., and Hirokawa, N. (1992). The phosphorylation of kinesin regulates its binding to synaptic vesicles. J Biol Chem *267*, 23930-23936.

Sayas, C.L., and Avila, J. (2014). Regulation of EB1/3 proteins by classical MAPs in neurons. Bioarchitecture *4*, 1-5.

Schaar, B.T., Kinoshita, K., and McConnell, S.K. (2004). Doublecortin microtubule affinity is regulated by a balance of kinase and phosphatase activity at the leading edge of migrating neurons. Neuron *41*, 203-213.

Schmidt, K., and Nichols, B.J. (2004). Functional interdependence between septin and actin cytoskeleton. Bmc Cell Biol *5*.

Schneider, A., Plessmann, U., Felleisen, R., and Weber, K. (1998). Posttranslational modifications of trichomonad tubulins; identification of multiple glutamylation sites. Febs Letters *429*, 399-402.

Schneider, A., Plessmann, U., and Weber, K. (1997). Subpellicular and flagellar microtubules of Trypanosoma brucei are extensively glutamylated. J Cell Sci *110 (Pt 4)*, 431-437.

Scholey, J.M. (2013). Kinesin-2: a family of heterotrimeric and homodimeric motors with diverse intracellular transport functions. Annu Rev Cell Dev Biol *29*, 443-469.

Schroder, H.C., Wehland, J., and Weber, K. (1985). Purification of brain tubulin-tyrosine ligase by biochemical and immunological methods. J Cell Biol *100*, 276-281.

Schroer, T.A. (2004). Dynactin. Annu Rev Cell Dev Biol *20*, 759-779.

Scott, M., McCluggage, W.G., Hillan, K.J., Hall, P.A., and Russell, S.E.H. (2006). Altered patterns of transcription of the septin gene, SEPT9, in ovarian tumorigenesis. Int J Cancer *118*, 1325-1329.

Seeger, M.A., Zhang, Y., and Rice, S.E. (2012). Kinesin tail domains are intrinsically disordered. Proteins *80*, 2437-2446.

Seitz, A., Kojima, H., Oiwa, K., Mandelkow, E.M., Song, Y.H., and Mandelkow, E. (2002). Single-molecule investigation of the interference between kinesin, tau and MAP2c. EMBO J *21*, 4896-4905.

Sellin, M.E., Holmfeldt, P., Stenmark, S., and Gullberg, M. (2011). Microtubules support a disk-like septin arrangement at the plasma membrane of mammalian cells. Mol Biol Cell *22*, 4588-4601.

Sellin, M.E., Stenmark, S., and Gullberg, M. (2012). Mammalian SEPT9 isoforms direct microtubule-dependent arrangements of septin core heteromers. Mol Biol Cell *23*, 4242-4255.

Sellin, M.E., Stenmark, S., and Gullberg, M. (2014). Cell type-specific expression of SEPT3-homology subgroup members controls the subunit number of heteromeric septin complexes. Mol Biol Cell *25*, 1594-1607.

Semenova, I., Ikeda, K., Resaul, K., Kraikivski, P., Aguiar, M., Gygi, S., Zaliapin, I., Cowan, A., and Rodionov, V. (2014). Regulation of microtubule-based transport by MAP4. Mol Biol Cell *25*, 3119-3132.

Setou, M., Nakagawa, T., Seog, D.H., and Hirokawa, N. (2000). Kinesin superfamily motor protein KIF17 and mLin-10 in NMDA receptor-containing vesicle transport. Science *288*, 1796-1802.

Setou, M., Seog, D.H., Tanaka, Y., Kanai, Y., Takei, Y., Kawagishi, M., and Hirokawa, N. (2002). Glutamate-receptor-interacting protein GRIP1 directly steers kinesin to dendrites. Nature *417*, 83-87.

Sharma, N., Bryant, J., Wloga, D., Donaldson, R., Davis, R.C., Jerka-Dziadosz, M., and Gaertig, J. (2007). Katanin regulates dynamics of microtubules and biogenesis of motile cilia. Journal of Cell Biology *178*, 1065-1079.

Sheffield, P.J., Oliver, C.J., Kremer, B.E., Sheng, S., Shao, Z., and Macara, I.G. (2003). Borg/septin interactions and the assembly of mammalian septin heterodimers, trimers, and filaments. J Biol Chem *278*, 3483-3488.

Shi, S.H., Cheng, T., Jan, L.Y., and Jan, Y.N. (2004). APC and GSK-3beta are involved in mPar3 targeting to the nascent axon and establishment of neuronal polarity. Curr Biol *14*, 2025-2032.

Shida, T., Cueva, J.G., Xu, Z., Goodman, M.B., and Nachury, M.V. (2010). The major alpha-tubulin K40 acetyltransferase alphaTAT1 promotes rapid ciliogenesis and efficient mechanosensation. Proc Natl Acad Sci U S A *107*, 21517-21522.

Shinoda, T., Ito, H., Sudo, K., Iwamoto, I., Morishita, R., and Nagata, K. (2010). Septin 14 is involved in cortical neuronal migration via interaction with Septin 4. Neurosci Res *68*, E251-E251.

Silverman-Gavrila, R.V., and Silverman-Gavrila, L.B. (2008). Septins: new microtubule interacting partners. ScientificWorldJournal *8*, 611-620.

Sirajuddin, M., Farkasovsky, M., Hauer, F., Kuhlmann, D., Macara, I.G., Weyand, M., Stark, H., and Wittinghofer, A. (2007). Structural insight into filament formation by mammalian septins. Nature *449*, 311-+.

Sirajuddin, M., Farkasovsky, M., Zent, E., and Wittinghofer, A. (2009). GTP-induced conformational changes in septins and implications for function. Proc Natl Acad Sci U S A *106*, 16592-16597.

Sirajuddin, M., Rice, L.M., and Vale, R.D. (2014). Regulation of microtubule motors by tubulin isotypes and post-translational modifications. Nat Cell Biol *16*, 335-344.

Sisson, J.C., Field, C., Ventura, R., Royou, A., and Sullivan, W. (2000). Lava lamp, a novel peripheral Golgi protein, is required for Drosophila melanogaster cellularization. Journal of Cell Biology *151*, 905-917.

Sitz, J.H., Baumgartel, K., Hammerle, B., Papadopoulos, C., Hekerman, P., Tejedor, F.J., Becker, W., and Lutz, B. (2008). The Down syndrome candidate dual-specificity tyrosine phosphorylation-regulated kinase 1A phosphorylates the neurodegeneration-related septin 4. Neuroscience *157*, 596-605.

Slep, K.C., Rogers, S.L., Elliott, S.L., Ohkura, H., Kolodziej, P.A., and Vale, R.D. (2005). Structural determinants for EB1-mediated recruitment of APC and spectraplakins to the microtubule plus end. J Cell Biol *168*, 587-598.

Song, Y., and Brady, S.T. (2014). Post-translational modifications of tubulin: pathways to functional diversity of microtubules. Trends Cell Biol.

Spiliotis, E.T. (2010). Regulation of Microtubule Organization and Functions by Septin GTPases. Cytoskeleton *67*, 339-345.

Spiliotis, E.T., and Gladfelter, A.S. (2012). Spatial guidance of cell asymmetry: septin GTPases show the way. Traffic *13*, 195-203.

Spiliotis, E.T., Hunt, S.J., Hu, Q., Kinoshita, M., and Nelson, W.J. (2008). Epithelial polarity requires septin coupling of vesicle transport to polyglutamylated microtubules. J Cell Biol *180*, 295-303.

Spiliotis, E.T., Kinoshita, M., and Nelson, W.J. (2005). A mitotic septin scaffold required for mammalian chromosome congression and segregation. Science *307*, 1781-1785.

Stamer, K., Vogel, R., Thies, E., Mandelkow, E., and Mandelkow, E.M. (2002). Tau blocks traffic of organelles, neurofilaments, and APP vesicles in neurons and enhances oxidative stress. Journal of Cell Biology *156*, 1051-1063.

Stauber, T., Simpson, J.C., Pepperkok, R., and Vernos, I. (2006). A role for kinesin-2 in COPI-dependent recycling between the ER and the Golgi complex. Curr Biol *16*, 2245-2251.

Stogbauer, F., Young, P., Timmerman, V., Spoelders, P., Ringelstein, E.B., Van Broeckhoven, C., and Kurlemann, G. (1997). Refinement of the hereditary neuralgic amyotrophy (HNA) locus to chromosome 17q24-q25. Hum Genet *99*, 685-687.

Stoothoff, W., Jones, P.B., Spires-Jones, T.L., Joyner, D., Chhabra, E., Bercury, K., Fan, Z., Xie, H., Bacskai, B., Edd, J., *et al.* (2009). Differential effect of three-repeat and four-repeat tau on mitochondrial axonal transport. J Neurochem *111*, 417-427.

Storer, P.D., and Houle, J.D. (2003). betaII-tubulin and GAP 43 mRNA expression in chronically injured neurons of the red nucleus after a second spinal cord injury. Exp Neurol *183*, 537-547.

Stowers, R.S., Megeath, L.J., Gorska-Andrzejak, J., Meinertzhagen, I.A., and Schwarz, T.L. (2002). Axonal transport of mitochondria to synapses depends on milton, a novel Drosophila protein. Neuron *36*, 1063-1077.

Su, X., Arellano-Santoyo, H., Portran, D., Gaillard, J., Vantard, M., Thery, M., and Pellman, D. (2013). Microtubule-sliding activity of a kinesin-8 promotes spindle assembly and spindle-length control. Nat Cell Biol *15*, 948-957.

Sudo, H., and Baas, P.W. (2010). Acetylation of Microtubules Influences Their Sensitivity to Severing by Katanin in Neurons and Fibroblasts. J Neurosci *30*, 7215-7226.

Sudo, K., Ito, H., Iwamoto, I., Morishita, R., Asano, T., and Nagata, K. (2007). SEPT9 sequence alternations causing hereditary neuralgic amyotrophy are associated with altered interactions with SEPT4/SEPT11 and resistance to Rho/Rhotekin-signaling. Hum Mutat *28*, 1005-1013.

Sugino, Y., Ichioka, K., Soda, T., Ihara, M., Kinoshita, M., Ogawa, O., and Nishiyama, H. (2008). Septins as diagnostic markers for a subset of human asthenozoospermia. J Urol *180*, 2706-2709.

Sullivan, K.F., and Cleveland, D.W. (1986). Identification of conserved isotype-defining variable region sequences for four vertebrate beta tubulin polypeptide classes. Proc Natl Acad Sci U S A *83*, 4327-4331.

Sun, F., Zhu, C., Dixit, R., and Cavalli, V. (2011). Sunday Driver/JIP3 binds kinesin heavy chain directly and enhances its motility. EMBO J *30*, 3416-3429.

Surka, M.C., Tsang, C.W., and Trimble, W.S. (2002). The mammalian septin MSF localizes with microtubules and is required for completion of cytokinesis. Molecular Biology of the Cell *13*, 3532-3545.

Suryavanshi, S., Edde, B., Fox, L.A., Guerrero, S., Hard, R., Hennessey, T., Kabi, A., Malison, D., Pennock, D., Sale, W.S., *et al.* (2010). Tubulin Glutamylation Regulates Ciliary Motility by Altering Inner Dynein Arm Activity. Current Biology *20*, 435-440.

Suzuki, G., Harper, K.M., Hiramoto, T., Sawamura, T., Lee, M., Kang, G., Tanigaki, K., Buell, M., Geyer, M.A., Trimble, W.S., *et al.* (2009). Sept5 deficiency exerts pleiotropic influence on affective behaviors and cognitive functions in mice. Hum Mol Genet *18*, 1652-1660.

Tada, T., Simonetta, A., Batterton, M., Kinoshita, M., Edbauer, D., and Sheng, M. (2007). Role of septin cytoskeleton in spine morphogenesis and dendrite development in neurons. Current Biology *17*, 1752-1758.

Takano, K., Miki, T., Katahira, J., and Yoneda, Y. (2007). NXF2 is involved in cytoplasmic mRNA dynamics through interactions with motor proteins. Nucleic acids research *35*, 2513-2521.

Takeda, S., Yamazaki, H., Seog, D.H., Kanai, Y., Terada, S., and Hirokawa, N. (2000). Kinesin superfamily protein 3 (KIF3) motor transports fodrin-associating vesicles important for neurite building. J Cell Biol *148*, 1255-1265.

Takeda, S., Yonekawa, Y., Tanaka, Y., Okada, Y., Nonaka, S., and Hirokawa, N. (1999). Left-right asymmetry and kinesin superfamily protein KIF3A: new insights in determination of laterality and mesoderm induction by kif3A-/- mice analysis. J Cell Biol *145*, 825-836.

Takei, Y., Teng, J.L., Harada, A., and Hirokawa, N. (2000). Defects in axonal elongation and neuronal migration in mice with disrupted tau and map1B genes. Molecular Biology of the Cell *11*, 363A-+.

Takemura, R., Okabe, S., Umeyama, T., Kanai, Y., Cowan, N.J., and Hirokawa, N. (1992). Increased microtubule stability and alpha tubulin acetylation in cells transfected with microtubule-associated proteins MAP1B, MAP2 or tau. J Cell Sci *103 (Pt 4)*, 953-964.

Tanaka-Takiguchi, Y., Kinoshita, M., and Takiguchi, K. (2009). Septin-mediated uniform bracing of phospholipid membranes. Curr Biol *19*, 140-145.

Tanaka, M., Tanaka, T., Kijima, H., Itoh, J., Matsuda, T., Hori, S., and Yamamoto, M. (2001). Characterization of tissue- and cell-type-specific expression of a novel human septin family gene, Bradeion. Biochem Biophys Res Commun *286*, 547-553.

Tanaka, M., Tanaka, T., Matsuzaki, S., Seto, Y., Matsuda, T., Komori, K., Itoh, J., Kijima, H., Tamai, K., Shibayama, M., *et al.* (2003). Rapid and quantitative detection of human septin family Bradeion as a practical diagnostic method of colorectal and urologic cancers. Med Sci Monit *9*, MT61-68.

Tanaka, T., Serneo, F.F., Higgins, C., Gambello, M.J., Wynshaw-Boris, A., and Gleeson, J.G. (2004). Lis1 and doublecortin function with dynein to mediate coupling of the nucleus to the centrosome in neuronal migration. Journal of Cell Biology *165*, 709-721.

Taylor, K.R., Holzer, A.K., Bazan, J.F., Walsh, C.A., and Gleeson, J.G. (2000). Patient mutations in doublecortin define a repeated tubulin-binding domain. Journal of Biological Chemistry *275*, 34442-34450.

Teng, J., Takei, Y., Harada, A., Nakata, T., Chen, J., and Hirokawa, N. (2001). Synergistic effects of MAP2 and MAP1B knockout in neuronal migration, dendritic outgrowth, and microtubule organization. J Cell Biol *155*, 65-76.

Teng, J.L. (2005). The KIF3 motor transports N-cadherin and organizes the developing neuroepithelium (vol 7, pg 474, 2005). Nature Cell Biology *7*, 637-637.

Tischfield, M.A., Baris, H.N., Wu, C., Rudolph, G., Van Maldergem, L., He, W., Chan, W.M., Andrews, C., Demer, J.L., Robertson, R.L., *et al.* (2010). Human TUBB3 mutations perturb microtubule dynamics, kinesin interactions, and axon guidance. Cell *140*, 74-87.

Tokhtaeva, E., Capri, J., Marcus, E.A., Whitelegge, J.P., Khuzakhmetova, V., Bukharaeva, E., Deiss-Yehiely, N., Dada, L.A., Sachs, G., Fernandez-Salas, E., *et al.* (2015). Septin dynamics are essential for exocytosis. J Biol Chem *290*, 5280-5297.

Tom Dieck, S., Hanus, C., and Schuman, E.M. (2014). SnapShot: local protein translation in dendrites. Neuron *81*, 958-958 e951.

Toth, K., Galamb, O., Spisak, S., Wichmann, B., Sipos, F., Valcz, G., Leiszter, K., Molnar, B., and Tulassay, Z. (2011). The influence of methylated septin 9 gene on RNA and protein level in colorectal cancer. Pathol Oncol Res *17*, 503-509.

Toure, A., Rode, B., Hunnicutt, G.R., Escalier, D., and Gacon, G. (2011). Septins at the annulus of mammalian sperm. Biological Chemistry *392*, 799-803.

Trinczek, B., Biernat, J., Baumann, K., Mandelkow, E.M., and Mandelkow, E. (1995). Domains of tau protein, differential phosphorylation, and dynamic instability of microtubules. Mol Biol Cell *6*, 1887-1902.

Trinczek, B., Ebneth, A., Mandelkow, E.M., and Mandelkow, E. (1999). Tau regulates the attachment/detachment but not the speed of motors in microtubule-dependent transport of single vesicles and organelles. J Cell Sci *112 (Pt 14)*, 2355-2367.

Tsang, C.W., Estey, M.P., DiCiccio, J.E., Xie, H., Patterson, D., and Trimble, W.S. (2011). Characterization of presynaptic septin complexes in mammalian hippocampal neurons. Biol Chem *392*, 739-749.

Tsang, C.W., Fedchyshyn, M., Harrison, J., Xie, H., Xue, J., Robinson, P.J., Wang, L.Y., and Trimble, W.S. (2008). Superfluous role of mammalian septins 3 and 5 in neuronal development and synaptic transmission. Mol Cell Biol *28*, 7012-7029.

Tsvetkov, A.S., Samsonov, A., Akhmanova, A., Galjart, N., and Popov, S.V. (2007). Microtubule-binding proteins CLASP1 and CLASP2 interact with actin filaments. Cell Motil Cytoskel *64*, 519-530.

Vale, R.D., Coppin, C.M., Malik, F., Kull, F.J., and Milligan, R.A. (1994). Tubulin GTP hydrolysis influences the structure, mechanical properties, and kinesin-driven transport of microtubules. J Biol Chem *269*, 23769-23775.

Vale, R.D., and Fletterick, R.J. (1997). The design plan of kinesin motors. Annu Rev Cell Dev Biol *13*, 745-777.

van Alfen, N. (2007). The neuralgic amyotrophy consultation. J Neurol *254*, 695-704.

van Alfen, N., Hannibal, M.C., Chance, P.F., and van Engelen, B.G.M. (1993). Hereditary Neuralgic Amyotrophy.

van Alfen N, H.M., Chance PF, van Engelen BGM (2008). Hereditary Neuralgic Amyotrophy, A.M. Pagon RA, Ardinger HH, Bird TD, Dolan CR, Fong CT, Smith RJH, Stephens K, ed. (Washington, Seattle, GeneReviews).

van Alfen, N., van Engelen, B.G., and Hughes, R.A. (2009). Treatment for idiopathic and hereditary neuralgic amyotrophy (brachial neuritis). Cochrane Database Syst Rev, CD006976.

van Dijk, J., Rogowski, K., Miro, J., Lacroix, B., Edde, B., and Janke, C. (2007). A targeted multienzyme mechanism for selective microtubule polyglutamylation. Mol Cell *26*, 437-448.

Verhey, K.J., and Gaertig, J. (2007). The tubulin code. Cell Cycle *6*, 2152-2160.

Verhey, K.J., and Hammond, J.W. (2009). Traffic control: regulation of kinesin motors. Nat Rev Mol Cell Bio *10*, 765-777.

Verhey, K.J., and Rapoport, T.A. (2001). Kinesin carries the signal. Trends Biochem Sci *26*, 545-550.

Versele, M., and Thorner, J. (2005). Some assembly required: yeast septins provide the instruction manual. Trends Cell Biol *15*, 414-424.

Vonmassow, A., Mandelkow, E.M., and Mandelkow, E. (1989). Interaction between Kinesin, Microtubules, and Microtubule-Associated Protein-2. Cell Motil Cytoskel *14*, 562-571.

Walenta, J.H., Didier, A.J., Liu, X., and Kramer, H. (2001). The Golgi-associated hook3 protein is a member of a novel family of microtubule-binding proteins. J Cell Biol *152*, 923-934.

Wang, X., and Schwarz, T.L. (2009). The mechanism of Ca2+ -dependent regulation of kinesin-mediated mitochondrial motility. Cell *136*, 163-174.

Webster, D.R., Gundersen, G.G., Bulinski, J.C., and Borisy, G.G. (1987). Assembly and turnover of detyrosinated tubulin in vivo. J Cell Biol *105*, 265-276.

Weems, A.D., Johnson, C.R., Argueso, J.L., and McMurray, M.A. (2014). Higher-order septin assembly is driven by GTP-promoted conformational changes: evidence from unbiased mutational analysis in Saccharomyces cerevisiae. Genetics *196*, 711-727.

Weirich, C.S., Erzberger, J.P., and Barral, Y. (2008). The septin family of GTPases: Architecture and dynamics. Nat Rev Mol Cell Bio *9*, 478-489.

Weisbrich, A., Honnappa, S., Jaussi, R., Okhrimenko, O., Frey, D., Jelesarov, I., Akhmanova, A., and Steinmetz, M.O. (2007). Structure-function relationship of CAP-Gly domains. Nat Struct Mol Biol *14*, 959-967.

Westermann, S., and Weber, K. (2003). Post-translational modifications regulate microtubule function. Nat Rev Mol Cell Biol *4*, 938-947.

Wloga, D., and Gaertig, J. (2010). Post-translational modifications of microtubules. J Cell Sci *123*, 3447-3455.

Wloga, D., Webster, D.M., Rogowski, K., Bre, M.H., Levilliers, N., Jerka-Dziadosz, M., Janke, C., Dougan, S.T., and Gaertig, J. (2009). TTLL3 Is a Tubulin Glycine Ligase that Regulates the Assembly of Cilia. Developmental Cell *16*, 867-876.

Wolyniak, M.J., Blake-Hodek, K., Kosco, K., Hwang, E., You, L., and Huffaker, T.C. (2006). The regulation of microtubule dynamics in Saccharomyces cerevisiae by three interacting plus-end tracking proteins. Mol Biol Cell *17*, 2789-2798.

Wong-Riley, M.T., and Besharse, J.C. (2012). The kinesin superfamily protein KIF17: one protein with many functions. Biomol Concepts *3*, 267-282.

Wong, R.W.C., Setou, M., Teng, J.L., Takei, Y., and Hirokawa, N. (2002). Overexpression of motor protein KIF17 enhances spatial and working memory in transgenic mice. P Natl Acad Sci USA *99*, 14500-14505.

Wordeman, L. (2005). Microtubule-depolymerizing kinesins. Curr Opin Cell Biol *17*, 82-88.

Wu, X.F., Xiang, X., and Hammer, J.A. (2006). Motor proteins at the microtubule plus-end. Trends in Cell Biology *16*, 135-143.

Xia, L., Hai, B., Gao, Y., Burnette, D., Thazhath, R., Duan, J., Bre, M.H., Levilliers, N., Gorovsky, M.A., and Gaertig, J. (2000). Polyglycylation of tubulin is essential and affects cell motility and division in Tetrahymena thermophila. Journal of Cell Biology *149*, 1097-1106.

Xie, H., Surka, M., Howard, J., and Trimble, W.S. (1999). Characterization of the mammalian septin H5: distinct patterns of cytoskeletal and membrane association from other septin proteins. Cell Motil Cytoskeleton *43*, 52-62.

Xie, Y.L., Vessey, J.P., Konecna, A., Dahm, R., Macchi, P., and Kiebler, M.A. (2007). The GTP-binding protein septin 7 is critical for dendrite branching and dendritic-spine morphology. Current Biology *17*, 1746-1751.

Xu, Y., Takeda, S., Nakata, T., Noda, Y., Tanaka, Y., and Hirokawa, N. (2002). Role of KIFC3 motor protein in Golgi positioning and integration. J Cell Biol *158*, 293-303.

Xue, J., Tsang, C.W., Gai, W.P., Malladi, C.S., Trimble, W.S., Rostas, J.A.P., and Robinson, P.J. (2004). Septin 3 (G-septin) is a developmentally regulated phosphoprotein enriched in presynaptic nerve terminals. Journal of Neurochemistry *91*, 579-590.

Yamada, K., Andrews, C., Chan, W.M., McKeown, C.A., Magli, A., de Berardinis, T., Loewenstein, A., Lazar, M., O'Keefe, M., Letson, R., *et al.* (2003). Heterozygous mutations of the kinesin KIF21A in congenital fibrosis of the extraocular muscles type 1 (CFEOM1). Nature Genetics *35*, 318-321.

Yamada, K.H., Hanada, T., and Chishti, A.H. (2007). The effector domain of human Dlg tumor suppressor acts as a switch that relieves autoinhibition of kinesin-3 motor GAKIN/KIF13B. Biochemistry-Us *46*, 10039-10045.

Yin, X., Feng, X., Takei, Y., and Hirokawa, N. (2012). Regulation of NMDA receptor transport: a KIF17-cargo binding/releasing underlies synaptic plasticity and memory in vivo. J Neurosci *32*, 5486-5499.

Yin, X.L., Takei, Y., Kido, M., and Hirokawa, N. (2011). Molecular motor KIF17 is fundamental for memory and learning via differential support of synaptic NR2A/2B levels. Neurosci Res *71*, E118-E118.

Yonekawa, Y., Harada, A., Okada, Y., Funakoshi, T., Kanai, Y., Takei, Y., Terada, S., Noda, T., and Hirokawa, N. (1998). Defect in synaptic vesicle precursor transport and neuronal cell death in KIF1A motor protein-deficient mice. Journal of Cell Biology *141*, 431-441.

Yu, I., Garnham, C.P., and Roll-Mecak, A. (2015). Writing and Reading the Tubulin Code. J Biol Chem *290*, 17163-17172.

Zhang, J., Kong, C., Xie, H., McPherson, P.S., Grinstein, S., and Trimble, W.S. (1999). Phosphatidylinositol polyphosphate binding to the mammalian septin H5 is modulated by GTP. Curr Biol *9*, 1458-1467.

Zhao, C., Takita, J., Tanaka, Y., Setou, M., Nakagawa, T., Takeda, S., Yang, H.W., Terada, S., Nakata, T., Takei, Y., *et al.* (2001). Charcot-Marie-Tooth disease type 2A caused by mutation in a microtubule motor KIF1Bbeta. Cell *105*, 587-597.

Zhu, M., Wang, F.S., Yan, F., Yao, P.Y., Du, J., Gao, X.J., Wang, X.W., Wu, Q., Ward, T., Li, J.J., *et al.* (2008). Septin 7 interacts with centromere-associated protein E and is required for its kinetochore localization. Journal of Biological Chemistry *283*, 18916-18925.

Zieger, B., Tran, H., Hainmann, I., Wunderle, D., Zgaga-Griesz, A., Blaser, S., and Ware, J. (2000). Characterization and expression analysis of two human septin genes, PNUTL1 and PNUTL2. Gene *261*, 197-203.

Zilberman, Y., Ballestrem, C., Carramusa, L., Mazitschek, R., Khochbin, S., and Bershadsky, A. (2009). Regulation of microtubule dynamics by inhibition of the tubulin deacetylase HDAC6. J Cell Sci *122*, 3531-3541.

VITA

Xiaobo Bai was born in Shaanxi, P.R.China on March 20th, 1985. After receiving his BS degree from Northwest A & F University in Yangling, China in 2002, Xiaobo entered Nankai University in Tianjin, China for his MS degree in molecular biology, and received it in 2009. During 2009-2015, he worked on his PhD degree in the Department of Biology in Drexel University, Philadelphia, Pennsylvania.

List of publications:

Bai X, Bowen RJ, Knox KT et al. (2013) Novel septin 9 repeat motifs altered in neuralgic amyotrophy bind and bundle microtubules. The Journal of Cell Biology 203(6): 895-905.

Angelis D, Karasmanis EP, Bai X, and Spiliotis ET (2014) In Silico Docking of Forchlorfenuron (FCF) to Septins Suggests that FCF Interferes with GTP Binding. PLOS ONE 9(5): e96390.

Bing T, Wu K, Cui X, Shao P, Zhang Q, **Bai X**, Tan J, Qiao W (2014) Identification and functional characterization of Bet protein as a negative regulator of BFV3026 replication. Virus Genes 48(3): 464-473.

Hu J, **Bai X**, Bowen JR, Dolat L et al. (2012) Septin-Driven Coordination of Actin and Microtubule Remodeling Regulates the Collateral Branching of Axons. Current Biology 22(12):1109-15.

DeMay BS, **Bai X**, Howard L et al. (2011) Septin filaments exhibit a dynamic, paired organization that is conserved from yeast to mammals. The Journal of Cell Biology 193(6): 1065-1081.

Bowen JR, Hwang D, **Bai X**, Roy D, Spiliotis ET (2011) Septin GTPases spatially guide microtubule organization and plus end dynamics in polarizing epithelia. The Journal of Cell Biololgy 194(2): 187-197.

Bai X, Qiao W, Chen Qi, Geng Yun. (2009) Development and Evaluation of a Loop-Mediated Isothermal Amplification Method for Rapid Detection of Prototype Foamy Virus. Chinese Journal of Microbiology and Immunology 29(2): 181-185.